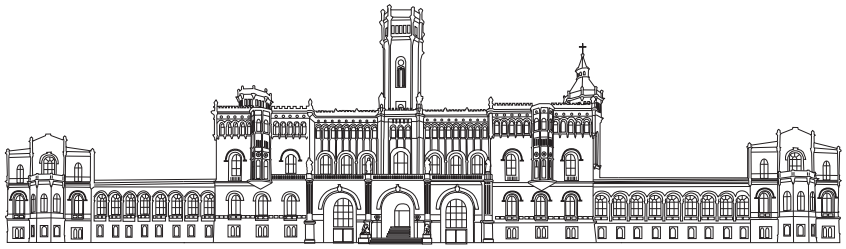

LEIBNIZ UNIVERSITÄT HANNOVER

QUANTUM BACK-ACTION EVASION AND FILTERING IN OPTOMECHANICAL SYSTEMS

Von der QUEST-Leibniz-Forschungsschule
der Gottfried Wilhelm Leibniz Universität Hannover
zur Erlangen des Grades

DOKTOR DER NATURWISSENSCHAFTEN
DR. RER. NAT.

genehmigte Dissertation
von

M. SC. JAKOB SCHWEER

2023

Referent:	Prof. Dr. Klemens Hammerer
Korreferenten:	Prof. Dr. Michèle Heurs
	Assoc. Prof. Dr. Stefan Danilishin
Tag der Promotion:	17. Februar 2023

ABSTRACT

The measurement precision of optomechanical sensors reached sensitivity levels such that they have to be described by quantum theory. In quantum mechanics, every measurement will introduce a back-action on the measured system itself. For optomechanical force sensors, a trade-off between back-action and measurement precision exists through the interplay of quantum shot noise and quantum radiation pressure noise. Finding the optimal power to balance these effects leads to the standard quantum limit (SQL), which bounds the sensitivity of force sensing. To overcome the SQL and reach the fundamental bound of parameter estimation, the quantum Cramér-Rao bound, techniques called quantum smoothing and quantum back-action evasion are required.

The first part of this thesis explores quantum smoothing in the context of optomechanical force sensing. Quantum smoothing combines the concepts of prediction and retrodiction to estimate the parameters of a system in the past. To illustrate the intricacies of these estimations in the quantum setting, two filters, the Kalman and Wiener filters, are introduced. Their prediction and retrodiction estimates are given for a simple optomechanical setup, and resulting differences are analyzed concerning the available quantum smoothing theories in the literature.

In the second part of this thesis, a back-action evasion technique called coherent quantum-noise cancellation (CQNC) is explored. In CQNC, an effective negative-mass oscillator is coupled to an optomechanical sensor to create destructive interference of quantum radiation pressure noise. An all-optical realization of such an effective negative-mass oscillator is introduced, and a comprehensive study of its performance in a cascaded CQNC scheme is given. We determine ideal CQNC conditions, analyze non-ideal noise cancellation and provide a case study.

Under feasible parameters, the case study shows a possible reduction of radiation pressure noise of 20% and that the effective negative-mass oscillator as the first subsystem in the cascade is the preferable order.

Keywords: Quantum smoothing, back-action evasion, cascaded quantum systems, coherent quantum-noise cancellation

ZUSAMMENFASSUNG

Die Messgenauigkeit optomechanischer Sensoren hat eine Sensitvität erreicht, sodass sie im Rahmen der Quantentheorie beschrieben werden müssen. Quantenmechanik besagt, dass jede Messung eine Rückkopplung auf das vermessene System induziert. Bei optomechanischen Kraftsensoren is ein Kompromiss zwischen Rückkopplung und Messgenauigkeit durch die Verzahnung von Schrotrauschen und Strahlungsdruckrauschen begründet. Die Verwendung der optimalen Leistung, derart dass diese beiden Prozesse in Waage liegen, führt zum Standardquantenlimit (SQL). Hierdurch wird die Messgenauigkeit begrenzt. Um das SQL zu überwinden und die fundamentale Grenze der Parameterschätzung zu erreichen, welche durch Quanten-Cramér-Rao-Ungleichung bestimmt ist, werden die Methoden der Quantenglättung und Rückkopplungsumgehung benötigt.

Im ersten Teil dieser Arbeit wird das Gebiet der Quantenglättung im Kontext von optomechanischer Kraftmessung untersucht. Die Quantenglättung kombiniert die Methoden der Vorhersage und Retrodiktion, um Abschätzungen an die Parameter eines Quantensystems zu tätigen, welche in der Vergangenheit liegen. Um die Feinheiten dieser Abschätzungen für Quantensysteme zu demonstrieren, werden zwei Filter, der Kalman- und der Wiener-Filter eingeführt. An einem einfachen optomechanischen System, werden deren Ergebnisse für die Vorhersage und Retrodiktion berechnet. Mögliche Diskrepanzen werden im Kontext der verfügbaren Theorien der Quantenglättung beleuchtet.

Im zweiten Teil dieser Dissertation wird eine Rückkopplungsumgehungsmethode, die kohärente Quantenrauschunterdrückung (coherent quantum-noise cancellation, CQNC) untersucht. Bei CQNC wird ein Oszillator mit effektiver negativer Masse an einen optomechanischen Sensor gekoppelt, um destruktiv mit dem Strahlungsdruckrauschen zu interferieren. Eine mögliche optische Realisierung eines solchen negativen Masse Oszillators wird vorgestellt und mit einem optomechanischem Kraftsensor kaskadiert. Dieser Aufbau wird hinsichtlich seiner Rauschünterdrückungfähigkeit untersucht. Diesbezüglich ermitteln wir die Bedingungen für eine vollständige Abwendung von Strahlungsdruckrauschen und analysieren den Einfluss von möglichen Abweichungen von diesen Bedingungen auf die Rauschünterdrückung. Zuletzt präsentieren wir eine Fallstudie eines möglichen experimentellen Aufbaus.

Die Fallstudie zeigt eine mögliche Strahlungsdrückreduzierung von 20% und dass der Oszillator mit effektiver negativer Masse als erstes System in der Kaskade zu bervorzugen ist.

Schlüsselwörter: Quantenglättung, Rückkopplungsumgehung, kaskadierte Quantensysteme, kohärente Quantenrauschünterdrückung

heehoaeheohoahae rahoroer heehaoaho

- Luka

ACKNOWLEDGMENTS

First, I would like to thank my supervisors, Klemens Hammerer, Michèle Heurs and Stefan Danilishin.

Thank you, Klemens; I can hardly describe how grateful I am to have you as my supervisor. I thank you for all the wisdom and help you gave me throughout these years. I am especially grateful for all the kindness and trust you gave me. After each of our meetings, I genuinely felt better about myself and that this Ph.D. endeavor will end well. Thank you from the bottom of my heart.

Thank you, Michèle, for keeping me in your group as a "theorist in residence" and never letting me feel like an outsider. I am grateful for your open ears to any of my problems, not just physics. Thank you for your kindness and all the Christmas chocolate, which was very helpful in these stressful last weeks. I also must apologize for writing this in American English.

Thank you, Stefan, for giving me this position in the first place. Coming from mathematical physics, I am grateful that you gave me the opportunity to switch gears and see some "physics" again. And even though we had to part ways, I am very thankful for your supervision in the first 2 years of my Ph.D. career.

To all three of you, thank you for this academic journey! With only 24h in a day, I can not believe how you do what you do. All of you have my deepest gratitude and respect!

To my colleagues in the Quantum Control group, thank you for making this time enjoyable! I am grateful to everybody coming to my office asking about theory or physics; these discussions always salvaged my day. Special thanks to Bernd, Daniel, Dennis, Jonas and Johny for the activities outside of the university – yes, I mean, thanks for the beers. To Margot and Jan, thank you for watching Luka when I was in Finland. Special thanks to everybody that proofread this thesis! I would also like to thank Jonas Lammers for introducing me to retrodiction at the beginning of my Ph.D.

I want to thank Birgit Ohlendorf, Birgit Gemmeke and Kirsten Labove for all the administrative magic they can do and for lots of support in this last few weeks.

To my family, I would like to thank my Grandmas Inge and Grete, my parents Gabi and Dieter, and my siblings and in-law Simon, Leon and Melanie for all their unconditional support, keeping me grounded in this world that is not just about physics. Also, thank you for all the good food and wine!

To my favorite person, Emi, thank you for being by my side for almost half our life's now! For lifting me up every time I thought I could not do it, rakastan sua!

To Merja ja Jokke, thank you for all the kindness and love over these years. I always felt like a part of the family from the beginning.

For my extended family, to my friends, Simon, Florian, Irina and Steffen, thank you for almost 20 years of friendship, for all the laughter and parties, lots of drinks and genuine support through all this time. When this is all over, let's grind again! To the friends I met in university, to the "lunch group", Nico, Pavel, Simon, Natascha, Eric and Inken, thanks for the lovely time, movie nights and pizzas. Also, to Eric and Inken, thanks for being the best virtual golf buddies.

To Luka, thank you for being the best of all the good boys!

CONTENTS

1 INTRODUCTION

Quantum mechanics describes light and matter on atomic scales. On these levels, things behave very differently from our macroscopic experience; they are neither waves nor particles. This *wave-particle duality* had only been observed for small particles up to the size of molecules – until recently. The rapid development of optomechanics in a push for high-precision displacement measurements has shifted quantum effects further into the realm of macroscopic objects, smearing the lines between classical and quantum behavior [23].

High-precision measurements at the quantum level come with their own set of constraints. Quantum mechanics is an inherently stochastic theory, and every measurement of a quantum system will inadvertently change its state. So not only are the measurement outcomes distributed randomly, but the process of collecting information will disturb the system. If one wants to monitor the state of a system over an extended time, this disturbance can pose a conundrum. For monitoring types of measurements, called *weak continuous measurements* [24], this is stated as follows. To increase the measurement precision, one needs to increase the measurement strength, which in turn will increase the *back-action* or disturbance on the system. This disturbance may reduce the precision at a later time of the measurement; thus, a trade-off between these effects needs to be found.

In optomechanical force or position measurements, light is used to monitor the change in the position of a movable object. It is the quantum nature of light that then limits the possible precision of the measurement. For a given energy, the number of photons in the field is distributed randomly by a *Poisson distribution*. Low light power will increase the uncertainty of the number of photons in the field, which leads to imprecision in the measuring photodetector. This imprecision noise is called *shot noise* and can be reduced relative to the signal by increasing the power. Conversely, increasing the power will increase the *radiation pressure*, and thus the disturbance on the monitored object. Finding the optimal power that balances these two effects leads to the *standard quantum limit* (SQL) and puts a lower bound to the measurement precision.

The SQL is not the fundamental limit. Many approaches have been suggested to achieve measurements with sub-SQL accuracy. Most of these ideas can be categorized in methods called *back-action evading* techniques. To reach the highest precision, back-action evasion will not be enough. The fundamental limit to parameter estimation in quantum systems is given by the *quantum Cramér-Rao bound*. It was shown by Tsang et al. [123] that to achieve this bound; one needs to use back-action evasion and *quantum smoothing*.

Smoothing is a filtering technique widely used in classical estimation theory. It estimates the state of a system at an intermediate time using measurement data from before and after the estimation time. The suggested quantum smoothing

extends this approach to the quantum regime. This extension to the quantum world is, however, not without controversy. The smoothing procedure can be split into two steps; one uses measurement data from before the estimation time and the other from after the estimation time. These approaches are called *prediction/filtering* and *retrodiction*. In the quantum context, there exists the theory of *quantum filtering* [9, 5], which relies on the *quantum non-demolition* principle [6]. For retrodiction, such a quantum theory does not exist, and the non-commuting nature of past and future measurement data makes the extension of smoothing to the quantum domain extremely delicate, and many different approaches are available. For example, the original idea of quantum smoothing proposed by Tsang [117] is a *hybrid classical-quantum parameter estimation* technique. Similarly, Gammelmark et al. [36] used quantum smoothing as a *Bayesian update* for quantum parameter estimation. Guevara and Wiseman [45] introduced a smoothing technique to produce a smoothed quantum state, and recently Chantasri, Laverick, and Wiseman [21] connected many available smoothing techniques.

To achieve force sensing at the quantum Cramér-Rao bound, it needs an excellent understanding of admissible smoothing techniques and available schemes for back-action evasion in optomechanical force sensors.

The goal of this thesis is thus two-fold. First, we want to address the intricacies of quantum smoothing for optomechanical systems. Optomechanical systems are often described by linear Gaussian quantum systems, a class closely related to classical stochastic systems. Due to their close relation to the classical world, many classical filtering techniques have been suggested for quantum smoothing, often prematurely, as we find. We aim to show that more caution is needed when applying these techniques to quantum systems by showing how different filters will result in different retrodiction estimates. The second part is aimed toward back-action evasion. Many suggested techniques are available, one of which is *coherent quantum-noise cancellation* (CQNC). Achieving insides into the noise canceling performance of different CQNC realizations, especially their behavior regarding mismatches in their parameter scope, is a valuable asset for future experiments. We contribute to this endeavor by giving a complete analysis of an all-optical cascaded realization of CQNC.

STRUCTURE OF THE THESIS

In Chapter 2, we lay out the fundamental concepts needed for the rest of the thesis. We start with an introduction to estimation theory in classical stochastic systems. Starting from the cornerstone of parameter estimation, Bayes' theorem, we will stray through the theory of continuous measurements and introduce the concepts of prediction, retrodiction and smoothing for parameter estimation. Turning to the quantum world, we give an elementary introduction to quantum mechanics and quantum measurements. Starting from the projective measurement postulate in closed quantum systems, we will generalize our notions step-by-step to open system dynamics, updating the measurement postulate along the way until its most general form. In the last section of this chapter,

we move to optomechanical systems. We will show how to quantize the optical and mechanical harmonic oscillator and couple them in an optomechanical cavity. The resulting back-action interaction will be linearized, and we will discuss how this interaction leads to the standard quantum limit.

Chapter 3 will focus on estimation theory for quantum systems. Starting with an introduction to continuous measurements in quantum mechanics, we will introduce the governing master equations that describe this evolution. The appropriate set of quantum systems for linearized optomechanics are the linear Gaussian quantum systems. We will introduce some practical concepts of these systems, such as the representation in phase space and Wigner functions. The close connection of this subclass of quantum mechanics will be shown as the master equations will turn to classical filter equations, the so-called Kalman filter. In addition, we provide another optional filter for this; the Wiener filter. Using a simple optomechanical example, the performance of these two filters will be discussed in the context of quantum smoothing. Accompanying this analysis, we will introduce the different notions of quantum smoothing available in the literature.

Chapter 4 is mainly based on our publication [106] and is devoted to back-action evasion in optomechanics. After an introduction to some back-action evading techniques, we discuss a setup for a cascaded all-optical scheme for coherent quantum-noise cancellation. We determine the conditions needed for a complete cancellation of quantum back-action noise and afterward analyze the parameter scope of the most likely deviations from these ideal conditions. Following this analysis, we will provide a set of parameters for which we conduct a case study for a possible experiment.

This thesis is concluded with a summation of our results and an outlook on further research ideas.

A FEW WORDS ON NOTATION

In this thesis, we denote vectors by boldface letters $\mathbf{x}$, operators, matrices by capital letters M and operators by hats $\hat{x}$. Consequently, a vector of operators will be boldface with a hat $\hat{\mathbf{x}}$. The exception to this rule is $\mathbb{1}$, which we will use for both the identity operator and identity matrix. We will also not always use a subscript at the identity matrix to denote its dimension; the dimension will be what is needed at that particular time. Complex conjugation is denoted by a star, a^*, the transpose of a matrix by $\top$ and Hermitian conjugation of operators and matrices by a dagger, thus $M^\dagger = (M^\top)^*$.

As in our publication [106], quadrature operators and force are dimensionless. The corresponding force spectral density will also be dimensionless, and we give it in arbitrary units. To find a spectral density in units of N^2/Hz for a given mechanical oscillator, one needs to multiply it with $\hbar m \gamma_m \omega_m$. Here, $\hbar$ is the reduced Planck constant, m the mass of the oscillator, γ_m its damping rate and ω_m its resonance frequency.

Many quantities in this thesis are rates that are represented in units of frequency (Hz) or units of angular frequency (rad/s). As we often use Fourier transforms, the standard dimensions of these rates will be that of angular frequencies. In connection to experiments, we find it more convenient to talk in Hz. We will omit the implicit conversion factor of 2π consistently.

The centerpiece of the suggested scheme in Chapter 4 is a system that acts as an effective negative-mass oscillator. For simplicity, we will often omit the "effective" without meaning that we deal with an actual negative mass.

2

PRELIMINARIES

This preliminary chapter introduces the basic concepts needed in this thesis. We start with an introduction to estimation theory for classical stochastic processes. Then we will give an overview of the kinematics and dynamics of quantum mechanics. In the last part of this chapter, we describe the basic setup for cavity optomechanics.

2.1 CLASSICAL ESTIMATION THEORY

In this section, we introduce the concepts of classical estimation theory. Classical estimation theory addresses the problem of determining a classical system's state from the information contained within available measurement data. Classical estimation theory has a long and rich history. The concepts of this section are found in many textbooks, such as [32, 114, 110, 116] for purely classical systems, and [143, 59] for both quantum and classical estimation. We give this review because many concepts will translate nicely into quantum mechanics; thus, gaining an intuition about these concepts is valuable.

2.1.1 *Bayesian Inference*

Before discussing measurements in quantum mechanics, it is beneficial to introduce the fundamental concept of classical measurement theory, also known as *Bayesian inference*. It tells us how our knowledge about some system variable x changes upon collecting measurement data y regarding this variable.

However, we first need to know what we mean by "knowledge" of x. Let us consider x to be a real-valued system parameter[1]. To infer its actual value, we perform a measurement with a value of uncertainty assigned to it. Thus, our knowledge of x is given by a probability distribution, $p(x)$, for the possible values of x. From this distribution, we gain the likelihood of x having some particular value. More generally, it measures our uncertainty of the actual value of x. The probability distribution $p(x)$ is called the *state-of-knowledge* of x, or simply the *state* of the system, as a classical system is described by its system variables.

To understand how the state changes upon acquiring measurement data y, we must understand how y is related to x. We first consider a simple example [59]. Assume we want to measure the length of an object using a simple ruler. In this case, our measurement will be the true length of the object plus

1 In general, this could be a vector of discrete or continuous values; for example, in a system of n interacting particles, it could be a vector of the n position and momentum vectors of the particles.

some random error, depending on how accurately we can measure the length. Therefore, there exists a probability distribution $p(y|x)$ for y, which is peaked around $y = x$. Because this probability distribution depends on the value of x, it is appropriately called the *conditional* probability distribution, or *conditional state* of y given x. It is referred to as the *likelihood function* for the measurement and is completely determined by the used measurement procedure. In order to determine the likelihood function, we note that it is often enough to relate the measurement result y to the system variable x as follows; $y = f(x) + \xi$. In this, $f(x)$ is some deterministic function of x, and ξ is a noise process introduced by our measurement apparatus with its independent probability distribution $p(\xi)$. Think of it as the error by reading off the ruler or some electrical noise added to some measurement instrument.

The likelihood function is one of the building blocks for *Bayes' theorem*, the pillar of Bayesian inference, which tells us how to derive the conditional probability distribution of x given a measurement result y. In essence, it is an elementary consequence of probability theory via the relationship of the joint probability $p(x \cap y)$ and the conditional probabilities $p(x|y)$ and $p(y|x)$. Their relationship is defined by [58]

$$p(x \cap y) = p(x|y)p(y) = p(y|x)p(x). \tag{2.1}$$

Rearranging Equation (2.1) leads to Bayes' theorem

$$p(x|y) = \frac{p(y|x)p(x)}{p(y)} = \frac{p(y|x)p(x)}{\mathcal{N}}\,, \text{with} \quad \mathcal{N} = \int_{-\infty}^{\infty} p(y|x)p(x)dx = p(y). \tag{2.2}$$

The right-hand side of Equation (2.2) is composed of the likelihood function, the probability distribution of x before the measurement occurred, called the *prior* and a normalization factor. Hence, Bayes' theorem tells us that the information about our state after performing a measurement is updated by multiplying our current knowledge about x with the likelihood function and normalizing the result.

2.1.2 *Stochastic Systems*

In an experimental scenario, the estimated systems will not be static as in the previous section but will undergo a dynamic evolution. Additionally, a perfectly closed system does not exist, and every system constantly interacts with its surroundings. This interaction is modeled by introducing a random noise process for the environment. Open systems of this kind are called *stochastic systems*.

We define a stochastic system as depicted in Figure 2.1 by a set of time-dependent system variables $\{\mathbf{x}_{t_k} : t_k \in \mathfrak{T}\}$, where $\mathfrak{T} \subseteq [t_0, T]$, is a finite time interval. If the system variables are affected by the incoming noise process in a time-dependent way, we will call this set a *stochastic process* [33].

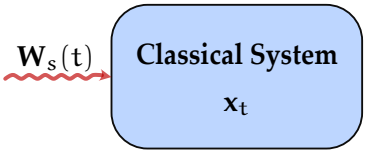

Figure 2.1: Simple model of a Classical Open System. The system described by $\mathbf{x}_t$ is in contact with a large environment, which effect is described by the system noise $\mathbf{W}_s(t)$.

Stochastic processes are characterized by the correlations of the system states at different times. These correlations can be described in terms of the conditional state. The simplest example of a stochastic process is given by

$$p(\mathbf{x}_{t_0}, \mathbf{x}_{t_1}, ...) = \prod_i p(\mathbf{x}_{t_i}). \tag{2.3}$$

This process does not hold any correlation with past or future system states at any time and is called a *completely independent process*. The next simplest possible stochastic process is the Markov process, and despite its simplicity, it covers enough stochastic evolutions for the purpose of this thesis.

In a Markov process, the conditional state of the system at a time t_n is completely determined by the system variables of the most recent time t_{n-1}, i.e.

$$p(\mathbf{x}_{t_n}|\mathbf{x}_{t_{n-1}}, ..., \mathbf{x}_{t_0}) = p(\mathbf{x}_{t_n}|\mathbf{x}_{t_{n-1}}). \tag{2.4}$$

As a consequence, any arbitrary state of a Markov process is given by a product of subsequent conditional states,

$$p(\mathbf{x}_{t_n}, \mathbf{x}_{t_{n-1}}, ..., \mathbf{x}_{t_0}) = p(\mathbf{x}_{t_n}|\mathbf{x}_{t_{n-1}}) ... p(\mathbf{x}_{t_1}|\mathbf{x}_{t_0})p(\mathbf{x}_{t_0}). \tag{2.5}$$

The conditional states in Equation (2.5), and thus the time evolution of the process is given by the famous *Chapman-Kolmogorov Equation* [22, 75]:

$$p(\mathbf{x}_{t_l}|\mathbf{x}_{t_n}) = \int d\mathbf{x}_{t_m} p(\mathbf{x}_{t_l}|\mathbf{x}_{t_m})p(\mathbf{x}_{t_m}|\mathbf{x}_{t_n}), \quad t_l \leqslant t_m \leqslant t_n. \tag{2.6}$$

Moving to the continuous time limit, the Chapman-Kolmogorov Equation turns into the *Fokker-Planck Equation*, which in turn can be described by a linear stochastic differential equation, called the *Langevin Equation* [38]. Thus, the evolution of the continuous Markov process is given by

$$d\mathbf{x}_t = A(\mathbf{x}_t)dt + E(\mathbf{x}_t)d\mathbf{W}_s(t), \tag{2.7}$$

where $d\mathbf{W}_s(t)$ is a vector of Wiener, or white noise, increments that satisfy

$$\mathbb{E}[d\mathbf{W}_s(t)] = 0, \quad d\mathbf{W}_s(t)(d\mathbf{W}_s(t))^\top = \mathbb{1}dt, \tag{2.8}$$

where $\mathbb{E}$ is an ensemble average [143]. Throughout this thesis, we will evaluate all stochastic differential equations in the Itô sense. To understand what

we mean by that, let us suppose we obtained a solution to Equation (2.7) by integrating both sides of Equation (2.7):

$$\mathbf{x}_t = \mathbf{x}_{t_0} + \int_{t_0}^{t} A(\mathbf{x}_\tau)d\tau + \int_{t_0}^{t} E(\mathbf{x}_\tau)d\mathbf{W}_s(\tau). \tag{2.9}$$

The second integral in Equation (2.9) is called a *stochastic integral* due to the inherent stochastic nature of the integrand. In physics, a common way of solving such kinds of integrals is the Itô stochastic integral [57], which we will use exclusively[2].

2.1.3 *Continuous Measurements and Effects*

Let us now introduce a measurement process $\mathbf{y}$, such that the measurement outcome $\mathbf{y}_t$ correlates with the system state $p(\mathbf{x}_t)$. We saw in Section 2.1.1 that by Bayes' theorem, our knowledge about the system state is inferred from the probability distribution, conditioned on the measurement results. At a particular time t, we arrive at

$$p_{\mathbf{y}_t}(\mathbf{x}_t) \equiv p(\mathbf{x}_t|\mathbf{y}_t, p_0) = \frac{p(\mathbf{y}_t|\mathbf{x}_t, p_0)p(\mathbf{x}_t, p_0)}{p(\mathbf{y}_t|p_0)}, \tag{2.10}$$

where $p_0 = p(\mathbf{x}_{t_0})$ is the prior state at the initial time t_0, and

$$p(\mathbf{y}_t|p_0) = \int d\mathbf{x}_t p(\mathbf{y}_t|\mathbf{x}_t, p_0)p(\mathbf{x}_t, p_0) = \mathcal{N}, \tag{2.11}$$

the normalization constant. Similarly to the system dynamics, in the continuous time limit, the measurement process can be described by a stochastic differential equation,

$$d\mathbf{y}_t = \mathbf{y}_t dt = C(\mathbf{x}_t)dt + d\mathbf{W}_m(t). \tag{2.12}$$

Here, we have introduced a new set of Wiener increments to account for possibly noisy measurements. The Wiener increments for the measurement process satisfy the same conditions as in Equation (2.8).

Next, we want to account for possible back-action of the measurement on the system, a process that will be unavoidable for quantum systems. An excellent example of a back-action measurement in the classical context is given in [143]. Imagine we want to determine whether a can contains petrol fumes by dropping a lit match into it. Clearly, the result will allow us to infer the presence of petrol in the can, but the system's state will "collapse" to a state with no petrol fumes in either case. In this example, the state is also conditioned on the measurement, but the state may undergo a transition from $p(\mathbf{x}'_t)$ to $p(\mathbf{x}_{t+\delta t})$, where δt denotes the length of the back-action interaction. This measurement back-action is described by a matrix $B_{\mathbf{y}_t}$, where the matrix entries define the

2 See Appendix A.1 for a definition.

probability of a state transition $B_{\mathbf{y}_t}(\mathbf{x}_{t+\delta t}|\mathbf{x}'_t) \geqslant 0$. Therefore, for all measurement results $\mathbf{y}_t$ and all $\mathbf{x}'_t$,

$$\int d\mathbf{x}'_t \, B_{\mathbf{y}_t}(\mathbf{x}_{t+\delta t}|\mathbf{x}'_t) = 1. \tag{2.13}$$

The conditional state after the measurement interaction is given by

$$p_{\mathbf{y}_t}(\mathbf{x}_{t+\delta t}) = \frac{\int d\mathbf{x}'_t \, B_{\mathbf{y}_t}(\mathbf{x}_{t+\delta t}|\mathbf{x}'_t) p(\mathbf{y}_t|\mathbf{x}'_t) p(\mathbf{x}'_t)}{p(\mathbf{y}_t)}, \tag{2.14}$$

which is an extension of Bayes' theorem by the additional back-action matrix element in the numerator. We can define a conditional transfer matrix by combining the part from Bayesian inference and the back-action. The elements of this matrix $\mathcal{E}_{\mathbf{y}_t}$ are defined by the product of the back-action and the likelihood function, i.e.

$$\mathcal{E}_{\mathbf{y}_t}(\mathbf{x}_{t+\delta t}|\mathbf{x}'_t) = B_{\mathbf{y}_t}(\mathbf{x}_{t+\delta t}|\mathbf{x}'_t) p(\mathbf{y}_t|\mathbf{x}'_t), \tag{2.15}$$

which maps the pre-measurement state to an unnormalized post-measurement state:

$$\check{p}_{\mathbf{y}_t}(\mathbf{x}_{t+\delta t}) = \int d\mathbf{x}'_t \, \mathcal{E}_{\mathbf{y}_t}(\mathbf{x}_{t+\delta t}|\mathbf{x}'_t) p(\mathbf{x}'_t). \tag{2.16}$$

From the forgoing properties, the state of the measurement instrument can be simplified

$$p(\mathbf{y}_t) = \int d\mathbf{x}_{t+\delta t} \int d\mathbf{x}'_t \, \mathcal{E}_{\mathbf{y}_t}(\mathbf{x}_{t+\delta t}|\mathbf{x}'_t) p(\mathbf{x}'_t) = \int d\mathbf{x}_t E_{\mathbf{y}_t}(\mathbf{x}_t) p(\mathbf{x}_t), \tag{2.17}$$

with $E_{\mathbf{y}_t}$ describing the effect of the measurement on the system state. It is thus known as the *effect operator* and is specifically given by

$$E_{\mathbf{y}_t}(\mathbf{x}_t) = p(\mathbf{y}_t|\mathbf{x}_t), \tag{2.18a}$$

$$\int d\mathbf{y}_t \, E_{\mathbf{y}_t}(\mathbf{x}_t) = 1. \tag{2.18b}$$

We see that this implies an interesting connection in that the effect of the measurement on the system is given by the likelihood function of achieving our measurement result given the system variable at that time.

To summarize our finding, the situation considered so far can be summarized by the stochastic differential equations:

$$d\mathbf{x}_t = A(\mathbf{x}_t)dt + E(\mathbf{x}_t)d\mathbf{W}_s(t), \tag{2.19a}$$

$$d\mathbf{y}_t = \mathbf{y}_t dt = C(\mathbf{x}_t)dt + d\mathbf{W}_m(t). \tag{2.19b}$$

For the purpose of this thesis, it is enough to consider a special class of Markov processes called linear Gaussian processes; see [46, 117, 118] for the general case. A Gaussian state is defined by a probability density function that is fully defined by its mean values $\langle \mathbf{x} \rangle$ and covariance matrix V; i.e.

$$p(\mathbf{x}) = f(\mathbf{x}; \langle \mathbf{x} \rangle, V) = \frac{1}{\sqrt{(2\pi)^n \det V}} \exp\left(-\frac{1}{2} (\mathbf{x} - \langle \mathbf{x} \rangle)^\top V^{-1} (\mathbf{x} - \langle \mathbf{x} \rangle)\right). \tag{2.20}$$

In order for a Gaussian state at the initial time t_0, $p(\mathbf{x}_{t_0}) = f(\mathbf{x}_{t_0}; \langle \mathbf{x}_{t_0} \rangle, V_0)$, to remain Gaussian the differential equations (2.19) simplify to the following [135, 116, 32, 143]:

$$d\mathbf{x}_t = A\, dt + E d\mathbf{W}_s(t), \tag{2.21a}$$

$$d\mathbf{y}_t = \mathbf{y}_t dt = C\, \mathbf{x}_t dt + d\mathbf{W}_m(t). \tag{2.21b}$$

Here, A, C, E are constant matrices[3]. The Wiener increments $d\mathbf{W}_s$ and $d\mathbf{W}_m$ satisfy the usual conditions, but we consider the possibility of cross-correlations between the measurement and system noises such that

$$\mathbb{E}[d\mathbf{W}_s] = 0, \quad d\mathbf{W}_s (d\mathbf{W}_s)^\top = \mathbb{1} dt, \tag{2.22a}$$

$$\mathbb{E}[d\mathbf{W}_m] = 0, \quad d\mathbf{W}_m (d\mathbf{W}_m)^\top = \mathbb{1} dt, \tag{2.22b}$$

$$E d\mathbf{W}_s (d\mathbf{W}_m)^\top = \Gamma^\top dt, \tag{2.22c}$$

where we have defined the cross-correlation matrix Γ between the noise sources similarly to [143].

2.1.4 *Bayesian Smoothing*

The typical scenario in estimation theory is that we have continuously measured a dynamically evolving system $p(\mathbf{x}_t)$ and, in the process, acquired a measurement record. We denote this record as a collection $\mathbf{Y}_{\mathfrak{T}} = \{\mathbf{y}_t : t \in \mathfrak{T}\}$, where $\mathfrak{T} \subseteq [t_0, T]$ is the time interval in which the measurement was performed. Given the record, we want to estimate the conditional state $p_{\mathbf{Y}_{\mathfrak{T}}}(\mathbf{x}_\tau)$ at a specific time $\tau \in [t_0, T]$. Depending on the position of τ, we differentiate three estimation types [114]: *prediction/filtering*, *retrodiction* and *smoothing*[4], see Figure 2.2 for an illustration.

When τ lies at the end of our measurement series, i.e., we want to infer the system state based on past measurement results $\overrightarrow{\mathbf{Y}}_\tau \equiv \mathbf{Y}_{[t_0,\tau)}$[5], we say we filter out the noise or predict the state. The state condition on the past measurements will be referred to as the filtered state: $p_f(\mathbf{x}_\tau) \equiv p_{\overrightarrow{\mathbf{Y}}_\tau}(\mathbf{x}_\tau) = p(\mathbf{x}_\tau | \overrightarrow{\mathbf{Y}}_\tau)$. For the reverse case, if τ is at the beginning of our measurement interval, we can use the measurement record to infer the system's state in the past. This state is called the retrodicted state: $p_r(\mathbf{x}_\tau) \equiv p_{\overleftarrow{\mathbf{Y}}_\tau}(\mathbf{x}_\tau)$, where the measurement record $\overleftarrow{\mathbf{Y}}_\tau = \mathbf{Y}_{[\tau,T)}$ of future results was used. Essentially, this is just the time reverse of filtering. Suppose we want to estimate the state at an intermediate time $t_0 < \tau < T$, we can combine both techniques using the whole measurement

3 Equation (2.21) is often referred to as a state space model. In fact, it is the noisy version of the so-called ABCD model, where we discarded the B and D matrix, which account for a possible additional controller input. The A matrix is usually called the *drift matrix* and C the *input matrix*.

4 Our terminology is in congruence to [36, 148, 54, 76], other authors [46, 81, 78] call these filtering and retro-filtering.

5 Other authors [46, 81, 78] use this arrow notation differently. For estimations using the past measurement record, they use a backward arrow to indicate that the record was made in the past. However, we find it more intuitive to use the arrow to indicate that we condition our state from a time t_0 to τ, moving forward in time.

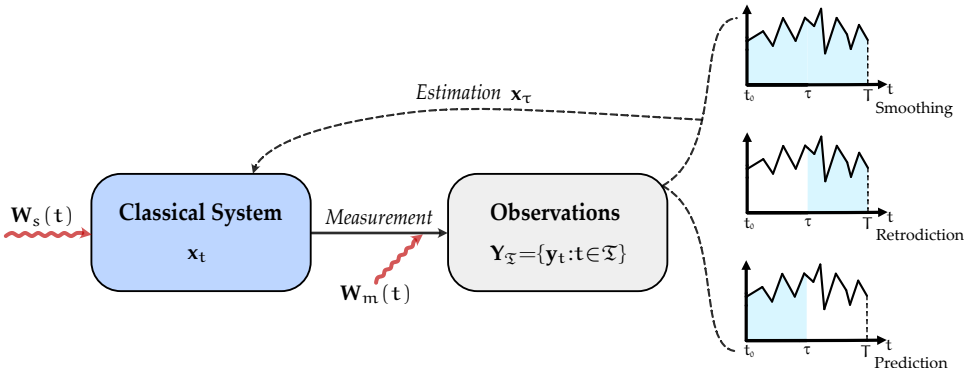

Figure 2.2: Model of the classical estimation problem. An open system $\mathbf{x}_t$ in the presence of system noise $\mathbf{W}_s$ is continuously measured with measurement noise $\mathbf{W}_m$. From the accessible measurement record $\mathbf{Y}_\mathfrak{T}$, the system state at time τ is estimated. Depending on the part of the measurement record used, we differentiate between prediction, retrodiction and smoothing.

record $\overleftrightarrow{\mathbf{Y}} = \mathbf{Y}_{[\tau,T)}$. This is called smoothing, and the inferred state is called the smoothed state: $p_s(\mathbf{x}_\tau) = p_{\overleftrightarrow{\mathbf{Y}}}(\mathbf{x}_\tau)$.

According to Bayes' theorem, the smoothed state can be expressed as

$$p(\mathbf{x}_\tau|\overleftrightarrow{\mathbf{Y}}) = \frac{p(\overleftrightarrow{\mathbf{Y}}|\mathbf{x}_\tau)\, p(\mathbf{x}_\tau)}{p(\overleftrightarrow{\mathbf{Y}})}, \tag{2.23}$$

$$p(\overleftrightarrow{\mathbf{Y}}) = \int d\mathbf{x}_\tau p(\overleftrightarrow{\mathbf{Y}}|\mathbf{x}_\tau)\, p(\mathbf{x}_\tau). \tag{2.24}$$

We will now split the measurement history into past $\overrightarrow{\mathbf{Y}}_\tau$ and future $\overleftarrow{\mathbf{Y}}_\tau$ components, relative to τ. We can then rewrite the first term in the numerator of (2.23):

$$p(\overleftrightarrow{\mathbf{Y}}|\mathbf{x}_\tau) = p(\overrightarrow{\mathbf{Y}}_\tau, \overleftarrow{\mathbf{Y}}_\tau|\mathbf{x}_\tau) \tag{2.25}$$

$$= p(\overleftarrow{\mathbf{Y}}_\tau|\overrightarrow{\mathbf{Y}}_\tau, \mathbf{x}_\tau)\, p(\overrightarrow{\mathbf{Y}}_\tau|\mathbf{x}_\tau) \tag{2.26}$$

$$= p(\overleftarrow{\mathbf{Y}}_\tau|\mathbf{x}_\tau)\, p(\overrightarrow{\mathbf{Y}}_\tau|\mathbf{x}_\tau). \tag{2.27}$$

For the last step, we used that our process is Markovian; thus, the future and past measurement records are independent for a given $\mathbf{x}_\tau$.

Now, we combine Equation (2.27) and Equation (2.23),

$$p_s(\mathbf{x}_\tau) = \frac{p(\overleftrightarrow{\mathbf{Y}}|\mathbf{x}_\tau)\, p(\mathbf{x}_\tau)}{p(\overleftrightarrow{\mathbf{Y}})} \tag{2.28}$$

$$= \frac{p(\overleftarrow{\mathbf{Y}}_\tau|\mathbf{x}_\tau)\, p(\overrightarrow{\mathbf{Y}}_\tau|\mathbf{x}_\tau) p(\mathbf{x}_\tau)}{p(\overleftrightarrow{\mathbf{Y}})} \tag{2.29}$$

$$= \frac{p(\overleftarrow{\mathbf{Y}}_\tau|\mathbf{x}_\tau)\, p(\mathbf{x}_\tau|\overrightarrow{\mathbf{Y}}_\tau)}{p(\overleftrightarrow{\mathbf{Y}})} \tag{2.30}$$

$$= \frac{p(\overleftarrow{\mathbf{Y}}_\tau|\mathbf{x}_\tau)\, p(\mathbf{x}_\tau|\overrightarrow{\mathbf{Y}}_\tau)}{\int d\mathbf{x}_\tau p(\overleftarrow{\mathbf{Y}}_\tau|\mathbf{x}_\tau)\, p(\mathbf{x}_\tau|\overrightarrow{\mathbf{Y}}_\tau)} \tag{2.31}$$

$$= \frac{E_r(\mathbf{x}_\tau) p_f(\mathbf{x}_\tau)}{\int d\mathbf{x}_\tau E_r(\mathbf{x}_\tau) p_f(\mathbf{x}_\tau)}. \tag{2.32}$$

Thus, the smoothed state, as a combination of filtering and retrodiction, is given by a combination of the filtered state and an effect operator associated with the future measurement record. In principle, we can turn this into a pure filtering or retrodiction problem by moving τ to the end or the beginning of the measurement procedure.

Turning our attention to the pure filtering problem, the filtered state for linear Gaussian systems is determined by the *Kalman-Bucy filter* [66], given by the following equations:

$$d\langle \mathbf{x}\rangle_f = A\langle \mathbf{x}\rangle_f dt + K^+[V_f] d\mathbf{W}_f, \tag{2.33a}$$

$$\dot{V}_f = AV_f + V_f A^\top + D - K^+[V_f] K^+[V_f]^\top, \tag{2.33b}$$

with the initial conditions $\langle \mathbf{x}\rangle_f(t_0) = \langle \mathbf{x}\rangle_0$ and $V_f(t_0) = V_0$. The matrix $D = EE^\top$ is called the diffusion matrix, and the increment $d\mathbf{W}_f := \mathbf{y}dt - C\langle \mathbf{x}\rangle_f$ is a vector of measurement pre-fits or innovations. Together with *Kalman gain* $K^\pm$, it refines the current estimate of the filter. The Kalman gain is given as a function of the covariance, as

$$K^\pm[V] := VC^\top \pm \Gamma^\top. \tag{2.34}$$

The Kalman-Bucy filter is the optimal estimate for a linear Gaussian process in the sense that it minimizes the mean square error [131].

To arrive at the solution for the effect operator, we observe that

$$p(\overleftrightarrow{\mathbf{Y}}) = \int d\mathbf{x}_\tau E_r(\mathbf{x}_\tau) p_f(\mathbf{x}_\tau), \tag{2.35}$$

is independent of the estimation time τ, i.e. $dp(\overleftrightarrow{\mathbf{Y}}) = 0$,

$$d\left[\int d\mathbf{x}_\tau E_r(\mathbf{x}_\tau) p_f(\mathbf{x}_\tau)\right] = 0 \tag{2.36}$$

$$\Rightarrow \int d\mathbf{x}_\tau dE_r(\mathbf{x}_\tau) p_f(\mathbf{x}_\tau) = -\int d\mathbf{x}_\tau E_r(\mathbf{x}_\tau) dp_f(\mathbf{x}_\tau). \tag{2.37}$$

Therefore, we see that for the linear differential equation for the filtered state

$$\mathrm{d}p_f(\mathbf{x}_\tau) = \hat{M}_{\mathbf{y}_\tau} p_f(\mathbf{x}_\tau), \tag{2.38}$$

defined by the state space model (2.21), there exists a corresponding adjoint equation for the effect operator

$$-\mathrm{d}E_r(\mathbf{x}_\tau) = \hat{M}^\dagger_{\mathbf{y}_\tau} E_r(\mathbf{x}_\tau). \tag{2.39}$$

We can thus find the solution for the effect operator via a backward Kalman-Bucy filter for the adjoint state space model. It is given by

$$-\mathrm{d}\langle \mathbf{x}\rangle_r = -A\langle \mathbf{x}\rangle_r + K^-[V_r]\mathrm{d}\mathbf{W}_r, \tag{2.40a}$$

$$-\dot{V}_r = -AV_r - V_rA^\top + D - K^-[V_r]K^-[V_r]^\top, \tag{2.40b}$$

and evolves backwards in time from the initial condition $E_r \propto \mathbb{1}$ at T, which corresponds to an uninformative state with $V_r(T) = \infty$. The backward filter was introduced by Mayne, Fraser and Potter [85, 35, 34] as a pragmatic solution to the above-illustrated smoothing problem. However, its connection to adjoint state space models was discovered later [131].

The smoothed state is defined by combining the two filter results. It is rightfully named the *two-filter smoother* [114, 32] or the *Mayne-Fraser-Potter smoother* after the aforementioned authors. The smoothed state is given by [85, 131]

$$\langle \mathbf{x}\rangle_s = V_s(V_f^{-1}\langle \mathbf{x}\rangle_f + V_r^{-1}\langle \mathbf{x}\rangle_r), \tag{2.41a}$$

$$V_s = (V_f^{-1} + V_r^{-1})^{-1}. \tag{2.41b}$$

The smoother is the *maximum likelihood* estimate of $\mathbf{x}$ given both measurement data from the past and the future, under the assumption that the errors from the two estimates are independent.

2.2 QUANTUM MECHANICS

In this section, we introduce the fundamental concepts of quantum mechanics. Our goal is to establish some basic notions and intuition about quantum mechanical states, their evolution and the measurement process. We will gradually introduce the idealized cases of these three building blocks and generalize them to the case of open quantum systems. However, a discussion of quantum state estimation based on continuous measurements will be reserved for Chapter 2. As in the previous chapter, this is a collection of concepts to build intuition and is found in many textbooks, we refer to [95, 16, 143] and [48, 15, 14] for a more mathematical perspective.

2.2.1 *Operational Approach to Quantum Mechanics*

Before we introduce the building blocks of quantum mechanics, we would like to talk about the broader scheme of the theory; especially, we would like to introduce our approach to quantum mechanics. Quantum mechanics is composed

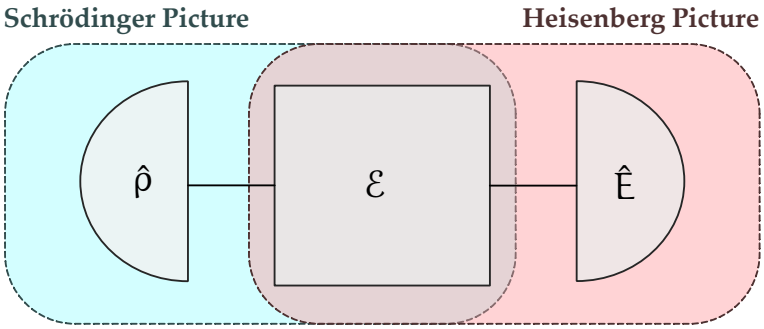

Figure 2.3: Depiction of the Schrödinger and Heisenberg picture. Assigning the time evolution $\mathcal{E}$ to the preparation stage $\hat{\rho}$ is called the Schrödinger picture and assigning the evolution to the measurement stage $\hat{E}$ is called the Heisenberg picture. Combinations of both are called the interaction picture.

of three concepts: *Preparations*, *time evolutions* and *measurements*. A preparation is a collection of attributes that describes our physical system, i.e., a preparation is a specific state of the system. After the preparation, the system may evolve freely before a measurement is performed. This time-evolution is *deterministic*[6] in the sense that states are uniquely determined by states at earlier times. Thus, this evolution is also *reversible*[6]. A measurement performed on a quantum state will give a classical bit of information, a measurement result. However, in quantum mechanics, measurements are fundamentally probabilistic and will always introduce back-action to the system. The amalgamation of these two conflicting concepts is known as the *measurement problem* [143, 59].

This description leaves us with a choice. We can assign the time evolution to the preparation stage, the measurement stage, or we can "cut" it up and assign parts of the evolution to both sides. All these views are equivalent; see Figure 2.3 for an illustration. We call the case where the preparations evolve the *Schrödinger picture*, the case of evolving measurements the *Heisenberg picture* and all the infinite cases of dividing the evolution the *interaction picture*.

2.2.2 *Closed Quantum Systems*

We begin our discussion with the case of *closed* systems. Closed or isolated systems do not exchange information with their environment. The description of the states, evolutions, and measurements in closed systems is also referred to as the *postulates* of quantum mechanics.

The classical description of quantum mechanics starts with a state space $\mathcal{S}$ given by a Hilbert space $\mathcal{H}$. A Hilbert space $\mathcal{H}$ is a complex vector space equipped with a scalar product $\langle .|. \rangle : \mathcal{H} \times \mathcal{H} \mapsto \mathbb{C}$. The elements of $\mathcal{H}$ are vectors $|\psi\rangle \in \mathcal{H}$, called *kets* in the Dirac notation. The dual of a ket $|\psi\rangle$ is called a *bra*. It is a linear map $\langle\psi| : \mathcal{H} \mapsto \mathbb{C}$, which maps any $|\phi\rangle \in \mathcal{H}$ to the inner Hilbert space product $\langle\psi, \phi\rangle$.

6 Only valid for closed systems, where we know the entire system. This will not be the case for an open system when only a subsystem is known.

The states of a closed system are the unit vectors $\||\psi\rangle\|^2 = \langle\psi|\psi\rangle = 1$, classically referred to as *wave functions*. States of this form are called *pure states* and hold the maximal information about the state space $\mathcal{S}$. The time evolution is determined by the system's interactions, which is described by a Hermitian operator $\hat{H} : \mathcal{H} \mapsto \mathcal{H}$. This operator, called the *Hamilton operator*, then gives rise to the *Schrödinger equation*:

$$\frac{i}{\hbar}\frac{d}{dt}|\psi(t)\rangle = \hat{H}|\psi(t)\rangle. \tag{2.42}$$

Observe, that for any Hamilton operator $\hat{H}$ the Schrödinger equation can be solved by an evolution operator $\hat{U}(t_0, t_1) : \mathcal{H} \mapsto \mathcal{H}$, which is defined by

$$\hat{U}(t_0, t_1) = \exp\left(-i\hat{H}(t_1 - t_0)\right), \tag{2.43}$$

where we set $\hbar = 1$[7]. We can then describe the time evolution in terms of these operators. For an initial state $|\psi(t_0)\rangle$, we find

$$|\psi(t_1)\rangle = \hat{U}(t_0, t_1)|\psi(t_0)\rangle, \quad t_0 \leqslant t_1. \tag{2.44}$$

The set of operators $\{\hat{U}_t\}_{t\in\mathbb{R}}$ forms a group of unitary operators, i.e., operators which fulfill $\hat{U}_t\hat{U}_t^\dagger = \mathbb{1}$ and the Hamiltonian $\mathcal{H}$ is the *generator* of this group. This implies that given some state $|\psi(t_1)\rangle$, we can find the initial state $|\psi(t_0)\rangle = \hat{U}^\dagger(t_0, t_1)|\psi(t_1)\rangle$. The time evolution defined by unitaries is thus called *reversible*. To summarize, closed quantum systems evolve by unitary transformations and are thus reversible.

Finally, we need to introduce the notion of measurement. This requires the interaction of our system to an external measurement device, or *observer*. Accordingly, our system is no longer closed at the moment of the measurement. Therefore, the system no longer needs to evolve via a unitary transformation; in fact, the measurement will result in an irreversible change in the system's state. This process is explained by the *measurement postulate*. It states that an ideal measurement Y on a quantum system is given by a set $\{(y, |y\rangle)\}$ of measurement outcomes $y \in \mathbb{R}$ and an orthogonal basis $|y\rangle$ of $\mathcal{H}$. The measurement procedure will then check which basis state the system is in. In this process, the state will be projected onto this basis state $|\psi_y = |y\rangle\rangle$, and the measurement device will output the result y. The result and state we achieve from the measurement are distributed randomly with a probability $p(y|\psi) = \langle y|\psi\rangle^2 = \langle\psi|\hat{P}_y|\psi\rangle$, where $\hat{P}_y = |\psi\rangle\langle\psi|$ is a *projection operator*. In contrast to classical measurement theory, we see that the randomness and back-action of the measurement process are inherent to the measurements in quantum mechanics. The procedure above can be formally written as

$$|\psi\rangle \overset{y}{\mapsto} |y\rangle = \frac{\hat{P}_y|y\rangle}{\sqrt{p(y|\psi)}}, \tag{2.45a}$$

$$p(y|\psi) = \langle\psi|\hat{P}_y|\psi\rangle. \tag{2.45b}$$

7 This convention will be kept for the rest of this section.

These are the idealized cases of measurements in quantum mechanics, called *projective measurements* or *von Neumann measurements* [127]. The procedure (2.45) gives the wave function its interpretation as a probability function and is called *Born's rule*[8].

From the measurement postulate, we find that for a Hermitian *observable*

$$\hat{O} = \sum_y y \hat{P}_y, \tag{2.46}$$

the expectation value of the measurement O given a prepared state $|\psi\rangle$ is given by

$$\langle \hat{O} \rangle_\psi := \langle \psi | \hat{O} | \psi \rangle = \sum_y p(y|\psi). \tag{2.47}$$

2.2.3 *Density Operators*

As stated in Section 2.1.2, a perfectly isolated system does not exist. We thus have to expand our notion and consider *open* quantum systems in analogy to the classical stochastic systems. We call a quantum system $\mathcal{S}$ open if it is embedded in a larger system $\mathcal{A}$, called *environment*, *bath* or *ancilla*. Because $\mathcal{S}$ is in constant contact with the environment, information can leave the system by leaking into the larger system. This process is called *dissipation* and similar to the noisy stochastic systems, this will introduce some uncertainty to our knowledge of the system state. Hence, pure states $|\psi\rangle$ are not feasible to describe this situation. The larger class to properly describe open systems are *density operators* $\hat{\rho} \in \mathcal{B}(\mathcal{H})$, which are Hermitian bounded operators on the Hilbert space $\mathcal{H}$. They are the quantum analog to the probability distributions introduced in the classical case, sometimes called *density matrices* or *mixed states*. Our discussion about closed systems is fully incorporated into this formalism. A pure state $|\psi\rangle$ is represented as a projection operator $\hat{\rho} = |\psi\rangle\langle\psi|$ and the dynamics of closed systems is given by the *von Neumann equation*

$$\frac{d}{dt}\hat{\rho}(t) = -i[\hat{H}, \hat{\rho}(t)] = -i(\hat{H}\hat{\rho}(t) - \hat{\rho}(t)\hat{H}), \tag{2.48}$$

which is equivalent to the Schödinger equation (2.42). Similarly, the von Neumann equation gives rise to a unitary time evolution,

$$\hat{\rho}(t_1) = \hat{U}(t_0, t_1)\hat{\rho}(t_0)\hat{U}^\dagger(t_0, t_1). \tag{2.49}$$

However, beyond this a general $\hat{\rho}$ can be given as a convex combination of pure states $|\psi_j\rangle$[9],

$$\hat{\rho} = \sum_j p_j |\psi_j\rangle\langle\psi_j|, \tag{2.50}$$

8 Sometimes this is also called the Born-Markov rule.

9 A consequence of the spectral decomposition theorem for Hermitian operators[26].

with $p_j \geqslant 0$ and $\sum_j p_j = 1$. Interestingly, every density operator $\hat{\rho}$ can itself be represented as a convex combination of density operators $\hat{\rho}_j$,

$$\hat{\rho} = \sum_j p_j \hat{\rho}_j. \tag{2.51}$$

Consequently, we see that the quantum states form a convex set and the pure states are the extreme points of this set. However, in contrast to classical probability theories, this decomposition in pure states is not unique[10]. To summarize, density operators satisfy the following conditions:

$$\hat{\rho} = \hat{\rho}^\dagger, \tag{2.52a}$$

$$\hat{\rho} \geqslant 0, \tag{2.52b}$$

$$\operatorname{tr} \hat{\rho} = \sum_y \langle y|\hat{\rho}|y\rangle = \sum_j p_j = 1. \tag{2.52c}$$

This subset, $\mathcal{T}(\mathcal{H}) \subset \mathcal{B}(\mathcal{H})$, is the set called *trace class operators* with unit trace.

The coefficients p_j are the probabilities of finding our state in a basis state $|\psi_j\rangle$. As long as the state is mixed, i.e., all $p_j < 1$, further knowledge about the system can be gained by collecting information[11]. This is different from a superposition $|\psi\rangle = \sum_j p_j |\phi_j\rangle$, which simply corresponds to the pure state $\hat{\rho} = |\psi\rangle\langle\psi|$, with a probability of 1. The right measure to infer this is the *purity*, defined by

$$\mathcal{P}(\hat{\rho}) = \operatorname{tr}(\hat{\rho}^2). \tag{2.53}$$

The measurement postulate can also be extended to density operators, by

$$\hat{\rho} \overset{y}{\mapsto} \hat{\rho}_y = \frac{\hat{P}_y \hat{\rho} \hat{P}_y}{p(y|\hat{\rho})}, \tag{2.54a}$$

$$p(y|\hat{\rho}) = \operatorname{tr}(\hat{P}_y \hat{\rho}). \tag{2.54b}$$

Similarly the mean of an observable $\hat{O}$ is obtained with

$$\langle \hat{O} \rangle_{\hat{\rho}} = \operatorname{tr}(\hat{O}\hat{\rho}). \tag{2.55}$$

2.2.4 *Open System Dynamics*

To understand how an open system evolves in time, we must first understand how to describe a coupled system. As mentioned before, an open system consists of a small system coupled to a large environment. The Hilbert space of the total system is then given by the composite system of the observed system $\mathcal{S}$, and the environment $\mathcal{A}$ [16]:

$$\mathcal{H}_{\text{total}} = \mathcal{H}_\mathcal{S} \otimes \mathcal{H}_\mathcal{A}. \tag{2.56}$$

10 In classical probability theories, the state space has the form of a simplex, hence every state has a unique decomposition in extreme points, c.f. [62].

11 For example, measuring the output field of an optical cavity. Here the laser light acts as an environment which we measure.

As the total system is a closed system, it evolves by a unitary transformation. Thus, by Equation (2.43) the total density operator evolves as

$$\hat{\rho}(t) = \hat{U}_t[\hat{\rho}_S(0) \otimes \hat{\rho}_A]\hat{U}_t^\dagger. \tag{2.57}$$

One approach is to write down the Hamiltonian for the composite system that generates the unitary transformation (2.57). For this, one needs to know the free Hamiltonian of each system and the Hamiltonian that covers all interactions. This leads to a total Hamiltonian on the composite system of the form

$$\hat{H}_{\text{total}} = \hat{H}_S \otimes \mathbb{1}_A + \mathbb{1}_S \otimes \hat{H}_A + \hat{H}_{\text{int}}. \tag{2.58}$$

In principle, one could then describe the dynamics in (2.57). However, this approach will only be feasible if the environment's dynamics are known. Another approach is to consider only the observable system S and describe the evolution of the reduced effective dynamics.

The physically suitable evolutions of this reduced state are described by a *quantum channel*. A quantum channel on the space of density operators, i.e., in the Schrödinger picture, is described by a map $\mathcal{E} : \mathcal{T}(\mathcal{H}) \to \mathcal{T}(\mathcal{H})$ that fulfills the three following conditions [144, Chapter 1.4]:

1. Linearity: This is an inherent requirement of quantum mechanics. Linearity means that

$$\mathcal{E}(\lambda\hat{\rho} + \hat{\sigma}) = \lambda\mathcal{E}(\hat{\rho}) + \mathcal{E}(\hat{\sigma}), \quad \forall\lambda \in \mathbb{C}, \quad \forall\hat{\rho}, \hat{\sigma} \in \mathcal{T}(\mathcal{H}). \tag{2.59}$$

2. Trace preserving: $\mathcal{E}$ has to map density operators onto density operators. Since every element in $\mathcal{T}(\mathcal{H})$ is a linear combination of density operators [77] we obtain by linearity

$$\operatorname{tr}\mathcal{E}(\hat{\rho}) = \operatorname{tr}\hat{\rho}, \quad \forall\hat{\rho} \in \mathcal{T}(\mathcal{H}). \tag{2.60}$$

   This condition says that the quantum channel will preserve probability. However, it can be useful to relax this condition and also allow for a loss of normalization. Consider, for example, a photodiode that detects a photon. In the detection process, this photon is "destroyed", and some probability has "left" the system. It is then convenient to introduce a set of *subnormalized states* $\tilde{\mathcal{T}}(\mathcal{H})$ which contains trace class operators $\hat{\rho}$ with $\operatorname{tr}\hat{\rho} \leqslant 1$. In this case, the evolution should map states to subnormalized states. Our condition above then translates into c.f. [48]:

$$\operatorname{tr}\tilde{\mathcal{E}}(\hat{\rho}) \leqslant \operatorname{tr}\hat{\rho}, \quad \forall\hat{\rho} \in \mathcal{T}(\mathcal{H}). \tag{2.61}$$

3. Complete positivity: The two foregoing conditions imply that $\mathcal{E}$ has to be a *positive map*, i.e., $\mathcal{E}(\hat{\rho}) \geqslant 0$ for all $\hat{\rho} \geqslant 0 \in \mathcal{B}(\mathcal{H})$. However, in the context of open systems, positivity is not enough. The necessary condition is that the evolution $\mathcal{E}$ is *completely positive*, which states that $\mathcal{E} \otimes \mathbb{1}_n \geqslant 0$, for all $n \in \mathbb{N}_0$. This ensures that the evolution maps the density operator as part of a larger system to a valid density operator.

We can find the associated evolution in the Heisenberg picture via $\mathrm{tr}\,[\mathcal{E}(\hat{\rho})\,\hat{O}] = \mathrm{tr}\,[\hat{\rho}\,\mathcal{E}^\dagger(\hat{O})]$. We will call $\mathcal{E}^\dagger : \mathcal{B}(\mathcal{H}) \to \mathcal{B}(\mathcal{H})$ the *adjoint channel*. It fulfills the same conditions as the quantum channel, but condition (2.60) translates to unitality (respectively (2.61) translates to subunitality):

$$\mathcal{E}^\dagger(\mathbb{1}) = \mathbb{1}, \quad \text{or} \quad \tilde{\mathcal{E}}^\dagger(\mathbb{1}) \leqslant \mathbb{1}.$$

A quantum channel $\mathcal{E}$ that satisfies the weaker condition of 2 is called a *quantum operation* [48].

To fully characterize all quantum channels, we need the concept of *partial trace*. Consider a composite system with a Hilbert space $\mathcal{H}_{AB} = \mathcal{H}_A \otimes \mathcal{H}_B$, the partial trace $\mathrm{tr}_B : \mathcal{T}(\mathcal{H}_A \otimes \mathcal{H}_B) \to \mathcal{T}(\mathcal{H}_A)$ is a mapping from the composite state space to reduced state space of $\mathcal{H}_A$. We say we "trace out" the system $\mathcal{H}_B$. By Stinesprings theorem [112], every quantum channel can be described by

$$\begin{aligned}\hat{\rho}_S(t) &= \mathcal{E}(\hat{\rho}_S(0)) && \text{(2.62a)}\\ &= \mathrm{tr}_{\mathcal{A}}\,[\hat{U}_t\,\hat{\rho}_S(0) \otimes \hat{\rho}_{\mathcal{A}}\,\hat{U}_t^\dagger] && \text{(2.62b)}\\ &= \hat{V}_t\,\hat{\rho}_S(0). && \text{(2.62c)}\end{aligned}$$

Thus, every evolution of an open system is essentially described by adding a large system to render the system closed, evolving the system according to the unitary transformation, and finally trace-out the added system.

We need to make further assumptions about the system-environment interaction to find a closed-form solution for $\hat{V}_t$. The system will generally be tiny compared to the whole environment, and the coupling is considered weak. Therefore, the many modes are barely affected by the system and the correlation time $\delta_{t_{\mathcal{A}}}$ will be very short. The correlation time denotes how long the information remains in the environment before dissipating. Crudely speaking, the environment has "forgotten" about the system after this time. Therefore, no information about the system at earlier times will flow back into the system later, and we can ignore the state of the environment. This approximation is the *Born-Markov* approximation, rendering the system evolution itself into a Markovian process. In this limit, the evolution of the quantum channel is generated by a generator $\mathcal{L}$, and the reduced state evolves with

$$\frac{d}{dt}\hat{\rho}_S = \mathcal{L}\hat{\rho} \equiv -i[\hat{H}, \hat{\rho}] + \sum_{k=1}^{N} \mathcal{D}[\hat{L}_k]\hat{\rho}. \tag{2.63}$$

This is the *Gorini-Kossakowski-Lindblad-Surdashan equation* or just *Lindblad equation* [83, 41]. It is composed of the usual unitary evolution governed by the Hamiltonian $\hat{H}$ and a dissipative part described by the super-operator

$$\mathcal{D}[\hat{L}_k]\hat{\rho} = \hat{L}_k\hat{\rho}\hat{L}_k^\dagger - \frac{1}{2}\left(\hat{\rho}\hat{L}_k\hat{L}_k^\dagger + \hat{L}_k\hat{L}_k^\dagger\hat{\rho}\right), \tag{2.64}$$

which describes the coupling of the reservoir to the system. In most cases, the operators $\hat{L}_k$[12] will be proportional to modes of the surrounding thermal bath or cavity field.

12 These operators are often called *Lindblad* or *jump* operators

2.2.5 *Generalized Measurements*

Like closed systems, the theory of projective measurements is an ideal case and is inadequate to describe the quantum measurement process. First, a realistic measurement apparatus will introduce classical noise to the measurement, adding additional uncertainty to the process. Measurements of this type are called *inefficient measurements* and need to be included in the measurement theory. Second, a measurement will generally not always "project" the system's state in an eigenstate of the measured observable. Third, a direct measurement does not always exist, and more frequently, it is the case that we perform an *indirect measurement*. In such a measurement, we couple the system to an external bath and then monitor the system by proxy through the environment.

Let us illustrate this in an example. Consider a mechanical oscillator $\mathcal{S}$ and a coherent laser field $\mathcal{A}$, acting as the ancilla. The total membrane-laser system is then described by the product Hilbert space $\mathcal{H}_\mathcal{S} \otimes \mathcal{H}_\mathcal{A}$. Assume we have perfect knowledge about our initial ancilla state, so it is initially prepared in a pure state $\hat{\rho}_\mathcal{A}(t_0) = |\alpha\rangle\langle\alpha|$. The system and ancilla are uncorrelated because no interaction has occurred up to this point. So, the initial state can be written as a product space $\hat{\rho}_{\text{total}}(t_0) = \hat{\rho}_\mathcal{S}(t_0) \otimes \hat{\rho}_\mathcal{A}(t_0)$. After some evolution time $t = t_1 - t_0$ by the unitary operator $\hat{U} = \exp(-\hat{H}_{\text{total}} t)$, the state will be in an *entangled* state. Such a state is non-separable, i.e., it can not be described as a product state. We write $\hat{\rho}_{\text{total}}(t_1) = \hat{U}\hat{\rho}_{\text{total}}(t_0)\hat{U}^\dagger$.

Now we measure some local observable of the ancilla $\hat{A} = \sum_y y(\mathbb{1}_\mathcal{S} \otimes \hat{P}_y)$, with some measurement output y. By the measurement postulate (2.54), we arrive at the post-measurement state

$$\begin{aligned}
\hat{\rho}_{\text{total}} \overset{y}{\mapsto} \hat{\rho}_{\text{total}|y} &\propto (\mathbb{1}_\mathcal{S} \otimes \hat{P}_y)\hat{\rho}_{\text{total}}(t_1)(\mathbb{1}_\mathcal{S} \otimes \hat{P}_y) && (2.65)\\
&= |y\rangle\langle y| \left(\hat{U}\hat{\rho}_{\text{total}}(t_0)\hat{U}^\dagger\right) |y\rangle\langle y| && (2.66)\\
&= \left(\langle y|\hat{U}|\alpha\rangle \hat{\rho}_\mathcal{S}(t_0) \langle\alpha|\hat{U}^\dagger|y\rangle\right) \otimes |y\rangle\langle y| && (2.67)\\
&= \left(\hat{M}_y \hat{\rho}_\mathcal{S}(t_0) \hat{M}_y^\dagger\right) \otimes |y\rangle\langle y|, && (2.68)
\end{aligned}$$

with measurement operators $\hat{M}_y = \langle y|\hat{U}|\alpha\rangle$. The normalization is given the probability

$$\begin{aligned}
p(y|\hat{\rho}_{\text{total}}(t_1)) &= \text{tr}\left[(\mathbb{1}_\mathcal{S} \otimes \hat{P}_y)\hat{\rho}_{\text{total}}(t_1)\right] && (2.69)\\
&= \text{tr}\left[\hat{M}_y \hat{\rho}_\mathcal{S}(t_0) \hat{M}_y^\dagger\right] && (2.70)\\
&= \text{tr}\left[\hat{M}_y^\dagger \hat{M}_y \hat{\rho}_\mathcal{S}(t_0)\right], && (2.71)
\end{aligned}$$

and needs to fulfill

$$\sum_y p(y|\hat{\rho}_{\text{total}}(t_1)) = \text{tr}\left[\sum_y \hat{M}_y^\dagger \hat{M}_y \hat{\rho}_\mathcal{S}(t_0)\right] \overset{!}{=} 1, \tag{2.72}$$

for all $\hat{\rho}_\mathcal{S}(t_0)$, which implies $\sum_y \hat{M}_y^\dagger \hat{M}_y \equiv \mathbb{1}$. Hence, by measuring the ancilla, we induce an effective measurement on the system, which is determined by

$\hat{U}$ and the initial ancilla state $|\alpha\rangle$. By Equation (2.68), we see that the system and ancilla are uncorrelated after the measurement. Hence we can trace out the ancilla and are left with the post-measurement system state

$$\hat{\rho}_{S|y} = \frac{\hat{M}_y \hat{\rho}_S(t_0) \hat{M}_y^\dagger}{p(y|\hat{\rho}_S(t_0))}. \tag{2.73}$$

Thus, we can reformulate the measurement postulate in terms of the measurement operators

$$\hat{\rho} \overset{y}{\mapsto} \hat{\rho}_y = \frac{\hat{M}_y \hat{\rho} \hat{M}_y^\dagger}{p(y|\hat{\rho})}, \tag{2.74a}$$

$$p(y|\hat{\rho}) = \mathrm{tr}\,(\hat{M}_y^\dagger \hat{M}_y \hat{\rho}). \tag{2.74b}$$

From the equation of the conditional probability, we find a Hermitian operator $\hat{E}_y = \hat{M}_y^\dagger \hat{M}_y$, which fulfills $\sum_y \hat{E}_y = \mathbb{1}$. By comparison to (2.18), we see that this is the quantum analog of the classical effect operator. In a broader sense, any collection of operators $\{\hat{E}_y, y \in Y\} \subset \mathcal{B}(\mathcal{H})$, with the conditions

$$\hat{E}_y = \hat{M}_y^\dagger \hat{M}_y, \tag{2.75}$$

$$\sum\nolimits_y \hat{E}_y = \mathbb{1}. \tag{2.76}$$

is a *positive operator-valued measure* (POVM) [48, 95].

To arrive at the most general quantum measurement theory, we must still incorporate inefficient measurements. These can be easily incorporated in the measurement postulate (2.74). An inefficient measurement is one in which the observer only detects a fraction of the whole measurement signal. In that case, a measurement result y can lead to many different system post-measurement states, and the composed system's post-measurement state will be in a mixture of these different outcomes. We can incorporate this into the measurement postulate by summing over the different measurement operators associated with y. Thus, the measurement postulate can be written as

$$\hat{\rho} \overset{y}{\mapsto} \hat{\rho}_y = \frac{\sum_n^N \hat{M}_{n|y} \hat{\rho} \hat{M}_{n|y}^\dagger}{p(y|\hat{\rho})}, \tag{2.77a}$$

$$p(y|\hat{\rho}) = \mathrm{tr}\left(\sum\nolimits_n \hat{M}_{n|y}^\dagger \hat{M}_{n|y} \hat{\rho}\right). \tag{2.77b}$$

2.2.6 *Beyond the Lindblad Equation*

So far, we have not discussed the dimension of the system's Hilbert space $\mathcal{H}$. In order to fully grasp the theory of quantum mechanics, the case of infinite dimensional Hilbert spaces is inevitable. This case is, however, riddled with mathematical intricacies. For example, in this case, there exist *unbounded* operators that are only defined on a domain, dom $\subset \mathcal{H}$. In general, many of the results presented in this section will not be valid for unbounded operators. For example, the Lindblad form (2.63) of the time evolution of a quantum Markov

system is only valid for bounded operators. In the unbounded case, there exist cases that do not fulfill this equation [108, 73, 2, 105, 53]. It is, however, unclear if there exists a physical realization of such non-Lindblad evolutions. For this thesis, we are only concerned with physical realizations, which are well approximated by the Lindblad equation. This is maybe not surprising, as any experiment will be energetically limited and thus can be approximated by a finite number of states. We will, therefore, only consider the finite-dimensional case and spare us the mathematical difficulties.

2.3 CAVITY OPTOMECHANICS

The experimental setups considered in this thesis lie in the field of cavity optomechanics, a branch of physics that studies the interaction between optical and mechanical systems. Many phenomena therein can not be described classically, and thus a quantum description is needed. We will start with the quantum description of light and then describe the interaction of light and matter on the quantum level. As described in the previous section, back-action interactions are unavoidable in quantum mechanics, leading to restrictions in the sensing capabilities. We will comment on these in the last part of this section.

2.3.1 *Quantum Optics*

The common starting point for the quantization of electromagnetic fields is the expansion into orthogonal eigenmodes. In a finite volume, such an expansion is always possible, and the classical Hamiltonian can be found as the volume integral over their energy density [40]

$$H \propto \int \left(\epsilon_0 \mathbf{E}^2 + \frac{1}{\mu_0} \mathbf{B}^2 \right) dV, \tag{2.78}$$

where $\mathbf{E}$ and $\mathbf{B}$ are the electric and magnetic field. For the orthogonal modes, one can rewrite this Hamiltonian in terms of independent harmonic oscillators as

$$H \propto \left(p^2 + \omega^2 x^2 \right), \tag{2.79}$$

with the correspond canonical coordinates x and p, and the angular frequency ω. The quantization procedure then turns these coordinates into operators and the classical Poisson bracket $\{.,.\}$ into the commutator $[.,.]$, and quantization is achieved by knowing how to quantize the harmonic oscillator.

A similar approach [132] identifies the field amplitudes of the electromagnetic field directly with non-Hermitian operators, i.e., $a_k \to \hat{a}_k$ and $a_k^* \to \hat{a}_k^\dagger$, and introduces the canonical commutation relations:

$$[\hat{a}_k, \hat{a}_{k'}^\dagger] = \delta_{kk'}. \tag{2.80}$$

These operators describe the energy excitations of this field and can thus be seen as the associated quantum particle, the *photon*. Applied to a field state,

the operators $\hat{a}_k$ will remove or annihilate a photon in mode k of the field. Conversely, the operators $\hat{a}_k^\dagger$ create a photon in mode k. Accordingly, these operators are called the *creation* and *annihilation* operators of the bosonic field.

Under the use of these operators, the Hamiltonian is written as

$$\hat{H} = \sum_k \hbar\omega_k \left(\hat{a}_k^\dagger \hat{a}_k + \frac{1}{2}\right), \tag{2.81}$$

with ω_k the eigenfrequency of the mode. The combined operator $\hat{a}_k^\dagger \hat{a}_k = \hat{n}_k$ is a Hermitian operator, the so-called *number* operator, describing the number of quanta in the mode ω_k. Thus, Equation (2.81) relates the field energy to the number of photons in all modes and the constant term associated with the energy of the *vacuum*.

Consider a single mode $\hat{a}$, we can form the corresponding (dimensionless) quadrature operators $\hat{x}$ and $\hat{p}$ via

$$\hat{x} = \frac{\hat{a} + \hat{a}^\dagger}{k}, \quad \hat{p} = i\,\frac{\hat{a}^\dagger - \hat{a}}{k}, \tag{2.82}$$

which satisfy the commutation relation

$$[\hat{x}, \hat{p}] = \frac{2i}{k^2}. \tag{2.83}$$

From this commutation relation follows the Heisenberg uncertainty principle

$$\Delta\hat{x}\,\Delta\hat{p} \geqslant \frac{1}{k^4}, \tag{2.84}$$

where Δ denotes the variance. We included the constant k to cover the common choices used in the literature. They comprise three choices, $k = \{1, \sqrt{2}, 2\}$[13]. The choice of k fixes many other parameters, for example, the vacuum uncertainty of the quadrature $\Delta\hat{x} = 1/k^2$. Throughout this thesis, we will choose $k = \sqrt{2}$.

In general, the systems in quantum optics are not made of only one or a few optical modes. Instead, there is a large environment of many modes coupling to the system, as described in Section 2.2.4. Assume the environment is in thermal equilibrium, then the Lindblad equation (2.63) for this case is [37]

$$\dot{\hat{\rho}} = -\frac{i}{\hbar}[\hat{H}, \hat{\rho}] + \kappa\,(\bar{n}(\omega_c) + 1)\,\mathcal{D}[\hat{o}]\hat{\rho} + \kappa\,\bar{n}(\omega_c)\mathcal{D}[\hat{o}^\dagger]\hat{\rho}, \tag{2.85}$$

where $\bar{n}(\omega_c) = \left(e^{\hbar\omega_c/k_B T} - 1\right)^{-1}$ is the average number of photons in the environment at frequency ω_c, $\hat{H}$ is the system's Hamiltonian, and κ is the coupling rate to the environment. For an optical cavity, $\bar{n}(\omega_c) \approx 0$, κ is the cavity linewidth or rate of energy decay through a transmissive mirror, and the system operator coupled to the environment is the cavity mode, i.e., $\hat{o} \equiv \hat{a}$. The Lindblad equation (2.85) reduces under these assumptions to

$$\dot{\hat{\rho}} = -\frac{i}{\hbar}[\hat{H}, \hat{\rho}] + \kappa\mathcal{D}[\hat{a}]\hat{\rho}, \tag{2.86}$$

13 $k = 1$ is used in, e.g. [132, 38]; $k = \sqrt{2}$ is used in [10] and our own work [106]; $k = 2$ can be found in [40].

with the Hamiltonian $\hat{H} = \hbar\omega_c(\hat{a}^\dagger\hat{a} + \frac{1}{2})$.

The state of the environment, in general, can be engineered to differ from a thermal state. A typically considered case is when one of the environmental modes is in a coherent state, as by driving the cavity with a laser. In this case, Equation (2.86) can still be used to describe the driven system.

In many cases, we are interested in the evolution of the field modes. Therefore, we deal with time-dependent operators, i.e., we switch to the Heisenberg or an interaction picture. For open systems, there exists an alternative, but equivalent, formulation to the Lindblad equation. It is the quantum analog to the classical Langevin equation (2.7), called the *quantum Langevin equation* [38]. For a driven cavity mode, $\hat{a}$, it reads

$$\dot{\hat{a}}(t) = -\left(i\Delta + \frac{\kappa}{2}\right)\hat{a}(t) + \sqrt{\kappa}\hat{a}_{in}(t). \tag{2.87}$$

Here, we have moved to a rotating frame at the laser frequency ω_L and set the detuning parameter $\Delta = \omega_c - \omega_L$. In a sense, the quantum Langevin equation is more general than the Lindblad equation [143, 107], because of the additional input field which was traced out to arrive at the Lindblad equation.

The input field, $\hat{a}_{in}(t)$, is a superposition of modes from the environment and is taken as a noise term. This superposition couples into the cavity at a time earlier than t and obeys the commutation relation

$$[\hat{a}_{in}(t), \hat{a}^\dagger_{in}(t')] = \delta(t - t'). \tag{2.88}$$

For times later than t, information about the cavity mode $\hat{a}$ is carried into the environment, forming output fields $\hat{a}_{out}$, which satisfy the same commutation relation as in Equation (2.88). The input and output are related to the cavity field by the *input-output relation*

$$\hat{a}_{in}(t) + \hat{a}_{out}(t) = \sqrt{\kappa}\hat{a}(t). \tag{2.89}$$

The output field is of utmost importance because it is the only accessible field that carries information about the internal cavity mode. The quantity of interest is often the two-time correlation of the intracavity field $\hat{a}$. As we argued to arrive at the quantum Markov approximation, the input field can be seen as a white noise process [38]. Thus,

$$\left\langle \hat{a}_{in}(t), \hat{a}^\dagger_{in}(t') \right\rangle = \langle \hat{a}_{in}(t)\hat{a}^\dagger_{in}(t')\rangle - \langle \hat{a}_{in}(t)\rangle\langle \hat{a}^\dagger_{in}(t')\rangle \tag{2.90}$$

$$= \delta(t - t'). \tag{2.91}$$

Combining Equations (2.89) and (2.91), one can show c.f. [132], that the output field satisfies

$$\left\langle \hat{a}_{out}(t), \hat{a}^\dagger_{out}(t') \right\rangle = \kappa \left\langle \hat{a}(t), \hat{a}^\dagger(t') \right\rangle, \tag{2.92a}$$

$$\left\langle \hat{a}_{out}(t), \hat{a}_{out}(t') \right\rangle = \kappa \mathrm{T}[\left\langle \hat{a}(t), \hat{a}(t') \right\rangle], \tag{2.92b}$$

where T is the *time-ordering* operator. Therefore, we can infer the correlations of the intracavity modes from the measurable output fields.

In this thesis, many estimations will be given in terms of spectral densities, a quantity often measured in experiments. The spectral density is the Fourier transform of the correlation function in the time domain. Thus, we introduce Fourier-transformed operators

$$\hat{a}(\omega) = \frac{1}{\sqrt{2\pi}} \int dt\, \hat{a}(t) e^{i\omega t}, \tag{2.93}$$

$$\hat{a}^\dagger(\omega) = \frac{1}{\sqrt{2\pi}} \int dt\, \hat{a}^\dagger(t) e^{i\omega t} \tag{2.94}$$

$$= (\hat{a}(-\omega))^\dagger . \tag{2.95}$$

Special care should be taken regarding the signs in front of the frequency[14]. The Fourier-transformed operators fulfill the commutation relation

$$[\hat{a}(\omega), \hat{a}^\dagger(\omega')] = \sqrt{2\pi}\, \delta(\omega - \omega'), \tag{2.96}$$

where the factor $\sqrt{2\pi}$ comes from the definition of the commutator (2.88) and the chosen convention for the pre-factor in the Fourier transform.

Assume we want to infer the noise spectral density of $\hat{x}$. By the *Wiener-Kinchin theorem*, the noise spectral density is given by the Fourier transform of the auto-correlation function of the signal, i.e.,

$$S_{xx}(\omega) = \langle \hat{x}(\omega) \hat{x}(\omega)^\dagger \rangle \tag{2.97}$$

$$= \frac{1}{\sqrt{2\pi}} \int d\tau\, \langle \hat{x}(t) \hat{x}(t+\tau) \rangle e^{-i\omega\tau} \tag{2.98}$$

$$= \frac{1}{\sqrt{2\pi}} \int d\tau\, C(\tau) e^{-i\omega\tau}, \tag{2.99}$$

$$\tag{2.100}$$

where C is the auto-correlation function and S_{xx} the noise spectral density. Since the operators, $\hat{x}(t)$ and $\hat{x}(t')$, do not commute and neither do their Fourier-transformed counterparts, the order of operators will influence the spectral density. There exist three ordering conventions. *Normal ordering* shuffles all annihilation operators to the right of the creation operators, *anti-normal ordering* does the converse. The third option is the *symmetrized* order, which reads

$$\bar{S}_{xx}(\omega) = \frac{1}{2}(S_{xx}(-\omega) + S_{xx}(\omega)) \tag{2.101}$$

$$= \int d\tau\, \frac{1}{2} \langle \hat{x}(0)\hat{x}(\tau) + \hat{x}(\tau)\hat{x}(0) \rangle\, e^{-i\omega\tau}. \tag{2.102}$$

Each of these conventions has its benefits; they lead to different variances for the vacuum state and will lead to different quasi-probability distributions, as we will see in Chapter 2. We choose the symmetrized version throughout this thesis, as it is most prominent in the experimental literature.

14 From personal experience, we emphasize giving special attention to the sign in front of the frequency.

2.3.2 *Optomechanical Interaction*

To complete the optomechanical setup, we have to couple a mechanical oscillator to an optical field. We start with a refresher on the quantization of the mechanical oscillator. Afterward, we explore its interaction with light.

A damped harmonic oscillator is characterized by its resonance frequency ω_m and linewidth γ_m. The ratio of these quantities, $Q_m = \frac{\omega_m}{\gamma_m}$, describes the rate at which energy will dissipate to the environment. A low value renders the oscillator very "stiff", as the kinetic energy of the movement is lost quickly to the environment. For a high value, the oscillator is "soft" because it will oscillate for many periods before the energy is fully dissipated. This quantity is called the mechanical *quality* factor Q_m. An oscillator is harmonic if the displacing force acting on it fulfills $F = m\ddot{X} = -kX$. Together with damping γ_m proportional to the velocity $v = \dot{X}$ and an additional external force F, we arrive at the equations of motion of a classical harmonic

$$\ddot{X} + \gamma_m \dot{X} + \omega_m^2 X = \frac{F(t)}{m}. \tag{2.103}$$

Without damping and external force ($\gamma_m = 0, F = 0$), we arrive at the classical Hamiltonian

$$H = \frac{m\omega_m^2 X^2}{2} + \frac{P^2}{2m}, \tag{2.104}$$

as the sum of the kinetic and potential energy. We see a close resemblance of Hamiltonian (2.104) to the classical Hamiltonian of the electromagnetic field (2.79). From Hamiltonian (2.104), the equations of motion are found via the Euler-Lagrange equations and are solved with boundary conditions $X(0) = X_0$ and $P(0) = P_0$:

$$X(t) = X_0 \cos \omega_m t + \frac{P_0}{m\omega_m} \sin \omega_m t. \tag{2.105}$$

As mentioned at the beginning of this section, to quantize, one can replace the classical parameters with operators and the Poisson brackets with the commutator. Following this procedure and requiring $[\hat{X}, \hat{P}] = i\hbar$, we arrive at

$$\hat{H} = \frac{m\omega_m^2 \hat{X}^2}{2} + \frac{\hat{P}^2}{2m}, \tag{2.106a}$$

$$\hat{X}(t) = \hat{X}_0 \cos \omega_m t + \frac{\hat{P}_0}{m\omega_m} \sin \omega_m t. \tag{2.106b}$$

The non-commutativity of momentum and position implies that both can not be known simultaneously with arbitrary good precision. Consequently, as

$$[\hat{X}(t), \hat{X}(0)] = \frac{\sin \omega_m t}{m\omega_m} [\hat{P}_0, \hat{X}_0] \neq 0, \tag{2.107}$$

there is a limit to the measurement accuracy when estimating the evolution of the mirror position.

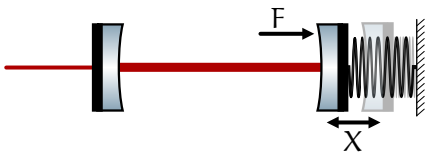

Figure 2.4: Simple optomechanical setup. An external force F causes the displacement X of a movable end mirror of an optical cavity.

For convenience, we rescale the position and momentum operators to dimensionless quantities: $\hat{x}_m = \hat{X}/x_{ZPF}$, $\hat{p}_m = x_{ZPF}\hat{P}/\hbar$ with the mechanical *zero-point fluctuation* x_{ZPF},

$$x_{ZPF} = \sqrt{\hbar/m\omega_m}. \tag{2.108}$$

In terms of these "new" operators, the former equations will match our definitions for the optical quadratures. The commutation relation is $[\hat{x}_m, \hat{p}_m] = i$. From this, we can rewrite the Hamiltonian as

$$\hat{H} = \frac{1}{2}\hbar\omega_m\left(\hat{x}_m^2 + \hat{p}_m^2\right) = \hbar\omega_m\left(\hat{b}^\dagger\hat{b} + \frac{1}{2}\right), \tag{2.109}$$

where $\hat{b}$ is the bosonic annihilation operator associated with mechanical field mode. It is a quasi-particle called the *phonon*. The equations of motion are accordingly

$$\dot{\hat{x}}_m = \omega_m\hat{p}_m, \quad \dot{\hat{p}}_m = -\omega_m\hat{x}_m, \quad \hat{x}(t) = \hat{x}_0\cos\omega_m t + \hat{p}_0\sin\omega_m t. \tag{2.110}$$

Now, consider a mechanical oscillator as a movable end mirror of an optical cavity, similar to the depiction in Figure 2.4. We recall that the resonance frequency of a cavity is $\omega_c = 2\pi cn/L$. Thus, due to the movement of the mechanical oscillator, the resonance frequency will be dependent on its position X via

$$\omega_c(X) = \frac{2\pi cn}{L(X)} = \frac{2\pi cn}{L+X} = \frac{2\pi cn}{L}\frac{1}{1+\frac{X}{L}} \tag{2.111}$$

$$= \omega_c\left(1 + \frac{X}{L} + \mathcal{O}\left(\frac{X}{L}\right)^2\right) \tag{2.112}$$

$$\approx \omega_c + \frac{\omega_c}{L}X, \tag{2.113}$$

assuming a small displacement. This approximation introduces an additional term in the optomechanical Hamiltonian. Using the dimensionless position operator $\hat{x}_m$ and a coupling parameter g_0, the optomechanical Hamiltonian reads[15]

$$\hat{H} = \hbar\omega_c(1 + g_0\hat{x}_m)\hat{a}^\dagger\hat{a} + \hbar\omega_m\hat{b}^\dagger\hat{b}. \tag{2.114}$$

15 We have dropped the vacuum energy term as it is irrelevant to the equations of motion.

This leads to the radiation pressure interaction Hamiltonian [82]

$$\hat{H}_{rp} = \hbar g_0 \hat{x}_m \hat{a}^\dagger \hat{a} \tag{2.115}$$

with the *single-photon coupling strength* g_0 defined by

$$g_0 = \frac{\omega_c}{L} x_{ZPF}. \tag{2.116}$$

The radiation pressure Hamiltonian exhibits non-linear coupling between the cavity modes and the mechanical motion; we turn to a linearized regime. The complete Hamiltonian is given by

$$\hat{H} = \hbar\omega_c \hat{a}^\dagger \hat{a} + \hbar\omega_m \hat{b}^\dagger \hat{b} + \hbar g_0 \hat{x}_m \hat{a}^\dagger \hat{a} + i\hbar\alpha \left(\hat{a}^\dagger e^{-\omega_L t} - \hat{a} e^{i\omega_L t} \right). \tag{2.117}$$

We added a driving field with laser frequency ω_L and field intensity $|\alpha| = \sqrt{P_L \kappa_c / \hbar\omega_L}$ with a laser power P_L and the cavity linewidth κ_c. Moving to an interaction frame via the unitary transformation $\hat{U}(t) = e^{i\omega_L \hat{a}^\dagger \hat{a} t}$ renders the Hamiltonian time invariant

$$\hat{H} = \hbar\Delta_c \hat{a}^\dagger \hat{a} + \hbar\omega_m \hat{b}^\dagger \hat{b} + \hbar g_0 \hat{x}_m \hat{a}^\dagger \hat{a} + i\hbar\alpha \left(\hat{a}^\dagger - \hat{a} \right), \tag{2.118}$$

where $\Delta_c = \omega_c - \omega_L$ as in our example of a driven empty cavity. We can now linearize the radiation pressure Hamiltonian by splitting the cavity field $\hat{a} \to \alpha + \delta\hat{a}$ with α a static part and $\delta\hat{a}$ a fluctuation term. Plugin this into the radiation pressure term, we get

$$\hat{H}_{rp} = \hbar g_0 (\alpha + \delta\hat{a})^\dagger (\alpha + \delta\hat{a}) \hat{x}_m \tag{2.119}$$

$$= \hbar g_0 \hat{x}_m \left(|\alpha|^2 + (\alpha \delta\hat{a}^\dagger + \alpha \delta\hat{a}) + \mathcal{O}(\delta\hat{a}^2) \right). \tag{2.120}$$

Assume now the cavity field is very strong, i.e., $\alpha \gg \delta\hat{a}$ so that the contributions $\mathcal{O}(\delta\hat{a}^2)$ can be neglected. The static term $|\alpha|^2$ can be eliminated by static length stabilization, and hence the radiation pressure Hamiltonian becomes

$$\hat{H}_{rp} = \hbar\alpha g_0 \hat{x}_m \left(\hat{a}^\dagger + \hat{a} \right) \tag{2.121}$$

$$= \hbar \frac{g}{2} \left(\hat{a}^\dagger \hat{b} + \hat{a} \hat{b}^\dagger \right) + \hbar \frac{g}{2} \left(\hat{a} \hat{b} + \hat{a}^\dagger \hat{b}^\dagger \right). \tag{2.122}$$

Here, we set $\delta\hat{a} \to \hat{a}$ and introduced the *cavity-enhanced* coupling strength g as

$$g = \sqrt{2}\alpha g_0 = \sqrt{2}\alpha \frac{\omega_c}{L} x_{ZPF} = \sqrt{2}\alpha \frac{\omega_c}{L} \sqrt{\frac{1}{m\omega_m}}. \tag{2.123}$$

We recognize that the radiation pressure splits into two terms in the linearized regime. The first term annihilates a cavity photon while creating a phonon, and vice versa; it acts like a beam-splitter. The second term has a parametric effect. At the same time, a phonon and photon are created or annihilated; it acts like a squeezing operator.

2.3.3 *The Standard Quantum Limit*

The existence of the radiation pressure interaction may become problematic if one is to observe the displacement of the mechanical oscillator. We consider the setup in Figure 2.4 to quantify its effect on the measurement precision. A cavity mirror moving due to subject to an external force F and radiation pressure noise. The force consists of a signal F_{sig} we want to measure and some Brownian thermal noise f_{th}. We will refer to this setup as an *optomechanical sensor* (OMS). With the linearized Hamiltonian, we can derive the quantum Langevin equations without detuning:

$$\dot{\hat{x}}_m = \omega_m \hat{p}_m, \tag{2.124a}$$

$$\dot{\hat{p}}_m = -\omega_m \hat{x}_m - \gamma_m \hat{p}_m - g\hat{x}_c + \sqrt{\gamma_m}\, F, \tag{2.124b}$$

$$\dot{\hat{x}}_c = -\frac{\kappa_c}{2}\hat{x}_c + \sqrt{\kappa_c}\, x_c^{in}, \tag{2.124c}$$

$$\dot{\hat{p}}_c = -\frac{\kappa_c}{2}\hat{p}_c - g\hat{x}_m + \sqrt{\kappa_c}\, \hat{p}_c^{in}. \tag{2.124d}$$

In these equations we scaled the force $F \to F/\sqrt{\hbar m \gamma_m \omega_m}$, with dimension $\sqrt{\text{Hz}}$. The scaled thermal noise satisfies $\langle f_{th}(t) f_{th}(t')\rangle = n_{th}\delta(t-t')$[16] with $n_{th} = k_B T/\hbar\omega_m$ the average phonon number of the mechanical oscillator. The Langevin equations form a system of linear differential equations, which can be easily solved in the Fourier space where differentiation is just multiplication. Together with the input-output relations (2.89), the output quadratures become

$$\hat{x}_c^{out} = e^{i\phi}\hat{x}_c^{in}, \tag{2.125a}$$

$$\hat{p}_c^{out} = e^{i\phi}\hat{p}_c^{in} - \chi_m g^2 \kappa_c \chi_c^2 \hat{x}_c^{in} + \chi_m \sqrt{\kappa_{om}}\, g \chi_{om} \sqrt{\gamma_m}\, F, \tag{2.125b}$$

with

$$e^{i\phi} = \frac{\kappa_c/2 - i\omega}{\kappa_c/2 + i\omega}, \quad \chi_c = \frac{1}{i\omega + \kappa_c/2}, \quad \chi_m = \frac{\omega_m}{\omega^2 - \omega_m^2 - i\gamma_m\omega}. \tag{2.126}$$

We see the force signal F is contained in the output phase quadrature $\hat{p}_c^{out}$, but so is the term proportional to the radiation pressure $\hat{x}_c^{in}$. The force can be estimated to be

$$\hat{F} = \frac{\hat{p}_c^{out}}{\sqrt{\gamma_m}\chi_m g\sqrt{\kappa_c}\chi_c} = F_{sig} + f_{th} + \frac{e^{i\phi}}{\sqrt{\gamma_m}\chi_m g\sqrt{\kappa_c}\chi_c}\hat{p}_c^{in} - \frac{g\sqrt{\kappa_c}\chi_c}{\sqrt{\gamma_m}}\hat{x}_c^{in}. \tag{2.127}$$

Thus, the force signal is masked by the thermal noise and added phase and amplitude quadrature terms. The sensitivity of the force measurement in the phase quadrature can be quantified by the spectral density of these added terms. We get

$$S_{FF}^{out} = \frac{k_B T}{\hbar\omega_m} + \frac{\Delta\hat{p}_c^{in}}{2G\gamma_m|\chi_m|^2} + \frac{G}{2\gamma_m}\Delta\hat{x}_c^{in}, \tag{2.128}$$

16 Technically only correct in the high temperature limit.

with a frequency-dependent measurement strength $G = \kappa_c|\chi_c|^2 g^2$. The thermal noise adds a flat background to our measurement sensitivity. We will assume that either our sensor is efficiently cooled, i.e., $k_B T \to 0$, or the back-action is large enough to be visible in the measurements. The measurement strength G is directly proportional to the input power because of the definition of $g \propto \alpha$. Increasing the measurement strength will increase the third term $\propto \Delta\hat{x}_c^{in}$; this is the radiation pressure or back-action part. Reducing the measurement strength increases the second term $\propto \Delta\hat{p}_c^{in}$; this is the shot noise or measurement imprecision part. Due to the inversely proportional terms, there exists an optimal value for G that minimizes this trade-off[17]. The optimal measurement strength

$$G_{SQL}(\omega) = \frac{1}{|\chi_m(\omega)|} \tag{2.129}$$

reduces the noise spectral density to an achievable level of

$$S_{FF}^{SQL}(\omega) = \frac{1}{\gamma_m|\chi_m(\omega)|}. \tag{2.130}$$

This lower bound is called the *standard quantum limit* (SQL) of force sensing [24, 10, 29]. A similar calculation can be made for a position measurement by setting $x_m^0 = \chi_m\sqrt{\gamma_m}F$ and arrives at a lower bound $S_{x_m x_m}^{SQL}(\omega) = |\chi_m(\omega)|$. Both position and force spectral densities and SQLs are plotted in Figure 2.5

Albeit posing a lower bound, the SQL is not a fundamental limit. Since its discovery, many ideas have been proposed to overcome this bound. We will discuss some of these ideas under the umbrella term *back-action evading* techniques in more detail in Chapter 4.

17 Due to the frequency dependence of G, the optimal power has to be found for every frequency.

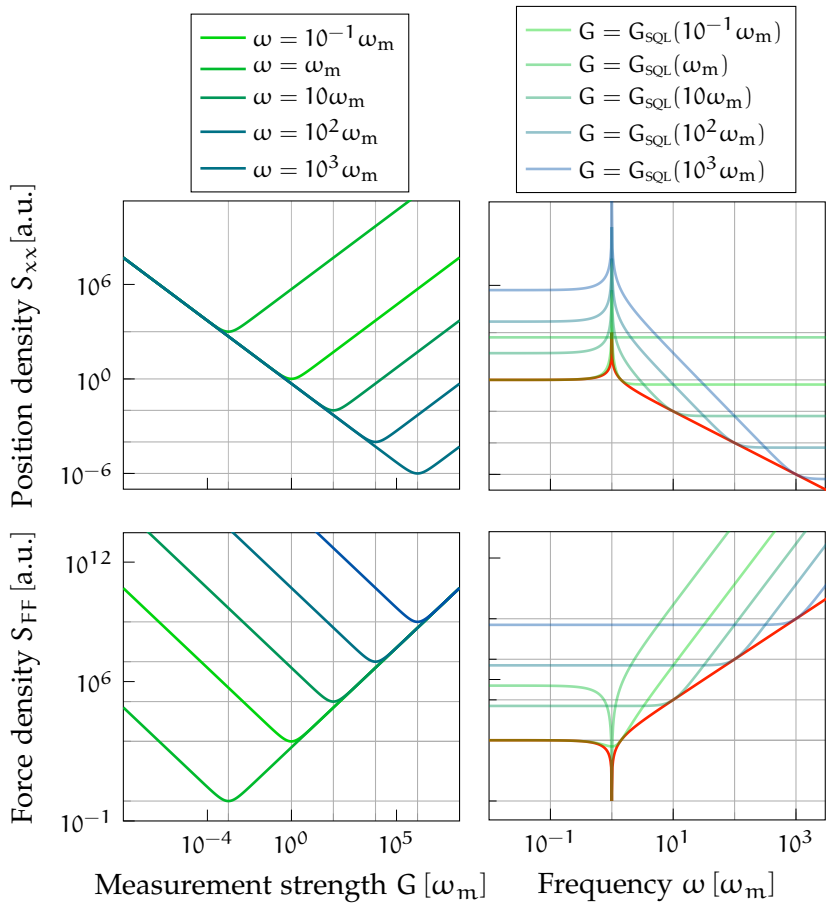

Figure 2.5: Spectral densities for measurements of an optomechanical sensor. Due to the normalization, given in arbitrary units. Top row: Sensitivity for position measurement. Bottom row: Sensitivity for force measurement. Left column: Noise spectral density for a fixed frequency over the measurement strength G. Chosen frequencies are $\omega_n = \{10^{-1}\omega_m, \omega_m, 10\omega_m, 10^2\omega_m, 10^3\omega_m\}$. The lowest achieved noise levels are at G_{SQL} for both position and force measurement. This lower bound is the standard quantum limit, S_{FF}^{SQL} and S_{xx}^{SQL} respectively. Right column: Noise spectral density over the frequency with measurement strength fixed to $G_{SQL}(\omega_n)$. Choosing the optimal measurement strength for all frequencies results in the red curve, which is the SQL. Plotted for a mechanical resonator with quality factor $Q_m = 1000$

3

CONTINUOUS MEASUREMENT AND QUANTUM SMOOTHING

This chapter discusses how quantum states can be estimated from continuous measurements. In Section 3.1, we introduce the Stochastic Master Equation of a monitored quantum system and the corresponding adjoint equation for the effect operator. Our discussion will be of similar rigor as Chapter 2, focusing on building intuition rather than mathematical precision. In Section 3.2, we apply the Stochastic Master Equation to the important class of linear Gaussian quantum systems. Due to their analogy to classical systems, the estimation problem will essentially reduce to a classical filter problem. We introduce two filter types as a solution; the Kalman and Wiener filter. In Section 3.3, we revise the field of Quantum Smoothing. We will introduce a simple optomechanical setup and discuss the performance of the Kalman and Wiener filter in terms of smoothing estimates in the quantum case.

3.1 STOCHASTIC MASTER EQUATIONS

In this section, we want to introduce the concepts of prediction and retrodiction to quantum systems. As seen in Chapter 2, any measurement in quantum mechanics will inadvertently affect the measured system and is inherently random. This randomness will be passed on to the system's dynamics by conditioning the evolution. Therefore, an in-depth discussion requires quantum stochastic calculus as in [143]. Pioneered by Belavkin [5] and Hudson and Parthasarathy [55], it is a generalization of classical stochastic calculus.

Our introduction will be rudimentary. We refer to [143, 59, 60, 30] for more details on the derivation of the *stochastic master equation* (SME). We find a combination of the texts above and the work of Lammers [76] especially helpful.

3.1.1 *Conditional States*

We start in the Schrödinger picture. The generic setup we consider here is a system $\mathcal{S}$, weakly coupled to possibly multiple ancillae $\mathcal{A}_k$. Here, we restrict ourselves to a specific class of quantum measurements called *monitoring*. These are Gaussian time-continuous measurements, with homodyne detection as an

example; see Appendix A.2. The SME for a quantum system, subjected to monitoring of the observables $\hat{o}_k$, is [76, 102]

$$\begin{aligned} d\hat{\rho}_c(t) = &-\frac{i}{\hbar}[\hat{H}, \hat{\rho}_c(t)]dt + \sum_k \mathcal{D}[\hat{o}_k]\hat{\rho}_c(t)dt \\ &+ \sum_k \sqrt{\eta_k}\mathcal{H}[\hat{o}_k]\hat{\rho}_c(t)dW_k(t), \end{aligned} \tag{3.1}$$

with the Wiener increment $dW_k(t)$, and the dissipation and measurement super-operators

$$\mathcal{D}[\hat{o}_k]\hat{\rho} = \hat{o}_k\hat{\rho}\hat{o}_k^\dagger - \frac{1}{2}\left(\hat{o}_k^\dagger\hat{o}_k\,\hat{\rho} + \hat{\rho}\,\hat{o}_k^\dagger\hat{o}_k\right), \tag{3.2}$$

$$\mathcal{H}[\hat{o}_k]\hat{\rho} = \left(\hat{o}_k - \langle\hat{o}_k\rangle_{\hat{\rho}}\right)\hat{\rho} + \hat{\rho}\left(\hat{o}_k - \langle\hat{o}_k\rangle_{\hat{\rho}}\right). \tag{3.3}$$

The measurement super-operator $\mathcal{H}$ describes the conditioning upon the measurement outcomes of the k-th measurement channel, with an efficiency η_k. Additionally, we can define the increment of the measurement outcomes Y_k,

$$dY_k(t) = \langle\hat{o}_k + \hat{o}_k^\dagger\rangle_{\hat{\rho}}\,dt + dW_k(t). \tag{3.4}$$

We see the conditional state $\hat{\rho}_c$ by the measurement outcomes through the Wiener increments dW_k.

Without detection, i.e., $\eta_k = 0$ or by averaging over all possible noise processes dW_k, we retrieve

$$d\hat{\rho} = -\frac{i}{\hbar}[\hat{H}, \hat{\rho}]dt + \sum_k \mathcal{D}[\hat{o}_k]\hat{\rho}dt, \tag{3.5}$$

with $\hat{\rho} = \mathbb{E}[\hat{\rho}_c]$ the ensemble average of the possible conditional states. Thus, without recording, the back-action of the measurement is fully described by the dissipator terms $\mathcal{D}[\hat{o}_k]$. Equation (3.5) is essentially the Lindblad equation (2.63) for an open system. Therefore, we can interpret an open system as a system monitored by the environment. As the "measurement record" of the environment is inaccessible, we retrieve the unconditional evolution.

The homodyne detection efficiency and the homodyne angle θ can also be cast directly in the measurement term by defining measurement operators $\hat{C}_k := \sqrt{\eta_k}e^{i\theta}\hat{o}_k$. Reintroducing the notion of Lindblad operators $\hat{L}_k = \hat{o}_k$, we arrive at a more general form of the SME,

$$\begin{aligned} d\hat{\rho}_c(t) = &-\frac{i}{\hbar}[\hat{H}, \hat{\rho}_c(t)]dt + \sum_j^{n_L} \mathcal{D}[\hat{L}_j]\hat{\rho}_c(t)dt \\ &+ \sum_k^{n_C} \mathcal{H}[\hat{C}_k]\hat{\rho}_c(t)dW_k(t). \end{aligned} \tag{3.6}$$

Here, n_L is the number of ancillae that couple to the system via Lindblad operators $\hat{L}_j$ and n_C is the number of measurement channels denoted by the measurement operators $\hat{C}_k$.

For a general derivation of the SME, the measurement and jump operators do not have a direct one-to-one correspondence as in our quantum optical setup. However, it still holds that [143]

$$\sum_{j}^{n_L} \hat{L}_j^\dagger \hat{L}_j - \sum_{k}^{n_C} \hat{C}_k^\dagger \hat{C}_k \geqslant 0 \tag{3.7}$$

is fulfilled. This relation holds because any information recorded by our measurement device needs to leak out of the system first.

3.1.2 *Conditional Effects*

In the classical case, we saw that the retrodiction is governed by an effect operator, which also naturally emerged in our discussion of quantum measurements. Similar to the classical case in Equation (2.39), we will construct the equations for retrodiction by an adjoint evolution. As discussed in 2.2.4, the time evolution of an open quantum system is governed by the notion of a quantum channel. Under the influence of the measurement, we can generalize this notion once more.

The time evolution of an open quantum system under monitoring is described by *conditional quantum channels* $\mathcal{E}_{t_0,T|y}$, also called quantum instruments [48, 144]. It describes the evolution of the quantum state conditioned upon the measurement outcome y. As a consequence it produces a conditional state $\hat{\rho}_y(T) = \mathcal{E}_{t_0,T|y}[\hat{\rho}(t_0)]$. Moving forward, we will consider conditional quantum operations, i.e., trace non-increasing channels as defined in Equation (2.61). The important feature of quantum instruments is that it yields

$$p(y|\hat{\rho}(T)) = \mathrm{tr}\left(\tilde{\mathcal{E}}_{t_0,T|y}[\hat{\rho}(t_0)]\right), \tag{3.8}$$

which is the conditional probability that the measurement y occurred given the initial state $\hat{\rho}(t_0)$. Thus, by the measurement postulate (2.77), we can connect the conditional channel to the measurement operators $\hat{M}_y$ as

$$\tilde{\mathcal{E}}_{t_0,T|y}[\hat{O}] = \sum_{n} \hat{M}_{n|y}^\dagger \hat{O} \hat{M}_{n|y}, \tag{3.9}$$

this result is *Kraus theorem* [95] and the decomposition above is the *Kraus decomposition* of a quantum channel. As a reminder, the measurement operators are connected to the POVM measurements, as $\hat{E}_y = \hat{M}_y^\dagger \hat{M}_y$.

Consider the case of a continuously monitored system $\mathcal{S}$. Its evolution from t_0 to T is governed by the quantum instrument $\tilde{\mathcal{E}}_{t_0,T|\mathcal{Y}}$ conditioned on the measurement record $\mathcal{Y} := \{Y(s), t_0 \leqslant s \leqslant T\}$, as

$$\tilde{\hat{\rho}}_{\mathcal{Y}}(T) = \tilde{\mathcal{E}}_{t_0,T|\mathcal{Y}}[\hat{\rho}(t_0)]. \tag{3.10}$$

The conditional state $\tilde{\hat{\rho}}_{\mathcal{Y}}$[1] is the solution to a SME with initial conditions $\hat{\rho}(t_0)$, which we obtained by integrating over the particular measurement record $\mathcal{Y}$.

1 Note, the tilde denotes that this state is un-normalized because we used the trace non-increasing channels.

Suppose now, we perform a POVM measurement $\{\hat{E}_x | x \in X\}$ on the state $\hat{\rho}_y(T)$ with an effect operator $\hat{E}_x$ and outcome set X. The conditional probability of receiving the outcome x is then

$$p(x|y, \hat{\rho}(t_0)) = \operatorname{tr}\left(\hat{E}_x \hat{\rho}_y(T)\right) = \frac{\operatorname{tr}\left(\hat{E}_x \tilde{\rho}_y(T)\right)}{p(y|\hat{\rho}(t_0))}. \tag{3.11}$$

We can rewrite the left-hand side as

$$p(x|y, \hat{\rho}(T)) = \frac{p(x, y|\hat{\rho}(t))}{p(y|\hat{\rho}(t_0))}, \tag{3.12}$$

and thus together with Equation (3.11) we find

$$p(x, y|\hat{\rho}(t_0)) = \operatorname{tr}\left(\hat{E}_x \tilde{\rho}_y(T)\right). \tag{3.13}$$

The joint probability of obtaining the result x and the measurement record y is given by a POVM measurement on the conditional state. Using this expression and the definition of the conditional channel (3.8), we can derive the adjoint channel via the associative law

$$p(x, y|\hat{\rho}(t_0)) = \operatorname{tr}\left(\hat{E}_x\, \tilde{\mathcal{E}}_{t_0,T|y}[\hat{\rho}(t_0)]\right) \tag{3.14a}$$

$$= \operatorname{tr}\left(\tilde{\mathcal{E}}^{\dagger}_{t_0,T|y}[\hat{E}_x]\, \hat{\rho}(t_0)\right). \tag{3.14b}$$

Thus, analogous to the conditional state, we can define a conditional effect operator

$$\hat{E}_{x,y}(t_0) := \tilde{\mathcal{E}}^{\dagger}_{t_0,T|y}[\hat{E}_x], \tag{3.15}$$

which acts as an effective POVM on the initial state $\hat{\rho}(t_0)$. Based on the measurement record y, it is propagated backward in time from T to t_0.

Starting from the trace non-increasing channels, the corresponding adjoint channel is sub-unital. This allows us to retrodict a trivial POVM element $\hat{E}(T) = \mathbb{1}$ and still derive a non-trivial effective POVM at time t_0 [76]. We find

$$\hat{E}_y := \tilde{\mathcal{E}}_{t_0,T|y}[\mathbb{1}] \tag{3.16}$$

which depends purely on the measurement record y. Therefore, we can understand the continuous observation of a quantum system as an effective instantaneous POVM measurement on the initial state. This interpretation of retrodiction as an instantaneous POVM measurement was examined extensively by Lammers [76] and yields a nice application for the verification of previously prepared quantum states. We will comment on this more in Section 3.3.

The considerations above are readily extended to a similar situation as the classical smoothing problem. Assume we monitored a system from t_0 to T and produced a measurement record $y := \{Y(s), t_0 \leqslant s \leqslant T\}$ in the process. This record can then be split around a time τ at which we want to verify the state

$\hat{\rho}_\tau$. We refer to the measurement record before τ as $\overrightarrow{y}$ and the record after τ as $\overleftarrow{y}$[2]. From Equation (3.14) we can write

$$\operatorname{tr}\left(\hat{E}(T)\tilde{\rho}_y(T)\right) = \operatorname{tr}\left(\hat{E}_y(t_0)\hat{\rho}(t_0)\right) \tag{3.17}$$

$$= \operatorname{tr}\left(\hat{E}_{\overleftarrow{y}}(\tau)\tilde{\rho}_{\overrightarrow{y}}(\tau)\right). \tag{3.18}$$

The first line does not depend on the estimation time τ. Similarly to Equation (2.36), we can derive the master equation for the conditional effect operator $\hat{E}$ as the adjoint of the master equation for the unnormalized conditional state $\tilde{\rho}$. For a derivation, we refer to [76]. The solutions are

$$\begin{aligned} d\tilde{\rho}_c(t) = &-\frac{i}{\hbar}[\hat{H}, \tilde{\rho}_c(t)]dt + \sum_j^{n_L} \mathcal{D}[\hat{L}_j]\,\tilde{\rho}_c(t)dt \\ &+ \sum_k^{n_C} \left(\hat{C}_k\tilde{\rho}_c(t) + \tilde{\rho}_c(t)\hat{C}_k^\dagger\right) dY_k(t), \end{aligned} \tag{3.19}$$

for the state and

$$\begin{aligned} -d\hat{E}(t) = &\frac{i}{\hbar}[\hat{H}, \hat{E}(t)]dt + \sum_j^{n_L} \mathcal{D}^\dagger[\hat{L}_j]\,\hat{E}(t)dt \\ &+ \sum_k^{n_C} \left(\hat{C}_k^\dagger\hat{E}(t) + \hat{E}(t)\hat{C}_k\right) dY_k(t) \end{aligned} \tag{3.20}$$

for the effect operator. We note that Equation (3.20) is not simply the adjoint equation to Equation (3.19), but also a stochastic *backward Itô equation*[3].

3.2 LINEAR GAUSSIAN QUANTUM SYSTEMS

We now introduce a particular class of quantum systems, the linear Gaussian quantum systems. Those systems are particularly interesting to us because the building blocks of quantum optomechanics, namely harmonic oscillators, are linear systems. Additionally, we saw in Section 2.3.2 that the mechanical and optical oscillator coupling via radiation pressure is readily linearized. This linearized regime is adequate for all experimental considerations in this thesis. Gaussian states are ubiquitous in linear systems as they remain Gaussian under linear evolution. In fact, it was shown in [76] that stable linear dynamics will "Gaussify" any initial state given enough time. The structure of linear Gaussian systems is closely related to those classical systems considered in Section 2.1, with some fundamental differences due to quantum mechanical constraints. Thus, many observations in this section can be seen as direct quantum mechanical extensions of the classical results presented in Chapter 2.

2 We use the same arrow notation as in Section 2.1.4.

3 See Appendix A.1 for details.

3.2.1 *Phase Space Representation*

When working with Gaussian states, it is advantageous to use the quadrature operators introduced in Equations (2.82). The underlying operator space is the phase space, in analogy to the space of canonical operators in Hamiltonian mechanics. We will first recall some aspects and related concepts of the *quantum phase space*. Moving to a system of n modes, with $2n$ associated canonical quadrature operators $\hat{\mathbf{x}} = (\hat{x}_j)_{j=1,\dots,2n}$. From the canonical commutation relation (2.83) for the $\hat{x}_j$

$$[\hat{x}_j, \hat{x}_k] := i\sigma_{jk}, \tag{3.21}$$

we find a skew-symmetric symplectic matrix $\sigma \in \mathbb{R}^{2n\times 2n}$. In our case, we choose

$$\hat{\mathbf{x}} = (\hat{x}_1, \hat{p}_1, \dots, \hat{x}_n, \hat{p}_n)^\top, \tag{3.22}$$

which implies

$$\sigma = \bigoplus_{k=1}^{n} \begin{pmatrix} 0 & 1 \\ -1 & 0 \end{pmatrix}. \tag{3.23}$$

The commutation relation (3.21) implies that the underlying Hilbert space $\mathcal{H}$ is infinite-dimensional and the operators $\hat{x}_j$ are unbounded. This statement is formal; as mentioned in Section 2.2.6, we will not deal with unbounded operators and infinite dimensions. However, a natural way to overcome this problem is by introducing a family of bounded operators. These are the *displacement operators*[4]

$$\hat{D}(\boldsymbol{\alpha}) \equiv \hat{D}_{\boldsymbol{\alpha}} = e^{i\boldsymbol{\alpha}^\top\cdot\sigma\cdot\hat{\mathbf{x}}}, \quad \text{for } \boldsymbol{\alpha} \in \mathbb{R}^{2n}; \quad \text{and } \hat{D}_0 = \mathbb{1}. \tag{3.24}$$

Hence, for our choice of σ and $\boldsymbol{\alpha} = (x_1, p_1, \dots, x_n, p_n)^\top$ the displacement operators are written explicitly as

$$\hat{D}_{\boldsymbol{\alpha}} = \exp\left(i\sum_{k}^{n}(x_k\hat{p}_k - p_k\hat{x}_k)\right). \tag{3.25}$$

By the commutation relation (3.21) the displacement operators satisfy the relations[5]

$$\hat{D}_{\boldsymbol{\alpha}}\hat{D}_{\boldsymbol{\beta}} = e^{-\frac{i}{2}\boldsymbol{\alpha}^\top\cdot\sigma\cdot\boldsymbol{\beta}}\,\hat{D}_{\boldsymbol{\alpha}+\boldsymbol{\beta}} \quad \text{and} \tag{3.26a}$$

$$\hat{D}_{\boldsymbol{\alpha}}\hat{D}_{\boldsymbol{\beta}} = e^{-i\boldsymbol{\alpha}^\top\cdot\sigma\cdot\boldsymbol{\beta}}\,\hat{D}_{\boldsymbol{\beta}}\hat{D}_{\boldsymbol{\alpha}} \tag{3.26b}$$

We note that the family of displacement operators is unitary and the inverse is

$$\hat{D}_{\boldsymbol{\alpha}}^\dagger = \hat{D}_{-\boldsymbol{\alpha}}. \tag{3.27}$$

4 In the more mathematically inclined literature displacement operators are called *Weyl operators* The collection of these are in turn called a *Weyl system* [107].

5 Also known as the *Weyl relations*.

This is in line with the notion of a displacement operator. If the operator $\hat{D}_\alpha$ "displaces" an operator in phase space by a value of $|\alpha|$, its inverse should undo this displacement.

The displacement operators implement a generalized form of the Fourier transform and thus establish an equivalence between operators on a Hilbert space to complex functions on phase space. This equivalence makes the phase space representation especially appealing. A density operator $\hat{\rho}$ is connected to a complex-valued function $\chi_{\hat{\rho}}(\alpha)$ on phase space via the *Fourier-Weyl transform* as

$$\hat{\rho} = \frac{1}{(2\pi)^n} \int d^{2n}\alpha \, \chi_{\hat{\rho}}(\alpha) \hat{D}_{-\alpha}, \tag{3.28a}$$

$$\chi_{\hat{\rho}}(\alpha) = \operatorname{tr}\left(\hat{D}_\alpha \hat{\rho}\right). \tag{3.28b}$$

In this sense, the pair $\hat{\rho}$ and $\chi_{\hat{\rho}}$ constitute a quantum Fourier transform by a quantum version of the Parseval relation [52].

The function $\chi_{\hat{\rho}}$ is called the *characteristic function* corresponding to the density operator $\hat{\rho}$. The name "characteristic function" is due to its analogy to classical probabilistic theory. In the classical case, the characteristic function is the Fourier transform of the probability distribution p. With this in mind, we can take the classical inverse Fourier transform and arrive at the quantum analog of the classical probability distribution. The result of this is the *Wigner function* [139] $\mathcal{W}_{\hat{\rho}}$ of $\hat{\rho}$,

$$\mathcal{W}_{\hat{\rho}}(\alpha) = \frac{1}{(2\pi)^{2n}} \int d^{2n}\beta \, e^{i\alpha^\top \cdot \sigma \beta} \, \chi_{\hat{\rho}}(\beta). \tag{3.29}$$

An equivalent and helpful definition of the Wigner function is given in terms of the Hermitian *parity operator* $\hat{\mathcal{P}}$. For n modes, it is the n-fold tensor product of a single-mode parity operator operator[6], and thus $\hat{\mathcal{P}}\,\hat{x}_k\,\hat{\mathcal{P}} = -\hat{x}_k$. The Wigner function is given in terms of expectations values of this operator [44]:

$$\mathcal{W}_{\hat{\rho}}(\alpha) = \frac{1}{\pi} \operatorname{tr}\left(\hat{\rho}\hat{D}_\alpha \, \hat{\mathcal{P}} \hat{D}_{-\alpha}\right). \tag{3.30}$$

The Wigner function plays the role of a *quasi probability distribution*[7] on phase space. In fact, it is normalized ($\int \mathcal{W}_{\hat{\rho}}(\alpha) d^{2n}\alpha = \operatorname{tr}(\hat{\rho}) = 1$) and its marginal distribution with respect to x and p returns the usual position and momentum probability distributions. However, the Wigner function can take on negative values because the parity operator is not positive.

If we have two Wigner function $\mathcal{W}_{\hat{\rho}}(\alpha)$ and $\mathcal{W}_{\hat{o}}(\alpha)$, corresponding to the two operators $\hat{\rho}$ and $\hat{o}$ then

$$\operatorname{tr}(\hat{\rho}\,\hat{o}) = (2\pi)^n \int \mathcal{W}_{\hat{\rho}}(\alpha) \mathcal{W}_{\hat{o}}(\alpha) \, d^{2n}\alpha. \tag{3.31}$$

6 This operator flips the sign of a single degree of freedom.

7 There exist other quasi probability distributions, the P- and Q-function. They are connected to the chosen operator ordering discussed in Section 2.3.1. For the symmetrized ordering, one arrives at the Wigner function.

Thus, the trace of an operator product translates to an overlap integral of the corresponding Wigner functions in phase space.

This leaves us with two equivalent descriptions of a quantum state. First as a Wigner function by a quasi-probability distribution on phase space and second as a quantum characteristic function. Similar to the classical characteristic function, the quantum analog translates its derivative to the *moments* of the corresponding field operators. In particular, the first moments (the means) and the second moments (the covariance) are derived in terms of the field operators as

$$-\mathrm{i}\frac{\partial}{\partial\alpha_k}\chi_{\hat\rho}(\boldsymbol{\alpha})\bigg|_{\boldsymbol{\alpha}=0} = \operatorname{tr}(\hat\rho\,\hat x_k) = \langle\hat x_k\rangle_{\hat\rho}, \tag{3.32a}$$

$$-\frac{\partial^2}{\partial\alpha_k\partial\alpha_l}\chi_{\hat\rho}(\boldsymbol{\alpha})\bigg|_{\boldsymbol{\alpha}=0} = \frac{1}{2}\sigma_{kl} + \operatorname{tr}(\hat\rho\,\hat x_k\hat x_l) = \frac{1}{2}\operatorname{tr}(\hat\rho\,\{\hat x_k,\hat x_l\}_+), \tag{3.32b}$$

where we introduced the anti-commutator $\{\hat x_k,\hat x_l\}_+ = \hat x_k\hat x_l + \hat x_l\hat x_k$. From these moments, we derive the covariance matrix V by

$$V_{kl} = \frac{1}{2}\operatorname{tr}\left(\hat\rho\,\{(\hat x_k - \langle\hat x_k\rangle_{\hat\rho}),(\hat x_l - \langle\hat x_l\rangle_{\hat\rho})\}_+\right) \tag{3.33}$$

$$= \frac{1}{2}\operatorname{tr}(\hat\rho\,\{\hat x_k,\hat x_l\}_+) - \langle\hat x_k\rangle_{\hat\rho}\,\langle\hat x_l\rangle_{\hat\rho} \tag{3.34}$$

By the commutation relation (3.21), we find this is equivalent to

$$\operatorname{tr}\left(\hat\rho\,(\hat x_k - \langle\hat x_k\rangle_{\hat\rho})(\hat x_l - \langle\hat x_l\rangle_{\hat\rho})\right) = V_{kl} + \mathrm{i}\sigma_{kl}. \tag{3.35}$$

We note that $V + \mathrm{i}\sigma \geqslant 0$ and by complex conjugation $V - \mathrm{i}\sigma \geqslant 0$. This implies

$$V \geqslant \mathrm{i}\sigma, \tag{3.36}$$

which is Heisenberg's uncertainty principle represented in phase space.

3.2.2 *Gaussian States*

A *Gaussian quantum state* [107, 134, 99] is a quantum state $\hat\rho(t)$[8] whose characteristic function, or equivalent Wigner function, has the shape of a classical Gaussian function, i.e.,

$$\chi_{\hat\rho}(\boldsymbol{\alpha},t) = \exp\left(\mathrm{i}\boldsymbol{\alpha}^\top\sigma^\top\mathbf{x}_{\hat\rho}(t) - \frac{1}{2}\boldsymbol{\alpha}^\top\sigma^\top V_{\hat\rho}(t)\,\sigma\boldsymbol{\alpha}\right). \tag{3.37}$$

Here, we defined $\mathbf{x}_{\hat\rho} = (\langle\hat x_1\rangle_{\hat\rho},\ldots,\langle\hat x_n\rangle_{\hat\rho})^\top$ the *displacement vector* and $V_{\hat\rho}$ the covariance matrix of the state $\hat\rho$. Hence, completely analogous to classical Gaussian states, a Gaussian quantum state is completely determined by its first and second moments. We obtain the corresponding Wigner function by inverse Fourier transformation of (3.37):

$$\mathcal{W}_{\hat\rho}(\boldsymbol{\alpha},t) = \frac{\exp\left(-\frac{1}{2}(\boldsymbol{\alpha}-\mathbf{x}_{\hat\rho}(t))^\top V_{\hat\rho}^{-1}(t)\,(\boldsymbol{\alpha}-\mathbf{x}_{\hat\rho}(t)\right)}{\pi^n\sqrt{\det(V_{\hat\rho}(t))}}. \tag{3.38}$$

8 For the following two definitions, we will write out the time dependence explicitly. It is not needed for many of the following discussions and will be dropped in the notation. When explicitly needed, the time dependence will be reintroduced.

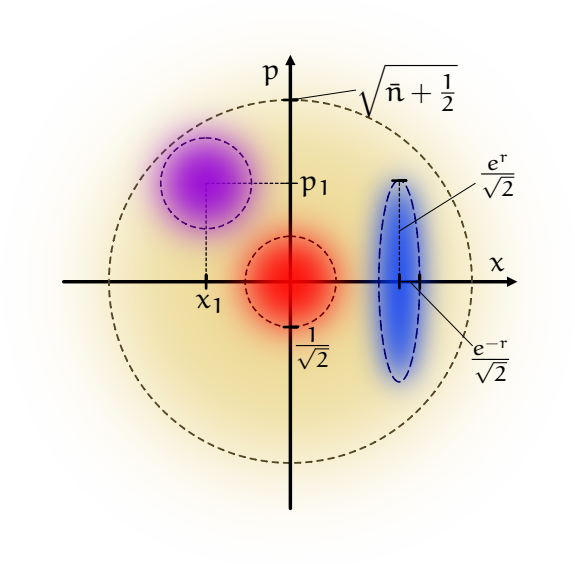

Figure 3.1: Plot of important Wigner functions in phase space. Dashed outlines correspond to the standard deviation of a given covariance matrix. The vacuum state (red) and coherent state (purple) have a variance of 1/2. A squeezed state (blue) with reduced variance in $\hat{x}$ quadrature and increased variance in $\hat{p}$. All states are encompassed in a centered thermal state (yellow) with standard deviation $\sqrt{\bar{n}+1/2}$ in both quadratures for an average thermal occupation $\bar{n}$.

Through these identifications, we can translate the purity of a state in Equation (2.53) to [107]

$$\mathcal{P}(\hat{\rho}) = \mathrm{tr}\left(\hat{\rho}^2\right) = 1/\sqrt{\det(2V_{\hat{\rho}})} = 1/\left(2^n\sqrt{\det(V_{\hat{\rho}})}\right). \tag{3.39}$$

Thus, for a Gaussian state, the purity is determined by its covariance matrix V. As the purity of a must be $\mathcal{P} \leqslant 1$, it is implied that $\det\left(V_{\hat{\rho}}\right) \geqslant 1/2^n$, which is again a consequence of Heisenberg's uncertainty principle. A single-mode Gaussian state is thus pure if its covariance obeys $\det(V_{\hat{\rho}}) = 1/2$. Single-mode Gaussian states can be nicely depicted as the contour of its Wigner function. The most common Gaussian states are coherent, squeezed, and thermal. We introduce these states in the single-mode case of a simple harmonic oscillator and depict them in Figure 3.1.

Coherent states are pure Gaussian states with variance $V = \frac{1}{2}\cdot\mathbb{1}$ and an arbitrary displacement vector $\mathbf{x}_{\hat{\rho}}$. Their characteristic function is given by

$$\chi_{\hat{\rho}}(\boldsymbol{\alpha}) = \exp\left(-\frac{1}{4}\boldsymbol{\alpha}^2 + i\boldsymbol{\alpha}^\top \mathbf{x}_{\hat{\rho}}\right). \tag{3.40}$$

Thus, as pure states, the coherent states correspond to a vector $|\alpha\rangle \in \mathcal{H}$ and are generated by the displacement operator acting on the vacuum state

$$|\alpha\rangle = \hat{D}_{\boldsymbol{\alpha}}|0\rangle. \tag{3.41}$$

A thermal state $\hat{\rho}$ is a mixed state. For a Gaussian mixed state, we can write the covariance matrix as a sum $V = V_{\text{pure}} + V_{\text{noise}}$ of a pure state $\hat{\rho}_{\text{pure}}$ and some arbitrary Gaussian noise profile. As a result of this decomposition, we can write the characteristic function as

$$\chi_{\hat{\rho}}(\boldsymbol{\alpha}) = \chi_{\text{pure}}(\boldsymbol{\alpha}) \exp\left(-\boldsymbol{\alpha}^\top \sigma^\top V_{\text{noise}} \sigma \boldsymbol{\alpha}/2\right). \tag{3.42}$$

Transforming the characteristic function back to the density operator, we find the resulting $\hat{\rho}$ as a convolution of the pure state $\hat{\rho}_{\text{pure}}$ and the Gaussian noise function [136]:

$$\hat{\rho} = \int \mathrm{d}\boldsymbol{\alpha} \exp\left(-\boldsymbol{\alpha}^\top \sigma^\top V_{\text{noise}} \sigma \boldsymbol{\alpha}/2\right) \hat{D}_{\boldsymbol{\alpha}} \hat{\rho}_{\text{pure}} \hat{D}_{-\boldsymbol{\alpha}}. \tag{3.43}$$

Therefore, a thermal state $\hat{\rho}_{\text{th}}$ with covariance matrix $V_{\text{th}} = (\bar{n} + 1/2) \cdot \mathbb{1}$ is a coherent state convolved with a Gaussian profile with covariance matrix $V_{\text{noise}} = \bar{n} \cdot \mathbb{1}$:

$$\hat{\rho}_{\text{th}} = \int \mathrm{d}\beta \exp\left(-\frac{1}{2}\beta^2 \bar{n}^{-1}\right) \hat{D}_\beta |\alpha\rangle\langle\alpha| \hat{D}_{-\beta}. \tag{3.44}$$

Contrary to coherent and thermal states, a squeezed state has one of its variances reduced, and its other variance increased accordingly. For a pure squeezed state, this implies that one variance will be $< \frac{1}{2}$, i.e., below Heisenberg's uncertainty limit. Generally, this reduction of one variance need not be along one of the phase space basis vectors but can be applied to an arbitrarily rotated field operator. For a pure single-mode squeezed state, we find its covariance matrix as

$$V_{\text{sqz}} = \frac{1}{2} R(\theta)^\top \begin{pmatrix} e^{2r} & 0 \\ 0 & e^{-2r} \end{pmatrix} R(\theta), \tag{3.45}$$

where the squeezing parameter r describes the deformation of a circle to the squeezing ellipse, and $R(\theta)$ is a rotation matrix with respect to the phase space basis.

3.2.3 *Gaussian Effect Operators*

Our discussion above is not limited to trace-class operators but remains valid for arbitrary Gaussian operators. The measurement scope we consider is restricted to monitoring, so it is natural only to consider Gaussian effect operators $\hat{E}$. As for Gaussian states, Lammers [76] showed that under stable backward dynamics, any effect operators will retrodict to a Gaussian effect operator.

Gaussian POVMs are defined similarly to Gaussian states and are fully determined by their means and covariance matrix. We find

$$\langle \hat{x}_k \rangle_{\hat{E}} := \frac{\operatorname{tr}\left(\hat{x}_k \hat{E}\right)}{\operatorname{tr}\left(\hat{E}\right)}, \tag{3.46}$$

$$V^{\hat{E}}_{kl} = \frac{1}{2} \operatorname{tr}\left(\hat{E}\{(\hat{x}_k - \langle \hat{x}_k \rangle_{\hat{E}}), (\hat{x}_l - \langle \hat{x}_l \rangle_{\hat{E}}\}_+\right). \tag{3.47}$$

The corresponding characteristic function in phase space is given by

$$\chi_{\hat{E}}(\boldsymbol{\alpha}, t) = \exp\left(i\boldsymbol{\alpha}^\top \sigma^\top \mathbf{x}_{\hat{E}}(t) - \frac{1}{2}\boldsymbol{\alpha}^\top \sigma^\top V_{\hat{E}}(t)\, \sigma\boldsymbol{\alpha}\right). \tag{3.48}$$

Our observations for Gaussian states can be translated to the Gaussian POVMs but are now interpreted in terms of measurements. Consider, for example, the situation in Equation (3.14). We have prepared a state $\hat{\rho}(t_0)$ at some initial time t_0, which we want to verify by a continuous measurement. The prepared state and the conditional effect operator are assumed to be Gaussian, hence taking the form of Gaussian Wigner functions. The operator product is then given by Equation (3.31) as the overlap integral of the Wigner functions. In turn, if we prepared a squeezed state but the measurement corresponds to a thermal effect operator, the features of the squeezed state will be "smeared out" and can not be verified. In this sense, the variance and corresponding purity of the effect operator give a measure of which states can be verified by a given measurement procedure.

3.2.4 *Linear Systems and the Kalman Filter*

Linear systems are those that follow linear Heisenberg equations of motion. The dynamics considered by us are governed by the SME (3.1). For this, the governing Hamiltonian is at most quadratic in the system's operators, while the measurement and Lindblad terms are only linear. We recast the Hamiltonian as

$$\hat{H} = \frac{1}{2}\hat{\mathbf{x}}^\top H \hat{\mathbf{x}}, \tag{3.49}$$

with $H \in \mathbb{R}^{2n\times 2n}$ a real-valued symmetric matrix, known as the Hamiltonian matrix [107]. We neglected possible linear and constant terms in the Hamiltonian (3.49), as no such term is present in the linearized optomechanical system in Section 2.3 and can always be absorbed by redefining the canonical operators $\hat{\mathbf{x}}$. The linear Lindblad operators are written as

$$\hat{L} = \Lambda\, \hat{\mathbf{x}}, \tag{3.50}$$

$$\Lambda^\dagger \Lambda = \Delta + i\Omega, \tag{3.51}$$

with the complex matrix $\Lambda \in \mathbb{C}^{n_L\times 2n}$ and real matrices $\Delta, \Omega \in \mathbb{R}^{2n\times 2n}$. Similarly, the linear measurement operators can be written as

$$\hat{C} = (A + iB)\hat{\mathbf{x}}, \tag{3.52}$$

with $A, B \in \mathbb{R}^{n_c\times 2n}$.

In this linear regime, the evolution of the means and covariance of a Gaussian state is governed by the following equations [76, 143, 148]:

$$d\mathbf{x}_{\hat{\rho}}(t) = M\mathbf{x}_{\hat{\rho}}(t)dt + \left(2V_{\hat{\rho}}(t)A^\top - \sigma B^\top\right) d\mathbf{W}(t) \tag{3.53a}$$

$$\begin{aligned}\dot{V}_{\hat{\rho}}(t) = {} & MV_{\hat{\rho}}(t) + V_{\hat{\rho}}M^\top + \sigma\Delta\sigma^\top \\ & - \left(2V_{\hat{\rho}}(t)A^\top - \sigma B^\top\right)\left(2V_{\hat{\rho}}(t)A^\top - \sigma B^\top\right)^\top,\end{aligned} \tag{3.53b}$$

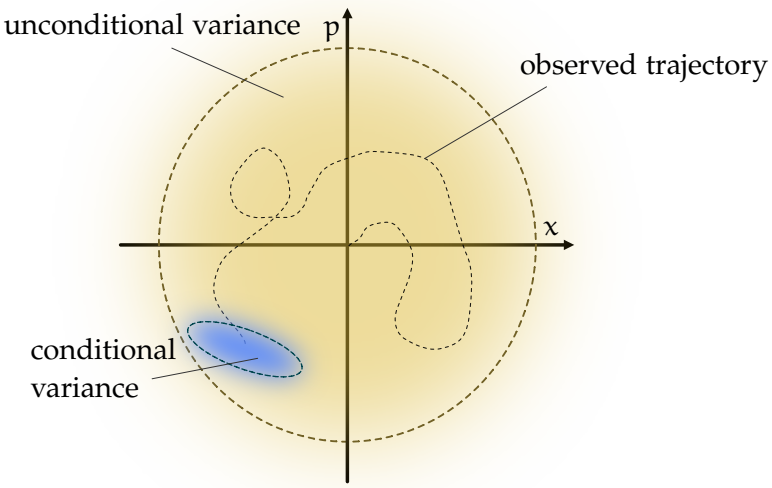

Figure 3.2: Evolution of a conditional state. The random propagation of its mean is revealed through the measurement process. The conditional variance gives the remaining uncertainty about the state (blue ellipse). Averaging over many of these trajectories would yield the unconditional variance (yellow circle).

with the drift matrix $M := \sigma(H + \Omega)$. The Wiener increments are related to the homodyne current via $d\mathbf{Y}(t) = 2A\mathbf{x}_{\hat{\rho}}(t)dt + d\mathbf{W}(t)$. We retrieve the unconditional open system dynamics without measurement, corresponding to $A, B \to 0$. In this case, the moments evolve according to the Hamiltonian and the diffusion and dissipation induced by the Lindblad terms Δ, Ω. Under conditional dynamics, the means evolve according to a white noise process $\mathbf{W}$ and the additional measurement terms in the evolution of the variance will reduce it below the unconditional level, see Figure 3.2.

Under similar considerations, the evolution of a Gaussian effect operator is governed by similar equations [76, 148]:

$$-d\mathbf{x}_{\hat{E}}(t) = -M\mathbf{x}_{\hat{E}}(t)dt + \left(2V_{\hat{E}}(t)A^\top + \sigma B^\top\right) d\mathbf{W}(t) \tag{3.54a}$$

$$\begin{aligned} -\dot{V}_{\hat{E}}(t) = &-MV_{\hat{E}}(t) - V_{\hat{E}}M^\top + \sigma\Delta\sigma^\top \\ &- \left(2V_{\hat{E}}(t)A^\top + \sigma B^\top\right)\left(2V_{\hat{E}}(t)A^\top + \sigma B^\top\right)^\top . \end{aligned} \tag{3.54b}$$

This shows the close resemblance of the linear Gaussian quantum systems to the classical stochastic systems discussed in Section 2.1.4. By the following comparison

$$A_{cl} = M = \sigma(H + \Omega), \tag{3.55a}$$
$$C_{cl} = 2A, \tag{3.55b}$$
$$D_{cl} = \sigma\Delta\sigma^\top, \tag{3.55c}$$
$$\Gamma_{cl}^\top = -\sigma B^\top, \tag{3.55d}$$

we see that Equations (3.53) and (3.54) are essentially the classical forward and backward Kalman filter equations (2.33) and (2.40)[9].

Even though we can map linear Gaussian quantum systems to their classical counterpart, there are still differences to the pure classical case. In the quantum case, the drift and diffusion matrices depend on the Lindblad operators via Δ and Ω. Thus, they can not be described independently from one another, or the diffusion process of the environment will also induce a drive on the system. Also, once the measurement operator includes an "imaginary" part B, there is always a cross-correlation between the system and measurement noises.

Suppose the measurement process has prolonged for a long enough time[10], the second moments will become stationary, i.e., time-independent. Consequently, the differential equations (3.53b) and (3.54b) turn into algebraic equations under $\dot{V} = 0$. Reintroducing the homodyne current, the quantum Kalman equations (3.53) can be rewritten [76]:

$$d\mathbf{x}_{\hat{\rho}}(t) = \tilde{M}_{\hat{\rho}}(t)\mathbf{x}_{\hat{\rho}}(t)dt + \left(2V_{\hat{\rho}}(t)A^\top - \sigma B^\top\right) d\mathbf{Y}(t) \tag{3.56a}$$
$$\begin{aligned}\dot{V}_{\hat{\rho}}(t) = {} & \tilde{M}_{\hat{\rho}}(t)V_{\hat{\rho}}(t) + V_{\hat{\rho}}\tilde{M}_{\hat{\rho}}^\top(t) + \sigma\tilde{\Delta}\sigma^\top \\ & + 4V_{\hat{\rho}}(t)A^\top A V_{\hat{\rho}}(t),\end{aligned} \tag{3.56b}$$

where $\tilde{M}_{\hat{\rho}}(t) = M + 2\sigma B^\top A - 4V_{\hat{\rho}}(t)A^\top A$ and $\tilde{\Delta} = \Delta - B^\top B$. Thus, returning to the stationary case, it is implied

$$0 = \tilde{M}_{\hat{\rho}}^{ss}V_{\hat{\rho}}^{ss} + V_{\hat{\rho}}^{ss}\tilde{M}_{\hat{\rho}}^{ss} + \sigma\tilde{\Delta}\sigma^\top + 4V_{\hat{\rho}}^{ss}A^\top A V_{\hat{\rho}}^{ss}. \tag{3.57}$$

Here, the matrices $V_{\hat{\rho}}^{ss}$ and $\tilde{M}_{\hat{\rho}}^{ss}$ are corresponding time-independent steady state matrices to $V_{\hat{\rho}}(t)$ and $\tilde{M}_{\hat{\rho}}(t)$. In this steady state limit, the evolution of the mean values is

$$\mathbf{x}_{\hat{\rho}} = e^{\tilde{M}_{\hat{\rho}}^{ss}(t-t_0)}\mathbf{x}_{\hat{\rho}}(t_0) + \int_{t_0}^{t} e^{\tilde{M}_{\hat{\rho}}^{ss}(t-\tau)}\left(2V_{\hat{\rho}}^{ss}A^\top - \sigma B^\top\right) d\mathbf{Y}(\tau). \tag{3.58}$$

It is shown in [76] that under stable dynamics, the initial condition will be damped out, and the means are only driven by the homodyne current. The

9 The subscript cl in Equations(3.55) denotes that these are the matrices of the classical linear Gaussian systems.

10 Assuming, the dynamics of the system are stable.

mean values are thus derived by the stochastic convolution of the measurement record $\mathbf{Y}$ and the matrix expression in the integrand by

$$\mathbf{x}_{\hat{\rho}}(t) = \int_{t_0}^{t} K_{\hat{\rho}}(t-\tau)\mathrm{d}\mathbf{Y}(\tau). \tag{3.59}$$

The components matrix $K_{\hat{\rho}}(t) := e^{\tilde{M}^{ss}_{\hat{\rho}}t}\left(2V^{ss}_{\hat{\rho}}A^{\top} - \sigma B^{\top}\right)$ are the (steady-state) Kalman filter that retrieves the means of the canonical quadratures. We will call these the forward Kalman filters. For the effect operator, one finds a matrix of backward Kalman filters $K_{\hat{E}}(t) := e^{\tilde{M}^{ss}_{\hat{E}}t}\left(2V^{ss}_{\hat{E}}A^{\top} - \sigma B^{\top}\right)$, with a different matrix $\tilde{M}_{\hat{E}}(t) = -M - 2\sigma B^{\top}A - 4V_{\hat{E}}(t)A^{\top}A$.

3.2.5 *The Wiener Filter*

Often the measurement proceeded long enough that we reached a steady state. In that case, the conditional quantum state can be derived by introducing *Wiener filtering* [101, 92, 89, 93], which allows for the calculation of the conditional state from the densities of the system. We will introduce this procedure for a single-mode and one measurement channel. It can be straightforwardly expanded to vector processes [92, 101]. Assume the equations of motion for the measured system and measurement process are known, we define $\hat{y}(t)$ as the operator of the measurement output and $\hat{x}(t)$ and $\hat{p}(t)$ as the position and momentum operators of the measured system. In order to apply the Wiener filter, these operators need to fulfill the following commutation relations

$$0 = [\hat{y}(t), \hat{y}(t')] \quad \forall t, t' \quad \text{and} \tag{3.60a}$$
$$0 = [\hat{x}(t), \hat{y}(t')] = [\hat{p}(t), \hat{y}(t')] \quad \forall t > t'. \tag{3.60b}$$

Equation (3.60a) is satisfied for all *simultaneously measurable* variables or *quantum non-demolition* (QND) measurements. For homodyne detection, this will be fulfilled. The second relation must be fulfilled due to causality, i.e., the measurement current that left the system and is detected outside can not influence future system variables. Both Equations (3.60) together is referred to as the *QND principle*, we will call it the *QND conditions*. It was introduced by Belavkin [5, 6] and entails that the measurement operators $\hat{y}(t')$ for $0 < t' < t$ can be regarded as a classical quantity [18, 23], as long as we consider the systems state at t.

We can then decompose the system variables $\hat{x}_n(t)$ as follows:

$$\hat{x}_n(t) = \int_{-\infty}^{t} \mathrm{d}t' \overrightarrow{K}_n(t-t')\hat{y}(t') + \hat{R}_n(t), \tag{3.61}$$

where the first term is the information about the system variable $\hat{x}_n(t)$ contained in the measurement record $\hat{y}(t)$ and $\hat{R}_n(t)$ denotes error to the estimation of $\hat{x}_n(t)$. We write $\overrightarrow{K}$ for the forward Wiener filter[11]. The error is not accessible

11 The arrow notation will be used to differentiate the Wiener and Kalman filter.

through the measurement and thus orthogonal to the measurement operator, i.e.

$$\langle \hat{R}_n(t)\hat{y}(t')\rangle = tr[\hat{\rho}\,\hat{R}_n(t)\hat{y}(t')] = 0, \quad \forall t' < t. \tag{3.62}$$

Inserting Eq. (3.61) into Eq. (3.62), we arrive at the well-known Wiener-Hopf equation [138, 65], which reads

$$C_{x_n y}(t-t'') = \int_{-\infty}^{t} dt'\, \overrightarrow{K}_n(t-t')C_{yy}(t'-t'') = 0 \quad \forall t'' \leqslant t. \tag{3.63}$$

In this $C_{x_n y}(t-t'')$ and $C_{yy}(t-t'')$ are the time-domain correlation functions between the operators. Since our filtering process proceeds until time t, we can assume $\overrightarrow{K}_n(t) = 0$ for $t' > t$ and using this we can extend the integral range to ∞ and rewrite Eq. (3.63) as

$$C_{x_n y}(t) = \int_{-\infty}^{\infty} dt'\, \overrightarrow{K}_n(t)C_{yy}(t-t') = 0 \quad \forall t \geqslant 0. \tag{3.64}$$

The solution to Eq. (3.64) can be found in the Fourier domain using the Wiener-Hopf method [96] and gives the famous Wiener filter. The solution for the optimal filter $\overrightarrow{K}_n(\omega)$ is

$$\overrightarrow{K}_n(\omega) = \frac{1}{s_y^+(\omega)}\left[\frac{S_{x_n y}(\omega)}{s_y^-(\omega)}\right]_+, \tag{3.65}$$

where have used the spectral densities $S_{x_n y}(\omega)$ and $S_{yy}(\omega)$ and have split $S_{yy}(\omega) = s_y^+(\omega)s_y^-(\omega)$ into two parts. $s_y^+(\omega)$ denotes the part which has no poles and zeros in the *upper-half complex plane* (UHP), i.e., s_y^+ and $(s_y^+)^{-1}$ are complex differentiable or holomorphic in the UHP. Similarly, s_y^- and $(s_y^-)^{-1}$ are holomorphic functions in the *lower-half complex plane* (LHP). The factor $[...]_+$ denotes the causal part of the function. It is built by first partial decomposition of $\frac{S_{x_n y}}{s_y^-}$ and then only keeping the components whose poles are located in the lower-half plane, i.e.

$$\begin{aligned}\frac{S_{x_n y}}{s_y^-} &= \sum_i \frac{\alpha_i}{\omega - P_i} \\ &= \sum_{P_i \in \text{LHP}} \frac{\alpha_i}{\omega - P_i} + \sum_{P_i \in \text{UHP}} \frac{\alpha_i}{\omega - P_i} \\ &= \left[\frac{S_{x_n y}(\omega)}{s_y^-(\omega)}\right]_+ + \left[\frac{S_{x_n y}(\omega)}{s_y^-(\omega)}\right]_-.\end{aligned} \tag{3.66}$$

The factors α_i are simply the residues of $\frac{S_{x_n y}}{s_y^-}$ at the poles of the decomposition. Hence, the causal part is calculated as

$$\left[\frac{S_{x_n y}}{s_y^-}\right]_+ = \sum_{P_i \in \text{LHP}} \frac{\text{Res}[\frac{S_{xy}}{s_y^-}, P_i]}{\omega - P_i}. \tag{3.67}$$

This is called the causal part because its inverse Fourier transform has support only for positive times. Similarly, the other term in (3.66) has support only for negative times; thus, we will call it the anti-causal part. By this reasoning, the optimal filter (3.65) is a causal function and is rightfully named the causal Wiener filter [138].

Assume we have reached a steady state where the system variables $\hat{x}_n$ have unconditional zero mean values. Then we can derive[12] the conditional first-order moments by a convolution of the Wiener filter with the measurement current,

$$\langle \hat{x}_n(t) \rangle^c = (\overrightarrow{K}_n * y)(t) = \int_{-\infty}^{t} \overrightarrow{K}_n(t-t')\, y(t')\, dt', \tag{3.68}$$

where $y(t)$ is the resulting measurement current of the output operator $\hat{y}(t)$. For the conditional moments derived by the Wiener filter, we use the superscript c to differentiate it from the results obtained by the Kalman filter. In addition, the conditional second-order moments[12] depend only on the remaining uncertainty $\hat{R}_n$ in (3.61). This can be formulated, as

$$V^c_{x_n x_m} = \langle \hat{R}_n(t) \hat{R}_m(t) \rangle \tag{3.69a}$$

$$= \langle [\hat{x}_n(t) - \langle \hat{x}_n(t) \rangle^c] \, [\hat{x}_m(t) - \langle \hat{x}_n(t) \rangle^c] \rangle \tag{3.69b}$$

$$= \int_{-\infty}^{\infty} \frac{d\omega}{2\pi} \operatorname{Re} \left[S_{x_n x_m}(\omega) - \left[\frac{S_{x_n y}(\omega)}{s_y^-} \right]_+ \left[\frac{S_{x_m y}(\omega)}{s_y^-} \right]^*_+ \right], \tag{3.69c}$$

where the first term is simply the unconditional variance $V^{uc}_{x_n x_m}$. Thus, the conditional variance is composed of the unconditional variance (first integrand) from which some measurement contribution is subtracted (second integrand). This contribution is the correlation between the output operator and the measured system variable.

Equation (3.69) shows that we can deduce the conditional variances from the spectral densities $S_{yy}(\omega)$ and $S_{x_n y}$, which can be obtained from measurement data, and predicted spectral densities $S_{x_n x_m}$ from theory. Additionally, we only assumed that a steady state has been reached and have not made further restrictions on the measurement noise. This is one of the appealing factors of the Wiener-Hopf procedure. The term $1/s_y^+$ acts as a pre-whitening tool. Therefore, the Wiener filter works identically for colored noises, which can be a significant advantage over the Kalman filter. Additionally, we saw that detailed knowledge of the dynamics is needed to set up the optimal Kalman filter. In cases where this is unknown, the Wiener filter can be an attractive alternative. For example, Meng et al. [86] used the Wiener filter for an optomechanical setup with structural damping, where temporal dynamics are unknown.

3.3 QUANTUM SMOOTHING FOR AN OPTOMECHANICAL SETUP

In the classical estimation problem, the combination of prediction and retrodiction lends nicely to the concept of smoothing. For linear Gaussian quantum

12 We refer to Appendix A.3.1 for motivation of these equations.

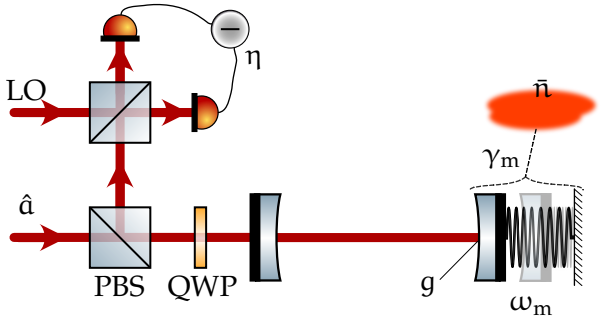

Figure 3.3: Optomechanical setup as suggested in [76]. A mechanical resonator coupled to a driven cavity. The linear polarized driving field is transmitted into the cavity through a polarizing beam-splitter (PBS) and a quarter-wave plate (QWP). After interacting with the mechanical oscillator with a coupling strength g, the field exits the cavity through the entry port. After another path through the QWP, the output field is reflected by the PBS and mixed with a strong local oscillator on a beam-splitter. From this, a homodyne detection with detection efficiency η is performed. The mechanical oscillator has an eigenfrequency ω_m and is coupled to a thermal bath with average phonon number $\bar{n}$ with a coupling rate γ_m.

systems, we saw the reemergence of classical filters in the form of Kalman and Wiener filters. Both of these filters have been used for filtering in the quantum regime. Retrodiction, and for that matter Smoothing, have no clear quantum mechanical description, and there are many different "versions" of Quantum Smoothing. In this section, we discuss this landscape on a simple optomechanical setup. We will calculate the Kalman and Wiener filters for prediction and retrodiction and discuss their discrepancies in the field of Quantum Smoothing. Many of the Wiener filter results were received in a dropped project. In cooperation with Lammers, we tried to compare the results of Wiener filtering to his Kalman filter results [76], especially for the retrodiction case. To our delight, the Wiener filters were used for prediction and retrodiction by Meng et al. [87, 86], who found similar solutions to ours.

3.3.1 *Optomechanical Setup*

We consider the setup given in [76, Section 8.2]. It is the generic optomechanical setup discussed in Section 2.3.2 subject to a continuous homodyne readout of the output field; see Figure 3.3. To reiterate, a single mode of harmonic oscillator ω_m and linewidth γ_m is coupled to a cavity field ω_c and driven by a strong coherent laser field ω_L. Following the linearization procedure laid out in Section 2.3.2, we arrive at the total Hamiltonian

$$\hat{H} = \hbar\omega_m \hat{b}^\dagger \hat{b} + \hbar\Delta_c \hat{a}^\dagger \hat{a} + \hbar\frac{g}{2}(\hat{b} + \hat{b}^\dagger)(\hat{a} + \hat{a}^\dagger), \tag{3.70}$$

with $\Delta_c = \omega_c - \omega_L$. The Lindblad equation of this setup is [102, 76]

$$\frac{d}{dt}\hat{\rho} = -\frac{i}{\hbar}[\hat{H}, \hat{\rho}] + \kappa\mathcal{D}[\hat{a}]\hat{\rho} + \gamma_m(\bar{n}+1)\mathcal{D}[\hat{b}]\hat{\rho} + \gamma_m\bar{n}\mathcal{D}[\hat{b}^\dagger]\hat{\rho}, \tag{3.71}$$

where $\bar{n}$ is the average phonon number of the mechanical bath. The limit of interest is the bad-cavity limit $\kappa \gg \omega_m, g$. In it, the cavity mode evolves much faster than the mechanics and its interaction and can thus be removed adiabatically [51, 50]. This reduces the problem effectively to the mechanical system alone. In a rotating frame at the mechanical frequency ω_m, the effective Lindblad equation reads

$$\begin{aligned}\frac{d}{dt}\hat{\rho}_m = &-i\,[\delta\omega_m \hat{b}^\dagger \hat{b}, \hat{\rho}_m] + \Gamma_- \mathcal{D}[\hat{b}]\hat{\rho}_m + \Gamma_+ \mathcal{D}[\hat{b}^\dagger]\hat{\rho}_m \\ &+ \gamma_m(\bar{n}+1)\mathcal{D}[\hat{b}]\hat{\rho}_m + \gamma_m \bar{n}\mathcal{D}[\hat{b}^\dagger]\hat{\rho}_m,\end{aligned} \tag{3.72}$$

with $\hat{\rho}_m$ the density operator of the mechanical system. The term $\delta\omega_m$ is the shift to the mechanical resonance frequency by the optical spring effect of the radiation pressure interaction and equals

$$\delta\omega_m = g^2(\omega_+ + \omega_-), \tag{3.73}$$

$$\omega_\pm = \frac{-\Delta_c \pm \omega_m}{(\kappa/2)^2 + (-\Delta_c \pm \omega_m)^2}. \tag{3.74}$$

The coupling rates $\Gamma_\pm$ of the mechanical operators to the bath are the Stokes and anti-Stokes rates (citation)

$$\Gamma_\pm = \frac{g^2\kappa}{(\kappa/2)^2 + (-\Delta_c \pm \omega_m)^2}. \tag{3.75}$$

Luckily, it is enough for our discussion to consider the cavity driven on resonance, i.e., $\Delta_c = 0$. We find, in this case, $\delta\omega_m = 0$ and for the bad cavity limit, the Stokes/anti-Stokes rates reduce the optomechanical *read out rate*,

$$\Gamma = \frac{4g^2}{\kappa}. \tag{3.76}$$

Its ratio to the coupling rate of the thermal bath γ_m is the *classical cooperativity*

$$C_{cl} = \frac{\Gamma}{\gamma_m} = \frac{4g^2}{\kappa\gamma_m}. \tag{3.77}$$

3.3.2 *Results of the Kalman Filter*

To derive the steady state Kalman filters for homodyne detection, we turn to the SME. It is noted that the procedure of adiabatic elimination of the cavity mode does not yield a valid SME. However, this can be circumvented by coarse-graining the system[13] and imposing the so-called *rotating wave approximation* (RWA). The effective conditional dynamics of the mechanical system is

$$\begin{aligned}d\hat{\rho}_m(t) = &\gamma_m(\bar{n}+1)\mathcal{D}[\hat{b}]\hat{\rho}_m(t)dt + \gamma_m\bar{n}\mathcal{D}[\hat{b}^\dagger]\hat{\rho}_m(t)dt \\ &+ \Gamma\mathcal{D}[\hat{x}]\hat{\rho}_m(t)dt + \Gamma\mathcal{D}[\hat{p}]\hat{\rho}_m(t)dt \\ &+ \sqrt{\eta\Gamma}\mathcal{H}[\hat{x}]dW_c(t) + \sqrt{\eta\Gamma}\mathcal{H}[\hat{p}]dW_s(t),\end{aligned} \tag{3.78}$$

13 For details on this procedure, see Sections 3 and 8 in [76].

where dW_c and dW_s are independent Wiener increments $\propto \cos(\omega_m t)$ and $\sin(\omega_m t)$ respectively [76, 50].

We can now translate this to the matrices needed for the linear Gaussian dynamics. We find for the Hamiltonian matrix $H = 0_2$, with the 2×2 zero matrix. From the Lindblad operators $\Delta = (\Gamma + \gamma_m(\bar{n} + \frac{1}{2}))\mathbb{1}$ and $\Omega = \frac{1}{2}\gamma_m \sigma$. The measurement operators yield the matrices $A = \sqrt{\eta\Gamma}\mathbb{1}$ and $B = 0_2$; hence there is no cross-correlation between the system and measurement noise.

Now, after a sufficiently long and stable measurement process, the steady state variance[14] is

$$V_{\hat{\rho}}^{ss} := V_{xx}^{\hat{\rho}} = V_{pp}^{\hat{\rho}} = \frac{-1 + \sqrt{1 + 8C_{cl}\eta(2C_{cl} + 2\bar{n} + 1)}}{8C_{cl}\eta}. \tag{3.79}$$

The covariance matrix is diagonal; hence the conditional state will not be squeezed, as typical in optomechanical setups [31, 103, 104]. By Equation (3.39), the variance gives us direct information about the purity of the prepared conditional state. For an efficient measurement ($C_{cl}\eta \gg 1$), the variance $V_{\hat{\rho}} \to \frac{1}{2}$ and, in turn, the prepared state is pure. For a very inefficient measurement $\eta \to 0$, we retrieve the unconditional state with $V_{\hat{\rho}} = \frac{1}{2} + \bar{n} + C_{cl}$, which is a thermal state plus additional back-action. With the steady-state variance the drift matrix $\tilde{M}_{\hat{\rho}}$ is

$$\tilde{M}_{\hat{\rho}} = -\lambda_{\hat{\rho}}\mathbb{1}, \quad \lambda_{\hat{\rho}} = \frac{\gamma_m}{2}\sqrt{1 + 8\eta C_{cl}\,(2C_{cl} + 2\bar{n} + 1)}. \tag{3.80}$$

From the drift matrix, we can derive the matrix of Kalman filters

$$K_{\hat{\rho}}(t) = e^{\tilde{M}_{\hat{\rho}} t}\left(2V_{\hat{\rho}}A^\top - \sigma B^\top\right) = 2\sqrt{\eta\Gamma}V_{\hat{\rho}}e^{-\lambda_{\hat{\rho}} t}\,\mathbb{1}, \tag{3.81}$$

and thus, the means are found by stochastic convolution

$$\langle\hat{x}\rangle_{\hat{\rho}} = (K_x^{\hat{\rho}} * dW_c)(t) = \int_{t_0}^{t} 2\sqrt{\eta\Gamma}V_{\hat{\rho}}e^{-\lambda_{\hat{\rho}}(t-\tau)}dW_c(\tau), \tag{3.82a}$$

$$\langle\hat{p}\rangle_{\hat{\rho}} = (K_p^{\hat{\rho}} * dW_s)(t) = \int_{t_0}^{t} 2\sqrt{\eta\Gamma}V_{\hat{\rho}}e^{-\lambda_{\hat{\rho}}(t-\tau)}dW_s(\tau). \tag{3.82b}$$

Under the same assumptions, the steady-state covariance of the effect is

$$V_{\hat{E}} := V_{xx}^{\hat{E}} = V_{pp}^{\hat{E}} = \frac{1 + \sqrt{1 + 8C_{cl}\eta(2C_{cl} + 2\bar{n} + 1)}}{8C_{cl}\eta}. \tag{3.83}$$

We find the steady-state variance of the effect operator, i.e., of the backward Kalman filter, is larger than the forward covariance. This fact is also true for the classical case [131, 130]; we will comment more on this when we compare the results of the Wiener and Kalman filters. For an efficient measurement $C_{cl}\eta \gg 1$, the difference $V_{\hat{E}} - V_{\hat{\rho}} = \frac{1}{4\eta C_{cl}}$ vanishes and in the inefficient case $\eta \to 0$ we find the covariance matrix $V_{\hat{E}}$ diverges. This fits our intuition. If we start from 0 information $\hat{E}(T) = \mathbb{1}$ and collect no information, there is nothing to retrodict.

14 We will drop the superscript ss in the following.

The backward drift matrix is identical to the forward case. We find the matrix $\tilde{M}_{\hat{E}}$ with the same $\lambda_{\hat{E}} = \lambda_{\hat{\rho}}$ and thus

$$\langle \hat{x} \rangle_{\hat{E}} = (K_x^{\hat{E}} * dW_c)(t) = \int_t^T 2\sqrt{\eta\Gamma} V_{\hat{E}} e^{-\lambda_{\hat{E}}(\tau - t)} dW_c(\tau), \tag{3.84a}$$

$$\langle \hat{p} \rangle_{\hat{E}} = (K_p^{\hat{E}} * dW_s)(t) = \int_t^T 2\sqrt{\eta\Gamma} V_{\hat{E}} e^{-\lambda_{\hat{E}}(\tau - t)} dW_s(\tau). \tag{3.84b}$$

Note that the integrals in (3.84) are backward Itô integrals as opposed to the forward Itô integrals in (3.82).

3.3.3 *Results of the Wiener Filter*

To analyze the Wiener filter, we first derive the spectral densities of our optomechanical setup, governed by the Equations (2.124). In a steady state and the bad cavity limit ($\kappa \gg \omega_m, g$), we arrive at [10]

$$S_{xx} = |\chi_m|^2 \left(2\Gamma + \gamma_m(2\bar{n} + 1)\right), \tag{3.85a}$$

$$S_{yy} = \frac{1}{2} + 4\Gamma\eta S_{xx}, \tag{3.85b}$$

$$S_{xy} = 2\sqrt{\Gamma\eta} S_{xx}, \tag{3.85c}$$

$$S_{pp} = \frac{\omega^2}{\omega_m^2} S_{xx}, \tag{3.85d}$$

$$S_{py} = \frac{i\omega}{\omega_m} S_{xy}, \tag{3.85e}$$

$$S_{xp} = -\frac{i\omega}{\omega_m} S_{xx}, \tag{3.85f}$$

We have used that in the Fourier domain $\hat{p} = -i\omega\hat{x}/\omega_m$. Again, Γ is the readout rate, η is the detection efficiency and $\bar{n}$ is the average phonon number. We begin with the causal filter. The spectral density S_{yy} can be decomposed in its causal and anti-causal parts as

$$S_{yy} = (s_y^+)(s_y^-) = \left(\frac{(\omega_{eff}^2 - \omega^2) - i\gamma_{eff}\omega}{\sqrt{2}(\omega_m^2 - \omega^2) - i\gamma_m\omega}\right)\left(\frac{(\omega_{eff}^2 - \omega^2) + i\gamma_{eff}\omega}{\sqrt{2}(\omega_m^2 - \omega^2) + i\gamma_m\omega}\right), \tag{3.86}$$

where we have defined an effective frequency $\omega_{eff} = \left(8\eta\gamma_m^2(2C_{cl} + 2\bar{n} + 1)\omega_m^2 + \omega_m^4\right)^{\frac{1}{4}}$ and a effective linewidth $\gamma_{eff} = \sqrt{\gamma_m^2 + 2\omega_{eff}^2 - 2\omega_m^2}$. The causal filter is constructed from this decomposition together with Equation (3.65). For the position filter, we arrive at[15]

$$\overrightarrow{K}_x(\omega) = \alpha(1 - i\omega\beta)\chi_{eff}(\omega), \tag{3.87}$$

recovering the results as in [87]. Here, we defined a effective mechanical susceptibility $\chi_{eff} = \frac{1}{\omega_{eff}^2 - \omega^2 - i\gamma_{eff}\omega}$, and the frequency independent coefficients

15 See Appendix A.3.2 for more details on the calculation.

$\alpha = 4\sqrt{\eta\gamma_m}\gamma_m(2C_{cl}+2\bar{n}+1)\frac{\omega_m^2}{\omega_m^2+\omega_{eff}^2}$ and $\beta = \frac{\gamma_m+\gamma_{eff}}{\omega_{eff}^2-\omega_m^2+\gamma_m^2+\gamma_{eff}\gamma_m}$. The effective susceptibility is peaked around the frequency ω_{eff} with the linewidth γ_{eff}, which are essentially the zeros of the spectral density S_{yy}. All these parameters depend on the optomechanical cooperativity C_{cl}, and we see that as C_{cl} increases, the effective frequency ω_{eff} and effective linewidth γ_{eff} will increase as well. Thus, for $C_{cl} \gg 1$, the filter becomes flat for a broad range below the resonance frequency ω_{eff}.

For the momentum filter, we use $\hat{p} = -i\omega\hat{x}/\omega_m$, and find

$$\overrightarrow{K}_p(\omega) = -\frac{\alpha\beta}{\omega_m}\left(\omega_m^2 + i\omega\frac{\omega_{eff}^2-\omega_m^2}{\gamma_{eff}+\gamma_m}\right)\chi_{eff}(\omega). \tag{3.88}$$

The conditional variances are found by Equation (3.69). Starting with the conditional variance for the position

$$V_{xx}^c = \frac{\gamma_{eff}-\gamma_m}{8\eta\gamma_m C_{cl}} \tag{3.89a}$$

$$= \frac{-\gamma_m + \sqrt{\gamma_m^2 + 2\omega_m\left(-\omega_m + \sqrt{8C_{cl}(2C_{cl}+2\bar{n}+1)\gamma_m^2\eta+\omega_m^2}\right)}}{8C_{cl}\eta\gamma_m}. \tag{3.89b}$$

For these results, we have not made any restrictions to the parameters except $\kappa \gg \omega_m, g$. We could employ the perfect oscillator $\gamma_m \to 0$ and free-mass limit $\omega_m \to 0$ as is common in the gravitational wave community. Doing so recovers the results of [93, 92, 101]. For our setup, however, we are in the regime $\omega_m \gg \Gamma, \gamma_m$, and can thus deep in a regime where the RWA holds. In this limit, the conditional variance reduces to

$$V_{xx}^c = \frac{-1+\sqrt{1+8C_{cl}\eta(2C_{cl}+2\bar{n}+1)}}{8C_{cl}\eta} = V_{xx}^{\hat{\rho}}, \tag{3.90}$$

which is the same as for the Kalman filter. For the remaining conditional covariance terms, we proceed similarly. We find

$$V_{pp}^c = \frac{\gamma_{eff}\omega_{eff}^2 - \gamma_m\omega_m^2 + \gamma_m(\gamma_m-\gamma_{eff})}{8C_{cl}\eta\gamma_m\omega_m^2}, \tag{3.91}$$

$$V_{xp}^c = \frac{\gamma_m^2 - \gamma_m\gamma_{eff} + \omega_{eff}^2 - \omega_m^2}{8\eta C_{cl}\gamma_m\omega_m}. \tag{3.92}$$

Again, employing the micro-mechanical limit, we find $V_{pp}^c = V_{xx}^c$ and $V_{xp}^c = 0$. To summarize, for the causal case, the Wiener-Hopf procedure yields the same covariance matrix as the Kalman filter.

Next, we will verify that the Kalman and Wiener filters are the same. For this, we perform the inverse Fourier transform on the above-calculated Wiener filter. After moving to the limit of large ω_m, we arrive at

$$\overrightarrow{K}_x(t) = 2\sqrt{\eta\Gamma}e^{-\lambda t}V_{xx}^c\Theta(t)\cos\omega_m t, \tag{3.93}$$

$$\overrightarrow{K}_p(t) = 2\sqrt{\eta\Gamma}e^{-\lambda t}V_{pp}^c\Theta(t)\sin\omega_m t, \tag{3.94}$$

with the envelope of the filter given by

$$\lambda = \frac{\gamma_m}{2}\sqrt{1 + 8\eta C_{cl}(2C_{cl} + 2\bar{n} + 1)}, \tag{3.95}$$

and Θ the Heaviside step function. We see the Wiener filters have the same envelop and pre-factor as the Kalman filter. Additionally, the x-filter contains the cosine and the p-filter sine components. Hence both Wiener and Kalman filters behave the same. This is not surprising, as the Kalman filter was initially derived as the time-varying version of the Wiener filter [66] and should be the same in the steady state limit.

In analogy to the backward Kalman filter for the effect operator, the anti-causal part of the Wiener filter was suggested for retrodiction [88, 86]. Here, we will see that the Wiener and Kalman filters do not behave similarly. We first note that the anti-causal filters are

$$\overleftarrow{K}_x(\omega) = \frac{1}{s^-}\left[\frac{S_{xy}}{s^+}\right]_-, \tag{3.96}$$

$$\overleftarrow{K}_p(\omega) = \frac{1}{s^-}\left[\frac{S_{py}}{s^+}\right]_-, \tag{3.97}$$

which for the spectral densities (3.85) are just the adjoints of the causal filters.

A similar situation is found for the variances; we observe

$$V^r_{xx} = \int_{-\infty}^{\infty}\frac{d\omega}{2\pi}\left(S_{xx}(\omega) - \left[\frac{S_{xy}}{s^+}\right]_-\left[\frac{S_{xy}}{s^+}\right]^*_-\right) \tag{3.98}$$

$$= \int_{-\infty}^{\infty}\frac{d\omega}{2\pi}\left(S_{xx}(\omega) - \left[\frac{S_{xy}}{s^-}\right]^*_+\left[\frac{S_{xy}}{s^-}\right]_+\right) \tag{3.99}$$

$$= V^c_{xx}. \tag{3.100}$$

We introduced the term V^r_{xx} for the retrodicted variance to differentiate it from the Kalman retrodiction and also note that $V^r_{xx} \neq V^{\hat{E}}_{xx}$ The same is true for $V^r_{pp} = V^c_{pp}$. However, the covariance will gather a minus sign $V^r_{xp} = -V^c_{xp}$ because $\hat{p} \to -\hat{p}$ under time-reverse. Since the covariance vanishes in the limit $\omega_m \gg \Gamma, \gamma_m$, we see that the Wiener filter gives the same estimate for the covariance regardless of whether future or past measurement data is used. Thus, due to the difference in the variance estimation, the anti-causal Wiener filter is not the same as the backward Kalman filter. We find,

$$\overleftarrow{K}_x(t) = 2\sqrt{\eta\Gamma}e^{\lambda t}V^c_{xx}\Theta(-t)\cos\omega_m t, \tag{3.101}$$

$$\overleftarrow{K}_p(t) = 2\sqrt{\eta\Gamma}e^{\lambda t}V^c_{pp}\Theta(-t)\sin\omega_m t. \tag{3.102}$$

These results are counter-intuitive. If we interpret the anti-causal Wiener filter similarly to the backward Kalman filter, its results should correspond to a Gaussian effect operator. In contrast to $V_{\hat{E}}$, the conditional variance given by the anti-causal part of the measurement spectrum will converge in the case of $\eta \to 0$. This is in strong contrast to what we discussed before. We start from a state of no knowledge about the effect operator $\hat{E}(T) = \mathbb{1}$ and collect no information. How can this yield an effect operator with finite variance $V_{\hat{E}} = \frac{1}{2} + \bar{n} + C_{cl}$?

A similar conundrum was noticed in the classical scenario and solved by Wall et al. [131, 130]. The classical forward Kalman filter was designed as the time-varying version of the Wiener filter; in turn, it will give identical results in the steady state limit. However, in this limit, the backward Kalman filter will always have a larger covariance than the forward case. Consequently, the anti-causal estimate from Wiener filtering and the backward Kalman filter did not yield the same results. The reason for this discrepancy lies in the way the forward and backward Kalman filter gain their estimate. In the forward case, the Kalman filter uses some a priori data and information from our measurement to infer the conditional state. For our optomechanical example, this a priori data is the unconditional variance $V_{uc} = C_{cl} + \bar{n} + \frac{1}{2}$. In the backward case, no prior data is present. The filter estimate is based on the measurement data alone. In context to our optomechanical example, the forward Kalman filter gives the conditional variance as a maximum-likelihood estimate of the measurement data and the a priori data of the state [131]. We find

$$V_{\hat{\rho}} = \left(V_{uc}^{-1} + V_{data}^{-1}\right)^{-1} \tag{3.103}$$

$$\stackrel{!}{=} \frac{-1 + \sqrt{1 + 8C_{cl}\eta(2C_{cl} + 2\bar{n} + 1)}}{8C_{cl}\eta} \tag{3.104}$$

$$\implies V_{data} = \frac{1 + \sqrt{1 + 8C_{cl}\eta(2C_{cl} + 2\bar{n} + 1)}}{8C_{cl}\eta} = V_{\hat{E}}. \tag{3.105}$$

Thus, this classical discussion fits the results derived from the SMEs. It also gives intuition to the limit of very efficient measurements $\eta C_{cl} \gg 1$, where the forward and backward filter estimates converge. In this limit, the information gained from the measurement is essentially perfect. Thus only the measurement record is needed for the best estimate, and the a priori information loses its "information value" as $V_{uc} \to \infty$.

The Wiener filter estimates the conditional variances from the spectral densities. We saw for the causal and anti-causal case that the variance is found by

$$V_{xx}^{c} = \int_{-\infty}^{\infty} \frac{d\omega}{2\pi} \left(S_{xx}(\omega) - \left[\frac{S_{xy}}{s^{-}}\right]_{+}^{*} \left[\frac{S_{xy}}{s^{-}}\right]_{+} \right) \tag{3.106}$$

$$= V_{uc} - \int_{-\infty}^{\infty} \frac{d\omega}{2\pi} \left[\frac{S_{xy}}{s^{-}}\right]_{+}^{*} \left[\frac{S_{xy}}{s^{-}}\right]_{+}. \tag{3.107}$$

Therefore, a priori information is always present in the Wiener filter calculation. Compared to the Kalman case, this missing asymmetry is why the results between the anti-causal Wiener and backward Kalman filter differ.

While appealing, we note that intuition gained from classical observations should only be applied to the quantum case with caution. Fundamentally, quantum mechanics considers two different objects for prediction and retrodiction, leading to many technicalities when combining both approaches for smoothing.

3.3.4 *Quantum Smoothing*

In the classical case, the combination of prediction and retrodiction led to the concept of smoothing by combining the filtered probability function p_f and retrodicted effect E_r into a smoothed probability function $p_s \propto p_f E_r$. The naive approach to the quantum case would be to combine the conditional density operator $\hat{\rho}$ and effect operator $\hat{E}$ similarly to derive a smoothed density operator $\hat{\rho}_s(\tau) \propto \hat{\rho}_c(\tau)\hat{E}(\tau)$. However, when we consider the causality condition (3.60b), introduced in Section 3.2.5

$$[\hat{\mathbf{x}}(t), \hat{\mathbf{y}}(t')] = 0 \quad \forall t > t', \tag{3.108}$$

we find that this is not the case for $t < t'$. This implies that, in general

$$[\hat{\rho}_c(\tau), \hat{E}(\tau)] \neq 0. \tag{3.109}$$

Therefore, $\hat{\rho}_s(\tau)$ is not a Hermitian operator, or for the symmetrized product[16], it is not a positive semi-definite operator [117]. The failure of the QND measurement conditions (3.60) for the future measurement record makes the quantum smoothing problem highly controversial. Introduced by Belavkin in his seminal work [6], the QND principle is an underlying assumption in the field of quantum filtering[17], and it is argued that Bayesian Inference may only apply to quantum systems when the QND conditions are fulfilled [42]. Nevertheless, many attempts have been made to tackle the restrictions given in Equation (3.109).

The term "quantum smoothing", also known as *hybrid smoothing*, was first introduced by Tsang [117, 118]. In this line of work, a classical parameter influences the evolution of a quantum system and Bayesian smoothing is employed using a smoothed estimate of that parameter. Our considerations fit right into this category. The classical parameter here is a classical force that acts upon the movable end mirror of a cavity, influencing the evolution of the intracavity field in the process. Tsang shows that in this hybrid case, the smoothing estimate is performed by a set of time-symmetric SMEs, and for linear Gaussian systems, it is reduced to a Wigner function

$$\mathcal{W}_s(\boldsymbol{\alpha}, \tau) = \frac{\mathcal{W}_{\hat{\rho}}(\boldsymbol{\alpha}, \tau)\mathcal{W}_{\hat{E}}(\boldsymbol{\alpha}, \tau)}{\int \mathcal{W}_{\hat{\rho}}(\boldsymbol{\alpha}, \tau)\mathcal{W}_{\hat{E}}(\boldsymbol{\alpha}, \tau)}. \tag{3.110}$$

Moreover, the moments of this smoothed estimate are given by the two-filter smoother (2.41). The hybrid smoothing technique is a valuable tool in estimating a varying optical phase as shown in theoretical works [122, 7] and experimentally [146, 137].

Following the work of Tsang, Gammelmark et al. [36] introduced the concept of *past quantum states*, which is given by the pair

$$\Xi(\tau) = (\hat{\rho}_c(\tau)), \hat{E}(\tau)). \tag{3.111}$$

16 As we use the symmetrized operator ordering, this is the case we consider.

17 We also used it for the Wiener filtering process.

In this sense, they do not define a quantum state but a measure that combines the information of past and future measurements. The authors then consider the case where a measurement $\hat{M}_{x_\tau}$ was performed at time τ with measurement result x_τ. It is shown that the past quantum state can estimate this measurement in the way of Bayesian inference as

$$p_\Xi(x_\tau) = \mathrm{tr}\left(\hat{M}_{x_\tau}\hat{\rho}_c(\tau)\hat{M}^\dagger_{x_\tau}\hat{E}(\tau)\right). \tag{3.112}$$

This technique was successfully implemented experimentally to estimate an unknown result of a measurement on superconducting qubits [115]. It also closely resembles the hybrid smoothing technique, and as argued by Tsang [119], it may be considered the same. Like hybrid smoothing, the theory of past quantum states was also extended to linear Gaussian systems [148]. Therein, the past quantum state estimate is also reduced to a Wigner function given by the two-filter estimates.

Employing the hybrid smoothing to our optomechanical setup, we find a "smoothed" state with variance

$$V_s = \left(V_{\hat{\rho}}^{-1} + V_{\hat{E}}^{-1}\right)^{-1} \tag{3.113a}$$

$$= \frac{1 + 2\bar{n} + 2C_{cl}}{2\sqrt{1 + 8\eta C_{cl}(2C_{cl} + 2\bar{n} + 1)}}\,\mathbb{1}. \tag{3.113b}$$

This can not be a real physical state, as the determinant

$$\det(V_s) \xrightarrow{\eta C_{cl} \gg 1} \frac{1}{16} < \frac{1}{4}, \tag{3.114}$$

violates Heisenberg's uncertainty principle. The estimates of the form above were found to have a close connection to *weak value estimates* [118, 148]. The concept of weak values was initially introduced by Aharonov et al. [1]. They considered the case of a system weakly coupled to probe so that the measurement yields minimal information about an observable $\hat{O}$ but also minimally disturbs the system. The weak value estimates are the ensemble average taken over a set of pre-selected and post-selected states. This means the weak value of an observable $\hat{O}$ is given by[1]

$$_\phi\langle\hat{O}\rangle_\psi = \mathbb{E}[o|\phi,\psi] = \mathrm{Re}\,\frac{\langle\phi|\hat{O}|\psi\rangle}{\langle\phi|\psi\rangle}, \tag{3.115}$$

where $|\psi\rangle$ is the state the system was prepared in, and $|\phi\rangle$ is the state in which the system was found after the measurement run.

This concept can be generalized to the smoothing setup [118, 46, 142], as a weak value estimate conditioned on the past and future measurement record. One can show that

$$_{\hat{E}}\langle\hat{O}\rangle_{\hat{\rho}} = \mathrm{Re}\,\frac{\mathrm{tr}\left(\hat{E}(\tau)\hat{O}\hat{\rho}_c(\tau)\right)}{\mathrm{tr}\left(\hat{E}(\tau)\hat{\rho}_c(\tau)\right)}. \tag{3.116}$$

This expression can be rearranged; we note that

$$
\begin{aligned}
{}_{\hat{E}}\langle \hat{O} \rangle_{\hat{\rho}} &\propto \operatorname{Re} \operatorname{tr}\left(\hat{E}(\tau)\hat{O}\hat{\rho}_c(\tau)\right) && (3.117)\\
&= \operatorname{tr}\left(\frac{\hat{E}(\tau)\hat{O}\hat{\rho}_c(\tau) + (\hat{E}(\tau)\hat{O}\hat{\rho}_c(\tau))^\dagger}{2}\right) && (3.118)\\
&= \operatorname{tr}\left(\frac{\hat{E}(\tau)\hat{O}\hat{\rho}_c(\tau) + \hat{\rho}_c(\tau)\hat{O}\hat{E}(\tau)}{2}\right) && (3.119)\\
&= \operatorname{tr}\left(\hat{O}\frac{\hat{E}(\tau)\hat{\rho}_c(\tau) + \hat{\rho}_c(\tau)\hat{E}(\tau)}{2}\right) = \operatorname{tr}(\hat{O}\tilde{\rho}_s), && (3.120)
\end{aligned}
$$

where we introduces the smoothed "state" $\tilde{\rho}_s$. Consequently, the weak value estimate of an operator $\hat{O}$ with preparation $\hat{\rho}_c$ and retrodiction effect $\hat{E}$ is given by

$$
{}_{\hat{E}}\langle \hat{O} \rangle_{\hat{\rho}} = \operatorname{Re} \frac{\operatorname{tr}(\hat{O}\,\tilde{\rho}_s)}{\operatorname{tr}(\tilde{\rho}_s)}. \tag{3.121}
$$

This value is only well defined in the case of commuting $\hat{\rho}_c$ and $\hat{E}$ because $\tilde{\rho}_s$ will not necessarily be positive otherwise.

The variance for the smoothed state (3.113) was calculated by the forward and backward Kalman filter. In this case, one could also choose the Wiener filter. For smoothing in the Wiener-Hopf context, one constructs the *non-causal* Wiener estimate by simultaneously using the whole measurement record [138]. The smoothed variance is found by

$$
V^s_{x_n x_m} = \int_{-\infty}^{\infty} \frac{d\omega}{2\pi} \operatorname{Re}\left[S_{x_n x_m}(\omega) - \frac{(S_{x_n y}(\omega))^* (S_{x_m y}(\omega))}{S_{yy}(\omega)}\right]. \tag{3.122}
$$

For our setup, we use the spectral densities (3.85) and arrive at the following

$$
\begin{aligned}
V^s_{xx} &= (C_{cl} + \bar{n} + \frac{1}{2})\frac{\gamma_m \omega_m^2}{\gamma_{eff}\omega_{eff}^2} && (3.123a)\\
V^s_{pp} &= (C_{cl} + \bar{n} + \frac{1}{2})\frac{\gamma_m}{\gamma_{eff}} && (3.123b)\\
V^s_{xp} &= 0. && (3.123c)
\end{aligned}
$$

In the limit $\omega_m \gg \gamma_m, g$ this turns into a diagonal matrix, with

$$
V_s = \frac{1 + 2\bar{n} + 2C_{cl}}{2\sqrt{1 + 8\eta C_{cl}(2C_{cl} + 2\bar{n} + 1)}}\,\mathbb{1} \tag{3.124}
$$

which reproduces the result given by the Mayne-Fraser-Potter smoother in Equation (3.113). Hence, the Kalman and Wiener filters are interchangeable in this hybrid smoothing setting.

So far, the described smoothing techniques did not yield a valid smoothed quantum state. Another method introduced by Wiseman and Guevara [45, 46] aims to resolve this problem. The scenario considered is that an observer named

Alice gains information about a quantum system by continuous measurement, from which she wants to infer the density operator of another observer called Bob. The key idea of this method is that Alice gains only partial information about the true state, while Bob is omniscient with complete access to the true observation record. Alice then tries to estimate the "true" from her observation record, which means she estimates an unknown rest in the past measurement data called the *unobserved record*. Following this idea, a series of papers applies it to linear Gaussian quantum systems [79, 80, 81, 78]. In these, Laverick et al. find the necessary criteria to produce a valid smoothed quantum state [80] and quantum analogs to the Mayne-Fraser-Potter [79], and Rauch-Tung-Striebel smoother [78]. Tsang argued [119] that this technique can be regarded as hybrid smoothing under the assumption that Bob's true density matrix is a classical stochastic process. We see there exist many proposals for the quantum smoothing problem with varying degrees of "overlap". In their work, Chantasri, Guevara, Laverick and Wiseman [21] aim to unify all these ideas.

3.3.5 *Verification through retrodiction*

The quantum smoothing problem can also be discussed through state verification. In this, the future measurement record is used to infer the prepared state of the past. Determining the conditional quantum state from filtering alone is not possible [104], as the observed trajectory in an experiment is random, whereas the variance undergoes a deterministic evolution. Thus, performing many measurements to determine the variance from the measured means yields the unconditional variance. Additional measurements are needed to infer the conditional variance through retrodiction. This was performed experimentally by Rossi et al. [104] for an optomechanical setup using Kalman filers, as discussed in this section. They generate the first moments from past and future measurement data to verify the state. Critical in matching the prepared to the retrodicted trajectories is the introduction of a relative distance between the two means, i.e., $\mathbf{d}(t) = \mathbf{x}_{\hat{E}}(t) - \mathbf{x}_{\hat{\rho}}(t)$. The difference between these two Gaussian processes is also Gaussian. As shown by Rossi et al., its variance can be calculated to be from the measured means. The variance of the relative distance is [104, 102]

$$V_{\mathbf{d}} = V_{\hat{\rho}} + V_{\hat{E}} = 2V_{\hat{\rho}} + \frac{1}{4\eta C_{cl}}\mathbb{1} \xrightarrow{\eta C_{cl} \gg 1} 2V_{\hat{\rho}}. \tag{3.125}$$

This fits well with intuition. The average over many experimental runs yields a variance as a sum of the preparation and retrodiction parts.

In 2021, Meng et al. [88] used verification based on this method but with Wiener filters. Their reasoning for not using Kalman filters lies in their experimental setup. They estimate a structurally damped oscillator for which information on the inner dynamics is unavailable, and thus the optimal Kalman filter can not be set up. Their work shows the verification of single- and multimode mechanical states to good precision. On a fundamental level, however,

we have concerns about applying the relative distance method from Rossi with the causal and anti-causal Wiener filters.

In the single mode example of this section, we can calculate the variance of distance in terms of the Wiener filters [88, 86][18] and find

$$V_{\Delta x\Delta x} = \frac{\alpha^2\beta^2}{\gamma_m + \gamma_{eff}}\left(1 + \frac{2\gamma_m\gamma_{eff}}{\omega_m^2 + \omega_{eff}^2}\right), \tag{3.126a}$$

$$V_{\Delta p\Delta p} = \frac{\alpha^2\beta^2}{\omega_m^2(\gamma_m^2 + \gamma_{eff}^2)}\left(\frac{\gamma_m\omega_m^2 + \gamma_{eff}\omega_{eff}^2}{2} + \frac{\gamma_m\gamma_{eff}(\gamma_m - \gamma_{eff})(\omega_{eff}^2 - \omega_m^2)}{2(\omega_{eff}^2 + \omega_m^2)}\right) \tag{3.126b}$$

$$V_{\Delta x\Delta p} = 0. \tag{3.126c}$$

In the limit of large ω_m, we find a diagonal matrix, with

$$V_{\mathbf{d}} = \frac{4C_{cl}\eta(2C_{cl} + 2\bar{n} + 1)^2)(1 + \sqrt{1 + 8C_{cl}(2C_{cl} + 2\bar{n} + 1)})}{(1 + 4C_{cl}\eta(2C_{cl} + 2\bar{n} + 1) + \sqrt{1 + 8C_{cl}(2C_{cl} + 2\bar{n} + 1)})^2}\,\mathbb{1} \tag{3.127}$$

$$= 2V_{\hat{\rho}} - \frac{2(2C_{cl} + 2\bar{n} + 1)}{1 + 4C_{cl}\eta(2C_{cl} + 2\bar{n} + 1) + \sqrt{1 + 8C_{cl}(2C_{cl} + 2\bar{n} + 1)}}\mathbb{1} \tag{3.128}$$

$$\xrightarrow{\eta C_{cl} \gg 1} 2V_{\hat{\rho}}. \tag{3.129}$$

Like the Kalman Filter, the Wiener filter produces a variance of the distance $\propto 2V\hat{\rho}$ in the limit of efficient measurements. However, without this limit, the difference does not match the Kalman filter estimate. We saw that fundamentally the anti-causal Wiener filter and the backward Kalman filter derive different estimates, and applying classical techniques to quantum systems should be done with great care. Even though the Kalman filters are essentially classical, the filter equations are derived as the linear Gaussian limit from the SMEs. Thus, we feel their validity is gained from first principle. For the Wiener filter, we only argued the validity in the causal case[19], where we used the QND conditions (3.60); for the anti-causal case, those are not fulfilled. We feel that despite the "small" difference in the filter estimates, without a more fundamental justification for the use of the anti-causal Wiener filter, its application should not be generally admissible.

3.4 SUMMARY

To summarize, this chapter aimed to show the intricacies of the quantum smoothing problem. For the filtering problem, there exists a well-established theory of quantum filtering [6]. Its application relies on the QND conditions (3.60), generally fulfilled in estimating a future system observable. In the linear Gaussian limit, this leads to many applications of classical estimation theory. For retrodiction and subsequently smoothing, the failure of the QND conditions while estimating a variable from the past is the major obstacle to the generalization

18 See also Appendix A.3.2 for details.

19 See Appendix A.3.1.

of Bayesian smoothing to the quantum domain. We hope our discussion of the smoothing problem for a simple optomechanical setup sufficiently illustrated these shortcomings. For filtering, we saw that both suggested filters yielded the same results but had different behaviors in the retrodiction case. Even though classical smoothing seems applicable for the hybrid quantum smoothing scenario, its estimates are often ill-defined [118], and for quantum state verification, the discrepancies of the Wiener and Kalman filter led to different estimates. While these differences will vanish for large cooperativities, blindly applying techniques from classical Bayesian inference to quantum systems seems unwise. Some authors even argue [42] that Bayesian inference may only be used once the QND conditions are fulfilled. Until a sufficient theory of quantum smoothing is found, from which classical smoothing can be obtained as a limit, we want to argue for caution when applying classical techniques to quantum scenarios.

4

COHERENT QUANTUM-NOISE CANCELLATION IN CASCADED SYSTEMS

In Chapter 2, we discussed how the back-action from radiation pressure inadvertently limits the measurement precision in optomechanical sensors. The imposed limit is the so-called *standard quantum limit* (SQL). Whereas the previous chapter discussed how to decrease the uncertainty about quantum systems based on estimation techniques, this chapter will discuss how to improve measurement accuracy by evading some of the back-action noise. Section 4.1 introduces some of these techniques under the umbrella term *back-action evading techniques*. One of these approaches, named *coherent quantum-noise cancellation* (CQNC) by Tsang and Caves [120], will be the focus of our subsequent discussion. In Section 4.2, we will introduce a possible realization of an all-optical CQNC scheme for application in a cascaded arrangement and give a theoretical investigation of its noise reduction performance. This chapter will conclude with an outlook on possible advancements upon our suggested setup and further research ideas regarding back-action evasion techniques in cascaded systems. Most of this chapter is based on our publication [106].

4.1 BACK-ACTION EVADING TECHNIQUES

The SQL, as introduced in Section 2.3.2, arises from two competing noise sources; the shot noise and the radiation pressure noise. Fundamentally this limit is induced by the uncertainty relation of the input amplitude and phase quadrature, $\hat{x}_{in}$ and $\hat{p}_{in}$. However, the SQL is not a fundamental limit, and many ideas to overcome this limit were already introduced in the 80's [20], long before experiments were able to reach the SQL.

For a continuous-time measurement, the limitation of the measurement precision is given by the fact that the position operator of a harmonic oscillator does not commute with itself for all times during the measurement. Under inspection of this commutation relation

$$[\hat{X}(t), \hat{X}(0)] = \frac{\sin \omega_m t}{m\omega_m} [\hat{P}_0, \hat{X}_0], \tag{4.1}$$

we see that for certain times the commutator will vanish. If we choose $t_n = \frac{n\pi}{\omega_m}$, where n is an arbitrary integer, $[\hat{X}(t_n), \hat{X}(0)] = 0$. Thus, the back-action will be evaded for measurements at these particular times[1], and the position can be measured with arbitrary precision. A measurement of this kind is called a *stroboscopic* measurement [20]. It was experimentally realized for atoms [126],

1 Technically, the back-action has not disappeared, but at these times, it is confined in the orthogonal quadrature, which is never measured.

and for mechanical resonators, there are stroboscopic schemes available [12, 17], but it has never been shown experimentally. We refer to the Ph.D. thesis of Rossi [102] for some preliminary results.

The basic principle of stroboscopic measurements and all the following techniques to beat the SQL was already introduced in Chapter 3; the concept of a *quantum non-demolition* (QND) measurement. For a QND measurement, one measures an auto-commuting variable, i.e., a variable which commutes with itself for all times t. In this, the measurement will not disturb the measured observable, and the back-action is *evaded*. Therefore, back-action evading and QND measurements can be treated synonymously.

A pragmatic approach to achieve a QND measurement is to measure a different observable altogether. In contrast to the position, the momentum of a mechanical oscillator forms an auto-commuting observable. This idea is called *speed meter* [11] and gained much consideration, especially in the gravitational wave community [71, 27, 43, 129, 28], but was not yet realized experimentally.

Another option, as described in [74], is to impose modifications upon the input or output of the OMS, rendering the apparatus itself into a QND device. One prominent example of such a modification used in gravitational wave detectors was also introduced in Chapter 3. In Figure 3.1, we showed a so-called squeezed state, which has one of its quadrature variances decreased while the other is enlarged. By choosing the squeezing angle of the input state wisely, one can surpass the SQL. This is akin to the interaction in Equation (2.128) that leads to the SQL itself, as based on the input power, the shot noise or radiation pressure can be enlarged or decreased relative to the signal. This frequency-dependent squeezing is called *ponderomotive squeezing* and entails that if we wanted to beat the SQL with squeezed input light, the squeezing angle needs to be different for each frequency, resulting in *frequency-dependent squeezing* [124, 8, 61]. Similarly, one could choose the measurement angle carefully for each frequency; this technique is known as *variational readout* [128, 74, 70]. Many of the techniques mentioned above were developed for gravitational wave detectors. For more details and further reading, we refer to the excellent review by Danilishin, Khalili and Miao [29].

In a more general approach, one can achieve a QND measurement by introducing another system that acts like a reference frame with an effective negative mass [100]. This can be seen in the following. Let us revisit the equations of motion of a harmonic oscillator with eigenfrequency ω_m and mass m as in Equation (2.106b),

$$\hat{X}(t) = \hat{X}_0 \cos \omega_m t + \frac{\hat{P}_0}{m\omega_m} \sin \omega_m t. \tag{4.2}$$

As stated above, $\hat{X}(t)$ can not be measured with arbitrary precision because of the commutation relation of $\hat{X}_0$ and $\hat{P}_0$. Including another harmonic oscillator as a reference system with the same eigenfrequency ω_m but momentum $\hat{P}'$,

position $\hat{X}'$, and mass m', one can then perform a measurement relative to this reference. The equation of motion of this relative position is

$$\hat{X}(t) - \hat{X}'(t) = (\hat{X}_0 - \hat{X}'_0)\cos\omega_m t + \left(\frac{\hat{P}_0}{m\omega_m} - \frac{\hat{P}'_0}{m\omega_m}\right)\sin\omega_m t. \tag{4.3}$$

By choosing the mass of the reference $m' = -m$, this turns into a commuting observable

$$\hat{X}(t) - \hat{X}'(t) = (\hat{X}_0 - \hat{X}'_0)\cos\omega_m t + \frac{\hat{P}_0 + \hat{P}'_0}{m'\omega_m}\sin\omega_m t, \tag{4.4}$$

because the difference of positions commutes with the sum of momenta, i.e.,

$$[\hat{X}_0 - \hat{X}'_0, \hat{P}_0 + \hat{P}'_0] = [\hat{X}_0, \hat{P}_0] - [\hat{X}'_0, \hat{P}'_0] = 0. \tag{4.5}$$

A negative mass amounts to a negative eigenfrequency for the dimensionless position and momentum operators $\hat{x}_m$ and $\hat{p}_m$. Thus, measuring with respect to a negative-mass reference can perform a QND measurement. This idea was first experimentally utilized in demonstrating Einstein-Podolsky-Rosen (EPR) states of two atomic spin oscillators of positive and negative mass [63]. Based on this, back-action cancellation was demonstrated by Wasilewski et al. [133] in the context of magnetometry. Extending this idea, several proposals have been made in a hybrid setting of a mechanical oscillator and atomic spin ensembles [47, 100]. The evasion of back-action noise in these spin ensembles was experimentally verified in [94].

Independently of this, Tsang and Caves [120] developed their idea of *coherent quantum-noise cancellation* (CQNC). The main principle is to introduce an "anti-noise" path to the dynamics of the optomechanical sensor, which couples the noise $\hat{x}_c^{in}$ to the measured phase quadrature $\hat{p}_{out}$ in just the right way that it cancels the radiation pressure noise[2]. This is best viewed in the form of the flowchart provided in [120], see Figure 4.1. The trick to ensure this cancellation happens correctly is introducing another oscillator that facilitates this "anti-noise" path. This oscillator will act like a negative-mass reference to the mechanical oscillator for perfect cancellation; we refer to this reference as (effective) *negative-mass oscillator* (NMO). Thus, CQNC can also be seen as measuring with respect to a negative mass. In the original proposal of CQNC, Tsang and Caves gave a possible implementation of a NMO by two optical cavities. Details and experimental feasibility of this all-optical NMO were discussed in more detail by Wimmer et al. [141]. Many other possible negative-mass oscillators and setups have been considered within the area of CQNC force sensing. Other setups include the use of ultra-cold atoms inside a separate cavity [4, 39], hybrid optomechanical cavity, i.e., implementing an atomic ensemble inside the optomechanical sensor [91, 109] and employing Bose-Einstein condensates [149]. Even a new all-optical setup was suggested using two detuned optical modes inside the force sensor [145]. These approaches can be categorized into integrated setups, where the effective negative mass is introduced directly into the

2 They interfere destructively, similar to how noise-canceling headphones work.

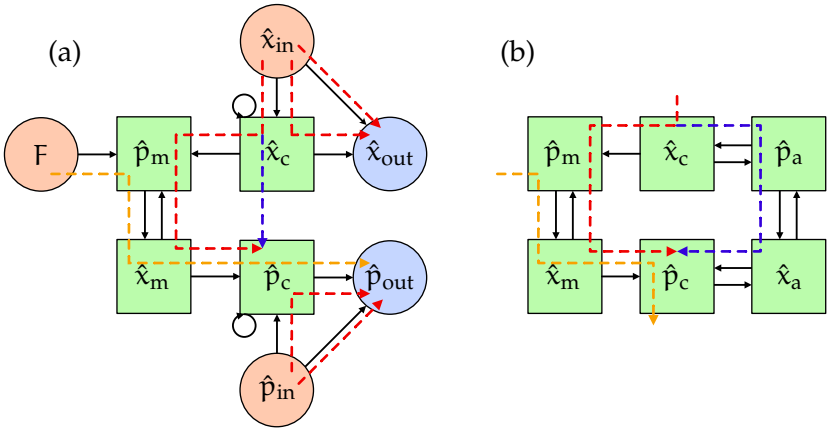

Figure 4.1: Flowchart of the Quantum Langevin equations (2.124) adapted from [120]. Green squares describe the quadratures of the systems, red circles the input variables and blue circles the output. Black lines show which terms enter the evolution of the quadratures. The orange dashed line depicts the signal flow, the red dashed line the noise flow, and the blue dashed the anti-noise flow. (a) shows the complete Langevin equations plus the suggested anti-noise path. (b) shows the suggested implementation of the anti-noise path in the form of the ancilla cavity $\hat{x}_a, \hat{p}_a$.

optomechanical force sensor, and cascaded setups [19, 37], where the NMO is a separate system. Recently, Zeuthen et al. [147] considered a broad class of NMOs in a cascaded setting and even considered a possible coupling between the positive- and negative-mass oscillators in a parallel topology.

All of these concepts, QND, back-action evasion or CQNC are connected under the term *quantum mechanics-free subspace* (QMFS) [121]. Essentially, this is a system composed of only QND observables, hence *free* from the limitations of quantum mechanics.

4.2 OPTICAL CQNC IN CASCADED SYSTEMS

The experimental realization of the all-optical CQNC scheme has been a significant driver in our group [140, 111]. Since the first study on the experimental feasibility of such a setup [141], the proposed design has undergone many design revisions, and many lessons were learned from the analysis of possible components for an all-optical CQNC experiment. A comprehensive overview of this can be found in the Ph.D. thesis of Steinmeyer [111]. Building on the work of our predecessors, we want to discuss the cascaded version of the original all-optical setup [120, 141]. Instead of implementing the "anti-noise" path directly into the optomechanical sensor, an all-optical NMO is built as a separate system. The back-action is then canceled by coupling the OMS to the NMO via a strong coherent field. We investigate the conditions for ideal CQNC of this setup, the effects of deviations from these ideal conditions, and provide a case study for a possible experiment. As the system order can be chosen freely in this cascaded scenario, all discussions will be with regard to the order of the subsystems.

4.2.1 *Cascaded Systems*

Our criterion for the performance of our scheme will be the force spectrum of the added noise in the output phase quadrature. To derive this quantity, we first note that our systems will be linear Gaussian systems. Thus, they obey Quantum Langevin equations, as shown for the OMS in (2.124), and the output is found via the input-output formalism. For a field operator $\hat{a}$, we find the Langevin equation

$$\frac{d}{dt}\hat{a} = \frac{i}{\hbar}[\hat{H}, \hat{a}] - \frac{\kappa}{2}\hat{a} + \sqrt{\kappa}\hat{a}_{in}, \tag{4.6}$$

which is essentially the Heisenberg equivalent of the Lindblad equation (2.86) with an additional driving term. The damping term $\propto \kappa\hat{a}$ can be inserted into the commutator by introducing an effective non-Hermitian Hamiltonian $\hat{H}_{eff} = \hat{H} - i\hbar\frac{\kappa}{2}\hat{a}^\dagger\hat{a}$. We can then write

$$\frac{d}{dt}\hat{a} = \frac{i}{\hbar}[\hat{H}_{eff}, \hat{a}] + \sqrt{\kappa}\hat{a}_{in}, \tag{4.7}$$

which resembles the classical Langevin equation (2.7) very closely.

We now consider a general linear quantum system with n quadrature operators $\hat{\mathbf{x}}$. The Langevin (4.7) turns into system of differential equations

$$\dot{\hat{\mathbf{x}}}(t) = M_{sys}\mathbf{x}(t) + K_{in}\hat{\mathbf{x}}_{in}(t) + K_{bath}\hat{\mathbf{x}}_{bath}(t). \tag{4.8}$$

Here, we have introduced the drift matrix M_{sys} for the system dynamics, i.e., the evolution given by commutator term with the effective Hamiltonian. The matrix K_{in} facilitates the coupling of the k input quadratures $\hat{\mathbf{x}}_{in}$, and additionally, we introduced m bath quadratures, which act like pure noise channels. This formalism is used frequently in quantum networks [25, 98], in which quantum systems are connected like classical circuits to build complex quantum systems. Again, we see the close connection between linear quantum and classical systems. In vector form, the input-output formalism can be written as

$$\hat{\mathbf{x}}_{out} + \hat{\mathbf{x}}_{in} = K_{in}^\top\hat{\mathbf{x}}, \tag{4.9}$$

connecting the k input quadratures to k output quadratures $\hat{\mathbf{x}}_{out}$. The equations of motion (4.8) can be solved in the Fourier domain, where $\dot{\hat{\mathbf{x}}}(t) = i\omega\hat{\mathbf{x}}(\omega)$. It follows,

$$\hat{\mathbf{x}} = (i\omega\mathbb{1} - M_{sys})^{-1}\left(K_{in}\hat{\mathbf{x}}_{in} + K_{bath}\hat{\mathbf{x}}_{bath}\right). \tag{4.10}$$

Together with Equation (4.9), we derive the output quadratures as

$$\begin{aligned}
\hat{\mathbf{x}}_{out} &= K_{in}^\top\hat{\mathbf{x}} - \hat{\mathbf{x}}_{in} && (4.11)\\
&= \left(K_{in}^\top(i\omega\mathbb{1} - M_{sys})^{-1}K_{in} - \mathbb{1}\right)\hat{\mathbf{x}}_{in} \\
&\quad + K_{in}^\top(i\omega\mathbb{1} - M_{sys})^{-1}K_{bath}\hat{\mathbf{x}}_{bath} && (4.12)\\
&= P_{in}\hat{\mathbf{x}}_{in} + P_{bath}\hat{\mathbf{x}}_{bath} && (4.13)\\
&= T\,\tilde{\mathbf{x}}_{in}, && (4.14)
\end{aligned}$$

where

$$\tilde{\mathbf{x}}_{\text{in}} = \begin{pmatrix} \hat{\mathbf{x}}_{\text{in}} \\ \hat{\mathbf{x}}_{\text{bath}} \end{pmatrix}, \tag{4.15}$$

$$T = (P_{\text{in}}, P_{\text{bath}})\,. \tag{4.16}$$

From this, we can calculate the (symmetrized) spectral density matrix as

$$\delta(\omega - \omega')S_{\text{out}}(\omega) = \frac{1}{2}\langle \hat{\mathbf{x}}_{\text{out}}(\omega)\hat{\mathbf{x}}^{\dagger}_{\text{out}}(\omega')\rangle + \text{c.c.} \tag{4.17}$$

$$= \frac{1}{2}\langle T(\omega)\tilde{\mathbf{x}}_{\text{in}}\tilde{\mathbf{x}}^{\dagger}_{\text{in}}T^{\dagger}(-\omega')\rangle + \text{c.c.} \tag{4.18}$$

$$= \frac{1}{2}\langle T(\omega)S_{\text{in}}T^{\dagger}(-\omega')\rangle + \text{c.c.}, \tag{4.19}$$

with S_{in} the input spectral density matrix.

For our upcoming setup, each subsystem will consist of two harmonic oscillators, i.e., of 4 quadrature operators. Hence the system matrices M_{sys} and bath input matrices K_{bath} are all 4×4-dimensional. The in- and output variables are the two quadratures of the laser light, making the input matrices K_{in} 4×2-dimensional. The bath coupling describes the intrinsic losses of each system. To model losses outside of the systems[3], the output quadratures are mixed with vacuum noise via a beam-splitter interaction[4], which are then

$$\hat{\mathbf{x}}'_{\text{out}} = \underbrace{\begin{pmatrix} 1 & 0 & 0 & 0 \\ 0 & 1 & 0 & 0 \end{pmatrix} \eta_{4\times4} \begin{pmatrix} T & 0 \\ 0 & \mathbb{1} \end{pmatrix}}_{T_{\text{loss}}} \begin{pmatrix} \tilde{\mathbf{x}}_{\text{in}} \\ \mathbf{x}_{\text{vac}} \end{pmatrix}. \tag{4.20}$$

The third matrix describes the transformation of the input variables to the output and introduces additional vacuum terms. The second matrix, $\eta_{4\times4}$, mixes the output and vacuum quadratures in a beam-splitter interaction, and the first matrix is the partial trace, which traces out the signal lost to the bath and vacuum.

Finally, we need to cascade the two subsystems. For this choose $\mathbf{x}_{\text{in},2} = \mathbf{x}'_{\text{out},1}$, where the subscripts 1 and 2 stand for the first and second system. The total output quadratures are then given by

$$\hat{\mathbf{x}}'_{\text{out},2} = T_2^{\text{loss}} \begin{pmatrix} T_1^{\text{loss}} & 0 & 0 \\ 0 & \mathbb{1}_{4\times4} & 0 \\ 0 & 0 & \mathbb{1}_{2\times2} \end{pmatrix} \begin{pmatrix} \hat{\mathbf{x}}_{\text{in}} \\ \hat{\mathbf{x}}_{\text{bath},1} \\ \hat{\mathbf{x}}_{\text{vac},1} \\ \hat{\mathbf{x}}_{\text{bath},2} \\ \hat{\mathbf{x}}_{\text{vac},2} \end{pmatrix} \tag{4.21}$$

$$= T_{\text{total}}\hat{\mathbf{x}}_{\text{in,total}}. \tag{4.22}$$

The spectral densities for the general cases considered here are then calculated from T_{total} in combination with Equation (4.19).

3 We call these propagation losses for the case between system 1 and 2, and detection losses between system 2 and the detector.

4 See Appendix A.2

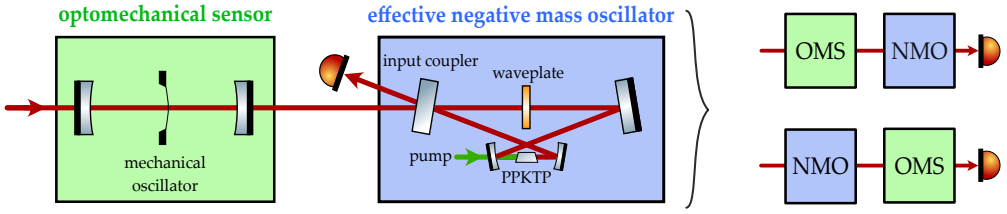

Figure 4.2: Schematic of the proposed cascaded setup. Left: The optomechanical sensor (green) consists of a mechanical oscillator inside an optical cavity, depicted in a membrane-in-the-middle (MiM) setup. The effective negative-mass oscillator (blue) comprises two optical modes coupled via a beam-splitter and down-conversion process. A non-linear (PPKTP) crystal exemplifies the coupling for the down-conversion and a wave plate for the beam-splitter coupling. Right: Simplified depiction of the cascaded scheme showing its two possible arrangements.

4.2.2 *Setup and Ideal CQNC*

A possible realization of our cascaded scheme is illustrated on the left of Figure 4.2. An OMS, subject to an external force and radiation pressure noise, is connected to a NMO by a coherent light field. The force is then measured by detecting outgoing light after the second system. The order of subsystems can be chosen freely, and the two possible arrangements are depicted on the right of Figure 4.2. In the first case, the light travels through the OMS, followed by the NMO. We will refer to this case as OMS $\mapsto$ NMO. In the second case, the order is reversed; hence the light will travel through the NMO first, and we will refer to this case as NMO $\mapsto$ OMS.

The OMS is modeled as described in Section 2.3.2. To arrive at the matrix expressions above, we quickly reiterate the linearized Hamiltonian of such a system. It is given by

$$\hat{H}_{\mathrm{OMS}} = \Delta_{\mathrm{om}}\hat{c}_{\mathrm{om}}^{\dagger}\hat{c}_{\mathrm{om}} + \frac{\omega_{\mathrm{m}}}{2}(\hat{x}_{\mathrm{m}}^2 + \hat{p}_{\mathrm{m}}^2) + \frac{g\hat{x}_{\mathrm{m}}}{\sqrt{2}}(\hat{c}_{\mathrm{om}} + \hat{c}_{\mathrm{om}}^{\dagger}), \tag{4.23}$$

where we introduced the subscript "om" to differentiate the cavity mode in contact with the mechanical resonator and the "main" cavity mode in the negative-mass system. From the Hamiltonian (4.23), we find the drift matrix and the input matrices of the drive and bath as

$$M_{\mathrm{OMS}} = \begin{pmatrix} -\kappa_{\mathrm{om}}/2 & \Delta_{\mathrm{om}} & 0 & 0 \\ -\Delta_{\mathrm{om}} & -\kappa_{\mathrm{om}}/2 & -g & 0 \\ 0 & 0 & 0 & \omega_{\mathrm{m}} \\ -g & 0 & -\omega_{\mathrm{m}} & -\gamma_{\mathrm{m}} \end{pmatrix},$$

$$K_{\mathrm{OMS}}^{\mathrm{in}} = \begin{pmatrix} \sqrt{\kappa_{\mathrm{om}}^{\mathrm{in}}} & 0 \\ 0 & \sqrt{\kappa_{\mathrm{om}}^{\mathrm{in}}} \\ 0 & 0 \\ 0 & 0 \end{pmatrix}, \quad K_{\mathrm{OMS}}^{\mathrm{bath}} = \mathrm{diag}\left(\sqrt{\kappa_{\mathrm{om}}^{\mathrm{bath}}}, \sqrt{\kappa_{\mathrm{om}}^{\mathrm{bath}}}, 0, \sqrt{\gamma_{\mathrm{m}}}\right), \tag{4.24}$$

$$\hat{\mathbf{x}} = (\hat{x}_{\mathrm{om}}, \hat{p}_{\mathrm{om}}, \hat{x}_{\mathrm{m}}, \hat{p}_{\mathrm{m}})^{\top},$$

$$\hat{\mathbf{x}}_{\mathrm{in}} = (\hat{x}_{\mathrm{in}}, \hat{p}_{\mathrm{in}})^{\top},$$

$$\hat{\mathbf{x}}_{\mathrm{bath}} = \left(\hat{x}_{\mathrm{om}}^{\mathrm{bath}}, \hat{p}_{\mathrm{om}}^{\mathrm{bath}}, \hat{x}_{\mathrm{m}}^{\mathrm{bath}}, \hat{p}_{\mathrm{m}}^{\mathrm{bath}}\right)^{\top}.$$

Here, $\Delta_{om} = \omega_{om} - \omega_L$ is the detuning of the optomechanical cavity to the incoming field. $\kappa_{om} = \kappa_{om}^{in} + \kappa_{om}^{bath}$ is the linewidth of the optomechanical cavity, with coupling constants κ_{om}^{in} to the driving field and κ_{om}^{bath} to the bath. ω_m is the eigenfrequency of the mechanical oscillator and γ_m its linewidth. The coupling strength between the light and the mechanical oscillator is g.

For the case of a resonant driving field ($\Delta_{om} = 0$) and no losses ($\kappa_{om}^{bath} = 0$), we recover the output quadratures

$$\hat{x}_{om}^{out} = e^{i\phi}\hat{x}_{om}^{in}, \tag{4.25a}$$

$$\hat{p}_{om}^{out} = e^{i\phi}\hat{p}_{om}^{in} - \chi_m g^2 \kappa_{om}\chi_{om}^2\hat{x}_{om}^{in} + \chi_m\sqrt{\kappa_{om}}g\chi_{om}\sqrt{\gamma_m}\,F, \tag{4.25b}$$

with

$$e^{i\phi} = \frac{\kappa_{om}/2 - i\omega}{\kappa_{om}/2 + i\omega}, \quad \chi_{om} = \frac{1}{i\omega + \kappa_{om}/2}, \quad \chi_m = \frac{\omega_m}{\omega^2 - \omega_m^2 - i\gamma_m\omega}. \tag{4.26}$$

The spectral density of the input into the OMS is given by

$$S_{OMS}^{in} = \frac{1}{2}\,\mathrm{diag}\,(1, 1, 0, 2S_F)\,, \tag{4.27}$$

which is composed of vacuum noise for the optical input and the spectral density of the applied force on the mechanical oscillator[5]. Using the matrix expressions (4.24), we can calculate the output spectral density. We find

$$S_{OMS}^{out} = \frac{1}{2}\begin{pmatrix} 1 & 2G_{om}\,\mathrm{Re}(\chi_m) \\ 2G_{om}\,\mathrm{Re}(\chi_m) & 1 + G_{om}^2|\chi_m|^2 + 2G_{om}|\chi_m|^2\gamma_m S_F \end{pmatrix}, \tag{4.28}$$

with the frequency-dependent measurement strength

$$G_{om} = \kappa_{om}|\chi_m|^2 g^2 = \Gamma_{om}\frac{(\frac{\kappa_{om}}{2})^2}{\omega^2 + (\frac{\kappa_{om}}{2})^2} \tag{4.29}$$

as defined in Section 2.3.2. We see the measurement strength has a Lorentzian shape, and its maximum is the optomechanical readout rate $\Gamma_{om} = \frac{4g^2}{\kappa_{om}}$. The spectral density of the added noise is given as the noise-to-signal ratio in the output phase spectrum in (4.28). Therefore, we simply need to divide $S_{\hat{p}_{om}\hat{p}_{om}}^{out}$ by the pre-factor of S_F. Doing so for the output of the OMS (4.28) recovers the SQL as given in Equation (2.128)[6].

The all-optical NMO, as suggested by [120], consists of two optical modes $\hat{c}_c$ and $\hat{a}$, with resonance frequencies ω_c and ω_a. In order to behave like an OMS, a beam-splitter and a down-conversion process are added. These should mimic the two components of the linearized radiation pressure interaction. In analogy to [141, 111], we refer to ω_c as the *meter* cavity and ω_a as the *ancilla* cavity. The Hamiltonian of this system is given by

$$\hat{H}_{NMO} = \Delta_c\hat{c}_c^\dagger\hat{c}_c + \Delta_a\hat{a}^\dagger\hat{a} + g_{BS}(\hat{a}\hat{c}_c^\dagger + \hat{a}^\dagger\hat{c}_c) + g_{DC}(\hat{a}\hat{c}_c + \hat{a}^\dagger\hat{c}_c^\dagger), \tag{4.30}$$

5 The force contains the thermal noise and all other forces. Thermal noise will be neglected until the case study.

6 Except for the thermal noise, which we neglect.

with the detunings $\Delta_{c,a} = \omega_{c,a} - \omega_L$, the beam-splitter coupling strength g_{BS} and the coupling strength of the down-conversion process g_{DC}. Similarly to the OMS, we can construct the matrix expressions of the NMO as

$$
\begin{aligned}
M_{NMO} &= \begin{pmatrix} -\kappa_c/2 & \Delta_c & 0 & g_{BS} - g_{DC} \\ -\Delta_c & -\kappa_c/2 & -(g_{BS} + g_{DC}) & 0 \\ 0 & g_{BS} - g_{DC} & -\kappa_a/2 & \Delta_a \\ -(g_{BS} + g_{DC}) & 0 & -\Delta_a & -\kappa_a/2 \end{pmatrix}, \\
K^{in}_{NMO} &= \begin{pmatrix} \sqrt{\kappa_c^{in}} & 0 \\ 0 & \sqrt{\kappa_c^{in}} \\ 0 & 0 \\ 0 & 0 \end{pmatrix}, \quad
\begin{aligned}
K^{bath}_{NMO} &= \operatorname{diag}\left(\sqrt{\kappa_c^{bath}}, \sqrt{\kappa_c^{bath}}, \sqrt{\kappa_a}, \sqrt{\kappa_a}\right), \\
\hat{\mathbf{x}} &= (\hat{x}_c, \hat{p}_c, \hat{x}_a, \hat{p}_a)^\top, \\
\hat{\mathbf{x}}_{in} &= (\hat{x}_{in}, \hat{p}_{in})^\top, \\
\hat{\mathbf{x}}_{bath} &= \left(\hat{x}_c^{bath}, \hat{p}_c^{bath}, \hat{x}_a^{bath}, \hat{p}_a^{bath}\right)^\top.
\end{aligned}
\end{aligned}
\tag{4.31}
$$

Here, κ_c is the linewidth of the meter cavity, and κ_a is the ancilla cavity linewidth. As we only drive the meter cavity, the linewidth of the ancilla cavity couples fully to the bath, i.e., it acts only as a noise channel. To imitate the radiation pressure interaction, we set $g_{BS} = g_{DC} = \frac{1}{2} g_a$ with the coupling strength g_a being the negative-mass counterpart to the coupling g. Assuming that the beam-splitter and down-conversion couplings are matched, we turn to a similar scenario for the OMS above. In the lossless case ($\kappa_c^{bath} = 0$) and driving the meter cavity on resonance ($\Delta_c = 0$), we find the output quadratures of the NMO as

$$
\begin{aligned}
x_c^{out} &= e^{i\theta} x_c^{in}, \\
p_c^{out} &= e^{i\theta} p_c^{in} - \chi_a g_a^2 \kappa_c \chi_c^2 x_c^{in} \\
&\quad + \chi_a \sqrt{\kappa_c} g_a \chi_c \sqrt{\kappa_a} \left(\frac{\kappa_a/2 + i\omega}{\Delta_a} x_a^{in} + p_a^{in} \right),
\end{aligned}
\tag{4.32}
$$

with

$$
e^{i\theta} = \frac{\frac{\kappa_c}{2} - i\omega}{\frac{\kappa_c}{2} + i\omega}, \quad \chi_c = \frac{1}{i\omega + \kappa_c/2}, \quad \chi_a = \frac{\Delta_a}{(\omega^2 - \Delta_a^2 - \frac{\kappa_a^2}{4}) - i\kappa_a \omega}. \tag{4.33}
$$

In analogy to the mechanical susceptibility χ_m, we have introduced χ_a as the susceptibility of the ancilla cavity. Because Δ_a can be negative, we can use the ancilla cavity detuning to make the NMO act like a negative-mass reference. The input spectral density of the NMO consists only of vacuum noise

$$
S^{in}_{NMO} = \frac{1}{2} \operatorname{diag}(1, 1, 1, 1), \tag{4.34}
$$

as it is only composed of optical modes. Undergoing the same procedure as for the OMS, we find the output spectral density matrix for the NMO as

$$
S^{out}_{NMO} = \frac{1}{2} \begin{pmatrix} 1 & 2G_a \operatorname{Re}(\chi_a) \\ 2G_a \operatorname{Re}(\chi_a) & 1 + G_a^2 |\chi_a|^2 + 2G_a |\chi_a|^2 \kappa_a \left(\frac{\omega^2 + \kappa_a^2/4}{\Delta_a^2} + 1 \right) \end{pmatrix}. \tag{4.35}
$$

To complete the symmetry between the OMS and the NMO, we introduced the frequency-dependent measurement strength of the NMO,

$$G_a(\omega) = g_a^2 \kappa_c |\chi_c(\omega)|^2 = \Gamma_a \frac{(\frac{\kappa_c}{2})^2}{\omega^2 + (\frac{\kappa_c}{2})^2}, \tag{4.36}$$

with $\Gamma_a = \frac{4\, g_a^2}{\kappa_c}$ the readout rate of the NMO. Under matched beam-splitter and down-conversion coupling, we see a complete symmetry between the output quadratures, Equations (4.25) and (4.32), and output spectra Equations (4.28) and (4.35) of the systems. Our setup aims to couple the two systems so that the back-action noise in the force spectrum will cancel, allowing for a sub-SQL performance. In our dual-cavity setup, this is done by cascading the two systems and matching the parameters of the NMO accordingly.

As seen in Figure 4.2, the whole scheme has two possible arrangements. Thus, to cascade the systems, we choose $x_c^{out} = x_{om}^{in}$ and $p_c^{out} = p_{om}^{in}$ for the case NMO $\mapsto$ OMS and $x_{om}^{out} = x_c^{in}$ and $p_{om}^{out} = p_c^{in}$ for OMS $\mapsto$ NMO. For ideal CQNC, the order will not matter, as shown in Appendix A.4. We will discuss cases that depend on the order in Sections 4.3.3 and 4.3.4. After cascading the two systems according to the procedure in Equation (4.21), we can find the noise-to-signal ratio in the phase spectrum. The added noise spectral density is

$$\begin{aligned} S_F = &\frac{1}{2G_{om}\gamma_m|\chi_m|^2} \\ &+ \frac{G_a^2|\chi_a|^2 + G_{om}^2|\chi_m|^2 + 2\, G_a G_{om}\Re(\chi_m \chi_a^*)}{2G_{om}\gamma_m|\chi_m|^2} \\ &+ \frac{G_a \kappa_a |\chi_a|^2}{2G_{om}\gamma_m|\chi_m|^2}\left(\frac{\omega^2 + \kappa_a^2/4}{\Delta_a^2} + 1\right). \end{aligned} \tag{4.37}$$

The terms in Equation (4.37) are shot-noise (first term), back-action noise (second term) and shot noise from the ancilla cavity (last term). The back-action noise is then canceled if the conditions are such that

$$g_{BS} = g_{DC} = \frac{1}{2} g_a, \tag{4.38}$$

$$G_{om}(\omega) = G_a(\omega), \tag{4.39}$$

$$\chi_m(\omega) = -\chi_a(\omega), \tag{4.40}$$

for all ω. This means that the NMO must admit a similar radiation pressure interaction as the OMS and that the light should couple to the ancilla cavity with the same strength as to the mechanical oscillator. Considering the explicit form of condition (4.40),

$$\chi_m(\omega) = -\chi_a(\omega) \tag{4.41}$$

$$\Leftrightarrow \frac{\omega_m}{(\omega^2 - \omega_m^2) - i\gamma_m\omega} = \frac{\Delta_a}{(\omega^2 - \Delta_a^2 - \frac{\kappa_a^2}{4}) - i\kappa_a\omega}, \tag{4.42}$$

this entails further restrictions:

1. The detuning of the ancilla cavity to the meter cavity is

$$\Delta_a = -\omega_m. \tag{4.42a}$$

As described in Section 4.1, a negative mass amounts to a negative eigenfrequency for harmonic oscillators. Therefore, detuning the ancilla cavity to $-\omega_m$ turns it into the negative-mass reference frame for the mechanical oscillator ω_m.

2. The linewidth of the ancilla cavity κ_a should match the damping rate of the mechanical oscillator

$$\kappa_a = \gamma_m, \tag{4.42b}$$

to mimic the oscillating behavior of the mechanical oscillator.

3. The susceptibilities χ_m and χ_a differ by a factor $\kappa_a^2/4$. This is because of the asymmetric coupling of the mechanical oscillator and the optical ancilla to the bath. To alleviate this, the detuning $|\Delta_a| \gg \kappa_a$, and together with forgoing items, implies the resolved sideband limit of the ancilla cavity

$$\omega_m \gg \kappa_a, \tag{4.42c}$$

and a large quality factor of the mechanical oscillator,

$$Q_m = \frac{\omega_m}{\gamma_m} \gg 1. \tag{4.42d}$$

These conditions are similar to the integrated setup [141], but instead of the coupling strength g_a and g, the measurement strengths G_a and G_{om} need to match. The effect of the NMO under these conditions is best seen in Figure 4.3. The output of the OMS experiences ponderomotive squeezing through the radiation pressure interaction. For the perfectly matched NMO, its output is squeezed such that the combination of both will result in a non-squeezed output. In this sense, CQNC can be understood as undoing ponderomotive squeezing[7].

Assuming conditions (4.38)–(4.40) are met, the back-action term in Equation (4.37) will vanish, and we arrive at

$$S_F = \frac{1}{2G_{om}\gamma_m|\chi_m|^2} + \frac{1}{2}\left(\frac{\omega^2 + \gamma_m^2/4}{\omega_m^2} + 1\right), \tag{4.43}$$

which contains only shot-noise contributions of the measured phase quadrature (first term) and the ancilla cavity (second term). The contribution of the OMS, proportional to the measurement strength G_{om} is the *quantum Cramér-Rao bound* [123, 90, 72], sometimes referred to as the *fundamental quantum limit* (FQL)[29] or *energetic quantum limit* [13]. If not for the residual shot noise of the ancilla cavity, this scheme would put us at the fundamental bound of parameter estimation.

7 We find this viewpoint extremely helpful.

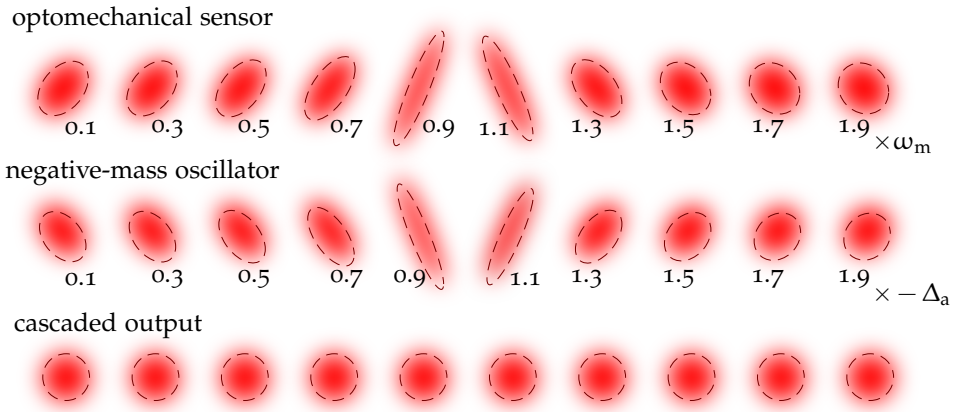

Figure 4.3: Output spectra of matched cascaded setup for different frequencies. First row, ponderomotive squeezing induced within the OMS. Second row, squeezing over frequency generated by the matched NMO. Third row is the output after a cascade of the first two rows. Adapted from [111].

However, in the limit of large measurement strength, we arrive at the lower bound of

$$S_F(\omega) \geqslant \frac{1}{2}\left(\frac{\omega^2+\gamma_m^2/4}{\omega_m^2}+1\right) \equiv S_{CQNC}(\omega). \tag{4.44}$$

Combining Equations (2.130) and (4.44) we find

$$S_{CQNC} = S_{SQL} \times \frac{1}{2Q_m}\left(\frac{\omega^2+\gamma_m^2/4+\omega_m^2}{\sqrt{(\omega^2-\omega_m^2)^2+\gamma_m^2\omega^2}}\right). \tag{4.45}$$

Thus, for $Q_m \gg 1$, we can summarize

$$S_{CQNC} = S_{SQL} \times \begin{cases} 1 & \text{on resonance } \omega = \omega_m \\ 1/(2Q_m) & \text{off resonance } \omega \lessgtr \omega_m. \end{cases} \tag{4.46}$$

In conclusion, under the additional condition that $G_{om} = G_a$, the cascaded setup reproduces the same findings of [141], leading to an enhancement in performance up to a factor of $2Q_m$ off-resonance and SQL performance on resonance. Due to the additional shot noise from the ancilla cavity, the CQNC scheme is not bounded by the quantum Cramér-Rao bound, showing that back-action evasion alone is not enough to achieve the fundamental limits in parameter estimation [123].

4.3 IMPERFECT CQNC

The conditions (4.38)–(4.40) are the ideal case for a perfect cancellation of quantum back-action noise and will not be satisfied in an actual experiment. Therefore, we will discuss possible imperfections and their impact on the performance of our cascaded scheme. These imperfections include mismatches to the

Table 4.1: Parameters of the optomechanical sensor used in Figs. 4.4 to 4.7

Parameter		Norm. value	Value
ω_m	mechanical resonance frequency	1	500 kHz
γ_m	mechanical linewidth	$10^{-3}\,\omega_m$	500 Hz
Q_m	mechanical quality factor	$\frac{\omega_m}{\gamma_m}$	1000
κ_{om}	optomechanical cavity linewidth	$10\,\omega_m$	5 MHz

parameters in Equations (4.38)–(4.40), and possible losses. Another degree of freedom of our setup is the order in which the light passes through the subsystems (NMO $\mapsto$ OMS or OMS $\mapsto$ NMO), but this will only affect the force sensing performance for imperfections that directly affect the force signal. The cases where the order does not matter are shown in Appendix A.4. Data shown in the figures of this section refer to an OMS given by the parameters in Table 4.1.

4.3.1 *Non-Ideal Ancilla Cavity Linewidth* $\kappa_a \neq \gamma_m$

The strictest requirement for an all-optical CQNC setup is to match the ancilla cavity linewidth to the damping rate of the mechanical oscillator. Assuming all conditions for ideal CQNC are matched, except $\kappa_a \neq \gamma_m$. Since the measurement strengths, $G_{om} = G_a$, are matched for all frequencies, and we assume no propagation losses between the system, this effectively reduces to the integrated CQNC setup [141]. The spectral density of added noise (4.37) in this case becomes

$$\begin{aligned} S_F = &\frac{1}{2G_{om}\gamma_m|\chi_m|^2} + \frac{G_{om}}{2\gamma_m}\left|\frac{\chi_m+\chi_a}{\chi_m}\right|^2 \\ &+ \frac{\kappa_a|\chi_a|^2}{2\gamma_m|\chi_m|^2}\left(\frac{\omega^2+\kappa_a^2/4}{\omega_m^2}+1\right). \end{aligned} \tag{4.47}$$

For an optimal G_{om}, we find the minimal spectral density for the added noise,

$$S_F = \frac{|\chi_m+\chi_a|}{\gamma_m|\chi_m|} + \frac{\kappa_a|\chi_a|^2}{2\gamma_m|\chi_m|^2}\left(\frac{\omega^2+\kappa_a^2/4}{\omega_m^2}+1\right) \tag{4.48}$$

This is composed of measurement shot and back-action noise (first term) and noise introduced by the ancilla cavity (second term). The second term will dominate the first one for frequencies off-resonance, setting a bound to the achievable performance. The ratio between the spectral density (4.48) and the SQL is

$$S_F = \frac{\kappa_a}{2\,\omega_m} \times S_{SQL}, \tag{4.49}$$

for $\kappa_a < 2\omega_m$. For $\kappa_a \gg \omega_m$, the effect of CQNC will vanish for low frequencies, converging to the SQL, while for large frequencies, the added noise is larger than

the SQL. This is illustrated in Figure 4.4. Condition 4.49 renders our setup unusable for gravitational wave detectors, as these operate in the free-mass limit $\omega_m \to 0$. However, this is not a show-stopper for tabletop experiments with micromechanical resonators. These mechanical oscillators usually have eigenfrequencies in the order of hundredth of kHz.

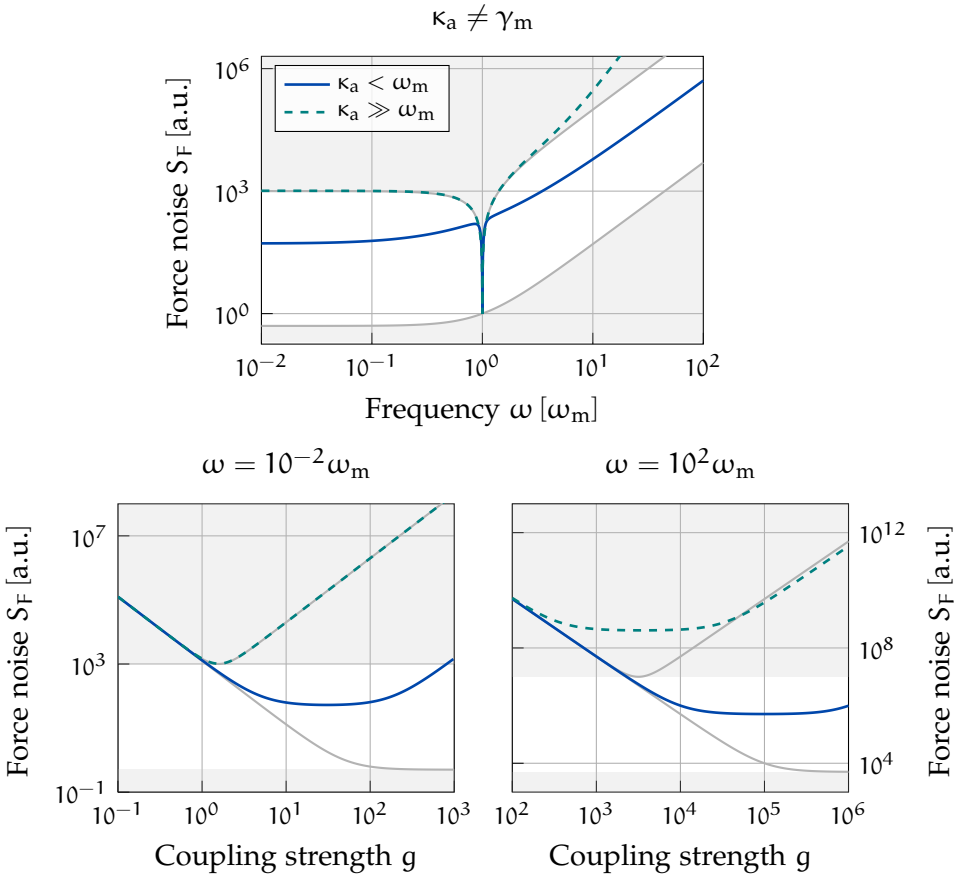

Figure 4.4: Imperfect matching of the ancilla cavity and mechanical linewidth. Top row: Achievable force noise levels for a mismatch between ancilla cavity linewidth κ_a and damping rate of the mechanical oscillator γ_m over frequency ω. For $\kappa_a < \omega_m$, an improvement of $\kappa_a/2\omega_m$ can be achieved off-resonance (solid blue). For $\kappa_a \gg \omega_m$, the effect of CQNC is completely canceled for low frequencies, and the sensitivity is worse than the SQL for high frequencies (dashed teal). Bottom row: Corresponding force sensitivity over coupling strength g for low frequencies (left) and high frequencies (right). The shaded areas mark the bounds for sub-SQL sensitivity, from below the fundamental limit given by Equation (4.44) and from above the SQL given by Equation (2.130). The gray lines in the bottom row show the force noise for ideal CQNC conditions and no back-action evasion. Parameters are given in Table 4.1.

4.3.2 *Unequal Measurement Strengths* $G_{om} \neq G_a$

Next, we consider a mismatch of the measurement strengths $G_a \neq G_{om}$, while matching the other CQNC conditions. This entails unmatched cavity linewidth $\kappa_c \neq \kappa_{om}$ and unmatched couplings $g_a \neq g$. Introducing parameters for the linewidth mismatch $\kappa_c = \epsilon\,\kappa_{om}$ and coupling mismatch $g_a = \sqrt{\delta}g$, we find for the spectral density

$$\begin{aligned} S_F = &\frac{1}{2G_{om}\gamma_m|\chi_m|^2} + \frac{G_{om}}{2\gamma_m}\left|1-\delta\epsilon\frac{|\chi_c|^2}{|\chi_{om}|^2}\right|^2 \\ &+ \delta\epsilon\frac{|\chi_c|^2}{|\chi_{om}|^2}\frac{1}{2}\left(\frac{\omega^2+\gamma_m^2/4}{\omega_m^2}+1\right). \end{aligned} \tag{4.50}$$

For suitable couplings g and cavity linewidth κ, we can find a frequency where the back-action term in Equation (4.50) will vanish, and ideal CQNC is possible. This is the case when the Lorentzians G_a and G_{om} are such that they will intersect at a frequency $\omega \neq 0$. We find that

$$\omega_* = \pm\sqrt{\frac{\delta\,\epsilon-\epsilon^2}{1-\delta\,\epsilon}}\frac{\kappa_{om}}{2} \tag{4.51}$$

is a real-valued frequency for the following parameters:

$$g_a = g \quad \Rightarrow \quad \kappa_c < \kappa_{om} \quad \text{or} \quad \kappa_c > \kappa_{om}, \tag{4.52a}$$

$$g_a < g \quad \Rightarrow \quad \epsilon > \frac{1}{\delta} \quad \text{or} \quad \epsilon < \delta, \tag{4.52b}$$

$$g_a > g \quad \Rightarrow \quad \epsilon > \delta \quad \text{or} \quad \epsilon < \frac{1}{\delta}. \tag{4.52c}$$

Consequently, a cavity linewidth mismatch can compensate for every possible matching condition of the couplings, and ideal CQNC can be achieved at ω_*. Equation (4.50) takes the shape of an inverse Lorentz around the frequency ω_*. To estimate the linewidth around the newfound dip, consider Equation (4.50) for an optimal G_{om}. We find,

$$S_F = \frac{1}{\gamma_m|\chi_m|}\left|1-\delta\epsilon\frac{|\chi_c|^2}{|\chi_{om}|^2}\right| + \delta\epsilon\frac{|\chi_c|^2}{|\chi_{om}|^2}\frac{1}{2}\left(\frac{\omega^2+\gamma_m^2/4}{\omega_m^2}+1\right) \tag{4.53}$$

$$= S_{SQL}\left|1-\delta\epsilon\frac{|\chi_c|^2}{|\chi_{om}|^2}\right| + \delta\epsilon\frac{|\chi_c|^2}{|\chi_{om}|^2}S_{CQNC} \tag{4.54}$$

$$= S_{SQL}|1-\delta\epsilon|\,|\chi_c|^2\,|(\omega+\omega_*)(\omega-\omega_*)| + \delta\epsilon\frac{|\chi_c|^2}{|\chi_{om}|^2}S_{CQNC}. \tag{4.55}$$

Moving now to the inverse, we determine the linewidth around ω_*

$$1/S_F = \frac{1}{S_{SQL}|1-\delta\epsilon|\,|\chi_c|^2\,|\omega^2-\omega_*^2| + \delta\epsilon\frac{|\chi_c|^2}{|\chi_{om}|^2}S_{CQNC}} \tag{4.56}$$

$$= \frac{1}{S_{SQL}|1-\delta\epsilon|\,|\chi_c|^2}\frac{1}{|\omega^2-\omega_*^2| + \frac{\delta\epsilon}{|\chi_{om}|^2}\frac{S_{SQL}}{S_{CQNC}}} \tag{4.57}$$

$$= \frac{1}{S_{SQL}|1-\delta\epsilon|\,|\chi_c|^2}\frac{1}{|\omega^2-\omega_*^2| + \frac{\delta\epsilon}{|\chi_{om}|^2}\frac{1}{2Q_m}}, \tag{4.58}$$

where we used Equation (4.46) for the last step, assuming we are far off-resonance. Thus, if ω_* is far away from the resonance frequency, the linewidth of this "dip" is $\propto 1/Q_m$.

For non-vanishing back-action, we can again minimize the spectral density (4.50) with an optimal G_{om}. Turning to the low-frequency limit ($\kappa_{c,om} \gg \omega$), the measurement strengths become frequency independent, $G_{om,a} \to \Gamma_{om,a}$, and the ratio $|\chi_c|^2/|\chi_{om}|^2 \to 1/\epsilon^2$. The minimal noise spectral density is then

$$S_F = |1 - \frac{\delta}{\epsilon}| \times S_{SQL} + \left(\frac{\delta}{\epsilon}\right) \times S_{CQNC}. \tag{4.59}$$

Ideal CQNC can be recovered for $\epsilon = \delta$, which means $\Gamma_{om} = \Gamma_a$. Hence, as long as the rate at which the back-action information leaks out of the system is matched, ideal CQNC is possible for low frequencies.

For the converse case ($\kappa_{c,om} \ll \omega$) the cavity susceptibilities $|\chi_c|^2 \approx |\chi_{om}|^2$, effectively cancelling in Equation (4.50). The optimal spectral density becomes

$$S_F = |1 - \delta\,\epsilon| \times S_{SQL} + (\delta\,\epsilon) \times S_{CQNC}. \tag{4.60}$$

In this case, ideal CQNC can be recovered for $\delta = 1/\epsilon$, which entails $g_a^2\kappa_c = g^2\kappa_{om}$. We have depicted our main findings in Figure 4.5.

We also considered a combination of the imperfections discussed in this section. If, for example, $G_{om} \neq G_a$ and additionally $\kappa_a \neq \gamma_m$, the noise spectral density will be a combination of Equations (4.47) and (4.50). In this case, the cancellation of back-action noise is possible for the cases discussed above, but the ancilla cavity noise floor is higher because of the linewidth mismatch $\gamma_m \neq \kappa_a$. Thus, our findings will remain the same, but the achievable performance off-resonance is given by the noise spectral density in Equation (4.49). Similar consideration is taken for the linewidth of the peak. The linewidth will be $\propto \kappa a/(2\omega_m)$ instead of $\propto 1/Q_m$.

4.3.3 *Losses*

We first consider propagation losses, which occur between the first and the second system. The propagation losses are modeled by mixing the first system's output signal with vacuum in a beam-splitter-like interaction; see Appendix A.2. This leads to a modified output signal,

$$x'_{out} = \sqrt{\eta}\, x_{out} + \sqrt{1-\eta}\, x_{vac}, \tag{4.61}$$

where x_{vac} represents the vacuum field and $\eta \in [0, 1]$ is the efficiency of the process. Due to this additional noise, information about the back-action interaction of the first system is lost to the vacuum; hence perfect cancellation of back-action noise is not possible. As before, we can find an optimal coupling strength to minimize the additional noise. For the system order NMO $\mapsto$ OMS, we achieve a minimal spectral density of

$$S_F = \sqrt{1-\eta} \times S_{SQL} + \eta \times S_{CQNC}. \tag{4.62}$$

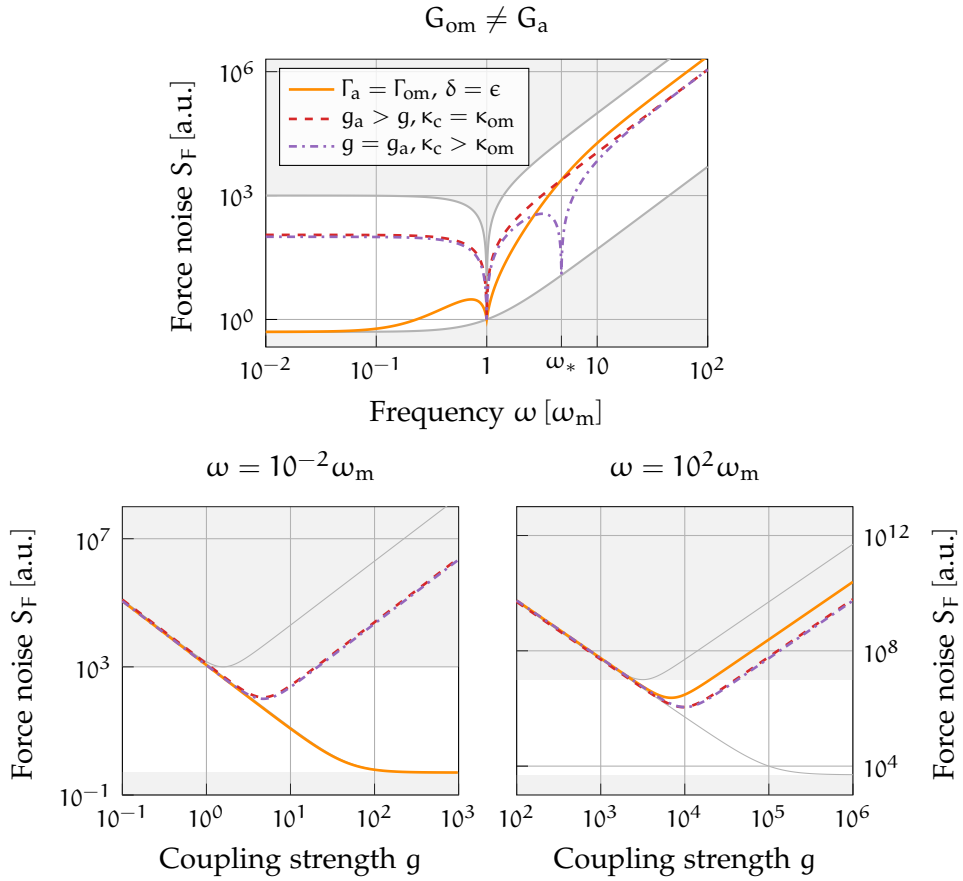

Figure 4.5: Imperfect matching of the measurement strength G_{om} and G_a. Top row: Achievable force noise levels for imperfect matching of measurement strength over frequency ω. For mismatched coupling strength compensated by linewidth mismatch,i.e., $\delta = \epsilon$, perfect noise cancellation can be recovered at low frequencies (solid orange for $\epsilon = \delta = 0.9$). For matched linewidth but mismatched coupling strength, noise cancellation is limited, but sub-SQL performance is possible (dashed red for $\delta = 0.9$). In the case of matched coupling strength but mismatched linewidth, we find a frequency (4.51) where perfect noise cancellation is possible (dash-dotted purple line, with $\epsilon = 0.9$). Bottom row: Corresponding force sensitivity over coupling strength g for low frequencies (left) and high frequencies (right). The shaded areas mark the bounds for sub-SQL sensitivity, from below the fundamental limit given by Equation (4.44) and from above the SQL given by Equation (2.130). The gray lines in the bottom row show the force noise for ideal CQNC conditions and no back-action evasion. Parameters are given in Table 4.1.

In contrast to the cases so far, losses reduce the performance of our setup even on resonance. Far away from resonance, where $S_{CQNC} \ll S_{SQL}$, we find that the minimal spectral density is

$$S_F = \sqrt{1-\eta} \times S_{SQL} + \eta \times S_{CQNC}. \tag{4.63}$$

In the opposite order OMS $\mapsto$ NMO, in addition to lost back-action information, some force signal will be lost due to propagation losses. Hence, the added noise will increase for this topology. We find

$$S_F = \frac{1}{\eta}\left(\sqrt{1-\eta} \times S_{SQL} + S_{CQNC}\right), \tag{4.64}$$

for the minimal spectral density and far off-resonance, it reduces to

$$S_F = \frac{\sqrt{1-\eta}}{\eta} \times S_{SQL}, \tag{4.65}$$

The spectral density is increased by $1/\eta$ compared to the case NMO $\mapsto$ OMS and hence directly proportional to the lost force signal. Losses after the second system constitute the detection efficiency and can be modeled similarly. Since this will not affect the cancellation of back-action noise, we will omit detection losses until the case study.

Apart from propagation losses, we take intracavity losses into account. Introducing a bath for each cavity, with coupling rates κ_c^{bath} and κ_{om}^{bath}, the intracavity losses can be described in terms of the escape efficiencies

$$\eta_{om,c}^{esc} = \frac{\kappa_{om,c}^{in}}{\kappa_{om,c}^{in} + \kappa_{om,c}^{bath}} = \frac{\kappa_{om,c}^{in}}{\kappa_{om,c}}. \tag{4.66}$$

Similar to propagation losses, introducing intracavity losses will always impede the cancellation of back-action noise, and depending on the order of the systems, the available force signal information will differ. For the case NMO $\mapsto$ OMS, with optimal measurement strength, we find the minimal spectral density

$$S_F = \frac{\sqrt{\eta_c^{esc} + \eta_{om}^{esc} - 2\eta_c^{esc}\eta_{om}^{esc}}}{\eta_{om}^{esc}} \times S_{SQL} + \frac{\eta_c^{esc}}{\eta_{om}^{esc}}|1 - \eta_{om}^{esc}\kappa_{om}\chi_{om}|^2 \times S_{CQNC}. \tag{4.67}$$

Again, moving away from resonance, the term $S_{CQNC} \ll S_{SQL}$ and thus the minimal spectral density is

$$S_F = \frac{\sqrt{\eta_c^{esc} + \eta_{om}^{esc} - 2\eta_c^{esc}\eta_{om}^{esc}}}{\eta_{om}^{esc}} \times S_{SQL}. \tag{4.68}$$

This encompasses both cases with propagation loss. For $\eta_{om}^{esc} \to 1$, we retrieve Equation (4.63) and for $\eta_c^{esc} \to 1$ Equation (4.65) respectively. Thus, for the configuration NMO $\mapsto$ OMS, the intracavity loss can be handled similarly to propagation loss.

For the case OMS $\mapsto$ NMO, we lose additional force signal due to intrinsic loss in the meter cavity. Moreover, the signal also picks up additional phase from the cavity $\propto e^{i\theta}$. We arrive at the minimal spectral density,

$$S_F = \frac{1}{\eta_{om}^{esc}|1 - \eta_c^{esc}\kappa_c\chi_c|^2}\left(\sqrt{\eta_c^{esc} + \eta_{om}^{esc} - 2\eta_c^{esc}\eta_{om}^{esc}} \times S_{SQL} + \eta_c^{esc} \times S_{CQNC}\right) \tag{4.69}$$

$$\xrightarrow{\text{off-resonance}} \quad \frac{\sqrt{\eta_c^{esc} + \eta_{om}^{esc} - 2\eta_c^{esc}\eta_{om}^{esc}}}{\eta_{om}^{esc}|1 - \eta_c^{esc}\kappa_c\chi_c|^2} \times S_{SQL}. \tag{4.70}$$

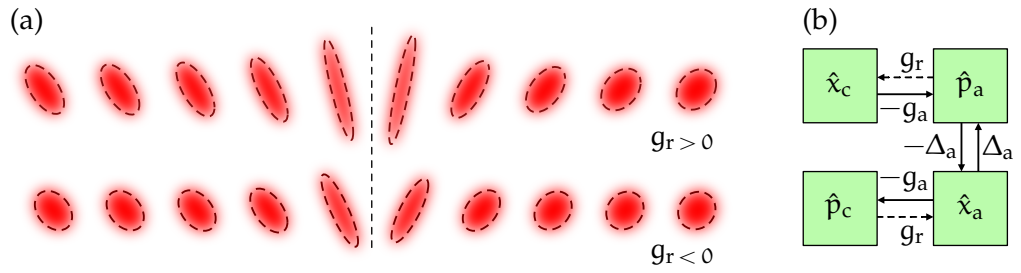

Figure 4.6: Effects of mismatch between beam-splitter and down-conversion coupling. (a) Output spectra for relative mismatch $g_r \neq 0$ for different frequencies. The dashed line denotes the resonance frequency ω_m. The mismatch between g_{BS} and g_{DC} breaks the rotational symmetry of ponderomotive squeezing around ω_m. (b) Flow chart between the mode of the ancilla and the meter cavity. The solid line shows the original back-action flow, and the dashed line shows the noise introduced by the relative mismatch g_r of the beam-splitter and down-conversion coupling.

The term $|1 - \eta_c^{esc}\kappa_c\chi_c|^2$ describes the meter cavity's phase and noise contribution. Due to its dependence on the meter cavity susceptibility χ_c, this difference is frequency-dependent and will vanish for frequencies $\omega > \kappa_c$. For low frequencies, it will be at a maximum of $|1 - 2\eta_c^{esc}|^2$, making intracavity losses extra punishing for configuration OMS $\mapsto$ NMO. We note that this term goes to infinity as $\eta_c^{esc} \to 0.5$. The reason for this lies in the way we modeled the intracavity loss. In essence, our cavities are built as two-mirror cavities and the noise couples through the end mirror. This is not realistic, but for low intracavity losses, a good approximation[8]. Our expressions from Equations (4.63)–(4.69) can be combined into a lengthy, yet simple, expression to encompass all the losses into a total loss expression. If we consider 1% losses from the sources above, we arrive at an optimal spectral density of

$$S_F \approx S_{SQL} \times \begin{cases} 17.4\% & \text{for NMO} \mapsto \text{OMS} \\ 18.3\% & \text{for OMS} \mapsto \text{NMO} \end{cases}, \tag{4.71}$$

for low frequencies. We see that introducing losses is detrimental to the possible noise reduction. As losses will never be avoidable, the system order NMO $\mapsto$ OMS should always be preferable since higher levels of noise reduction are achieved.

4.3.4 *Relative Mismatch of g_{BS} and g_{DC}*

In addition to losses, a relative mismatch between the beam-splitter coupling g_{BS} and down-conversion coupling g_{DC} will also affect the noise cancellation depending on the system order. So far, we assumed $g_{BS} = g_{DC} = 1/2\, g_a$ in order to mimic the back-action interaction of the OMS. We will now fix $g_{BS} + g_{DC} =$

8 Nobody wants to have 50% losses!

g and introduce a mismatch between the beam-splitter and down-conversion couplings

$$\frac{g_{BS} - g_{DC}}{g_{BS} + g_{DC}} = g_r \neq 0. \tag{4.72}$$

Effects of this relative mismatch are shown in Figure 4.6. As seen in Figure 4.6(b), the relative mismatch g_r allows the phase quadratures to couple back into the amplitude quadrature and thus deviate from the back-action interaction of the OMS. This introduces a noise path and will limit the cancellation of back-action noise. It also affects the force noise differently for the different system orders. For the case OMS $\mapsto$ NMO, the force signal is imprinted on the output phase quadrature of the OMS, and with the introduced mismatch, it is possible for the signal to couple to the amplitude quadrature. Contrary, for NMO $\mapsto$ OMS, the force signal will remain fully in the output phase quadrature. Thus, this results in different spectral noise densities for our phase measurement. For general mismatches, this will not reduce to a simple expression. No analytic expressions were found for the minimized spectral density. We exported our expressions and calculated the resulting spectral densities numerically. These results are shown in Figure 4.7. The CQNC performance is limited for low frequencies, but sub-SQL levels are still possible. Contrary to losses, the order OMS $\mapsto$ NMO seems advantageous for a relative mismatch of the couplings. CQNC will vanish entirely in the high-frequency limit, and no sub-SQL performance is possible. Interestingly, the achievable level of noise reduction does not depend on the sign of the mismatch parameter g_r.

4.4 CASE STUDY

After discussing ideal CQNC and the most relevant deviations from the ideal parameters, we now turn to a realistic situation one would expect in an actual experiment. For an integrated setup, reasonable parameters have been discussed in [141], which were revised in [111] for a cascaded setup, and two reasonable sets of parameters were given. From there, we found a new set of parameters that achieve broadband noise reduction for frequencies below the mechanical resonance of the oscillator with eigenfrequency $\omega_m = 500\text{kHz}$. The low-frequency range is chosen because a large coupling strength is needed to achieve sub-SQL performance at high frequencies[9]. Losses are particularly interesting in our case study, as they influence the noise reduction depending on the system order. Our set of parameters is shown in Table 4.2.

Our scheme considers a NMO, where the two modes are not spatially separated, as depicted in Figure 4.2. In this scenario, the ancilla cavity linewidth κ_a will directly contribute to the escape efficiency as a noise channel. Discussions in our group deem an ancilla cavity linewidth of $\kappa_a = 200$ kHz feasible. Combined with a meter cavity linewidth of $\kappa_c = 2$ MHz, this results in an escape efficiency of 90% for the NMO. We hope to achieve similar escape efficiencies for

9 This can be seen from the force noise curves over the coupling strength

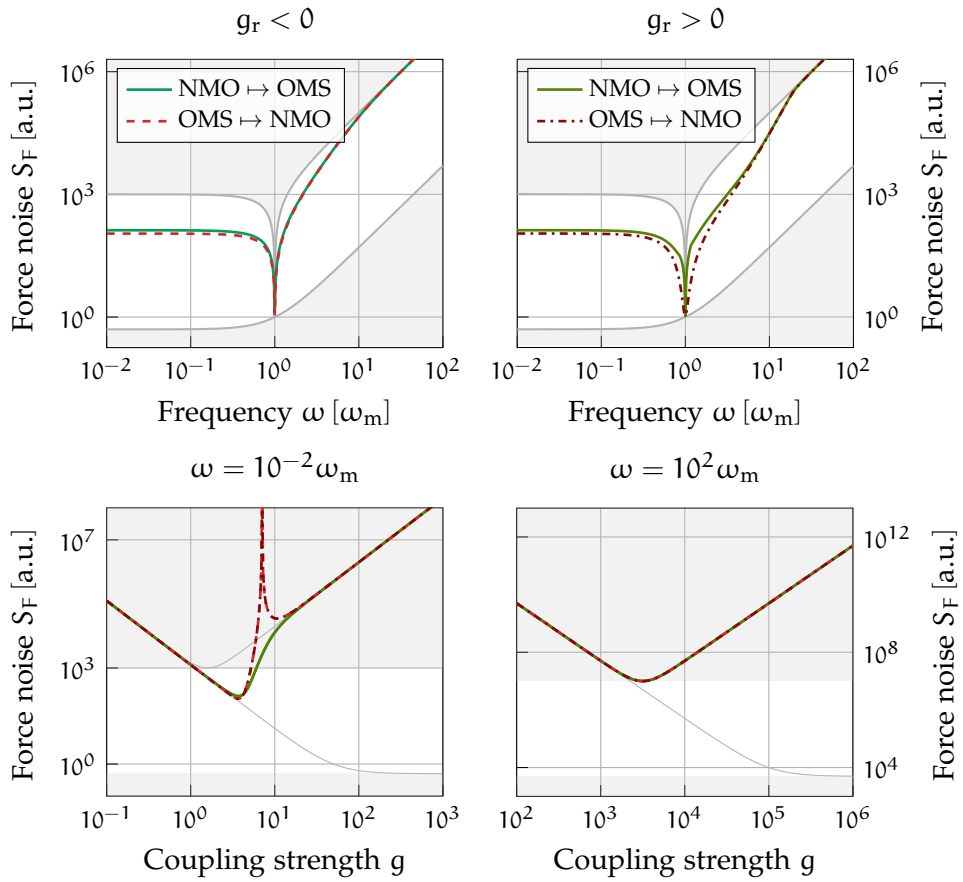

Figure 4.7: Force noise for relative mismatch of beam-splitter and down-conversion coupling. Top row: Achievable force noise levels over frequency ω. Left: Plotted for $g_r = -0.2$. Right: Plotted for $g_r = 0.2$. The relative mismatch introduces additional noise by modifying the effective back-action term of the NMO. Perfect noise cancellation is impossible, but sub-SQL levels are achievable for low frequencies. For high frequency, no noise reduction is possible. Traversing through the OMS first seems advantageous for noise cancellation. Bottom row: Corresponding force sensitivity over coupling strength g for low frequencies (left) and high frequencies (right). As seen by the line shapes over the coupling strength, the sign of the relative mismatch plays no role in the achievable noise performance. We see a sharp rise in the noise-to-signal ratio for low frequencies at a particular coupling strength. This is where the entire force signal is rotated to the amplitude quadrature. The shaded areas mark the bounds for sub-SQL sensitivity, from below the fundamental limit given by Equation (4.44) and from above the SQL given by Equation (2.130). The gray lines in the bottom row show the force noise for ideal CQNC and no back-action evasion. Parameters are given in Table 4.1.

Table 4.2: Proposed set of parameters

Parameter		Norm. value	Value
ω_m	mechanical resonance frequency	1	500 kHz
γ_m	mechanical linewidth	$10^{-8}\,\omega_m$	5 mHz
κ_c	meter cavity linewidth	$4\,\omega_m$	2 MHz
Δ_a	ancilla cavity detuning	$-0.99\,\omega_m$	−495 kHz
κ_a	ancilla cavity linewidth	$\frac{2}{5}\,\omega_m$	200 kHz
g_{BS}	beam-splitter coupling strength	$1.01\,\frac{g}{2}$	253 kHz
g_{DC}	down-conversion coupling strength	$0.97\,\frac{g}{2}$	243 kHz
η_c^{esc}	escape efficiency NMO		0.9
κ_{om}	optomechanical cavity linewidth	$0.99\,\kappa_c$	1.98 MHz
g	optomechanical coupling strength	ω_m	500 kHz
η_{om}^{esc}	escape efficiency OMS		0.9
η_{prop}	propagation efficiency		0.97
η_{det}	detection efficiency		0.97
T	temperature		4K

the OMS. Detection efficiencies over 97% were already realized [125]. Similarly, propagation losses between the systems should not be an issue. We assume 3% losses from both propagation and detection.

Matching most parameters, such as ancilla cavity detuning Δ_a and the cavity linewidth κ_c and κ_{om} should not be a problem; we assume them to be closely matched. More delicate to match are the coupling strengths. A down-conversion coupling of $g_{DC} = 250$ kHz and a beam-splitter coupling of $g_{BS} \geqslant 235$ kHz was readily achieved [111]; thus, we set the optomechanical coupling strength to $g = 500$ kHz.To check if the proposed coupling strength is needed to achieve sub-SQL noise levels, we define the gain parameter

$$R = 1 - \frac{S_F}{S_{SQL}}. \tag{4.73}$$

The plot of this parameter can be seen in Figure 4.8. We see, a sub-SQL performance is possible for $g \approx 0.9 - 2.6\,\omega_m$ with a maximum performance at $g \approx 1.5\,\omega_m$. Optomechanical coupling strengths of $g = 440$ kHz have been reported in micro-mechanical setups [94] and higher couplings in the order of MHz should be possible [97]. Hence, our assumed coupling strength is achievable and also necessary. Suppose these levels cannot be reached for the optomechanical coupling strength; one could still compensate for this mismatch by the cavity linewidths, as described in Equation (4.48) and increase the performance for low frequencies.

The OMS must be limited by quantum back-action noise to measure the possible cancellation of back-action noise. For this, the quantum back-action noise

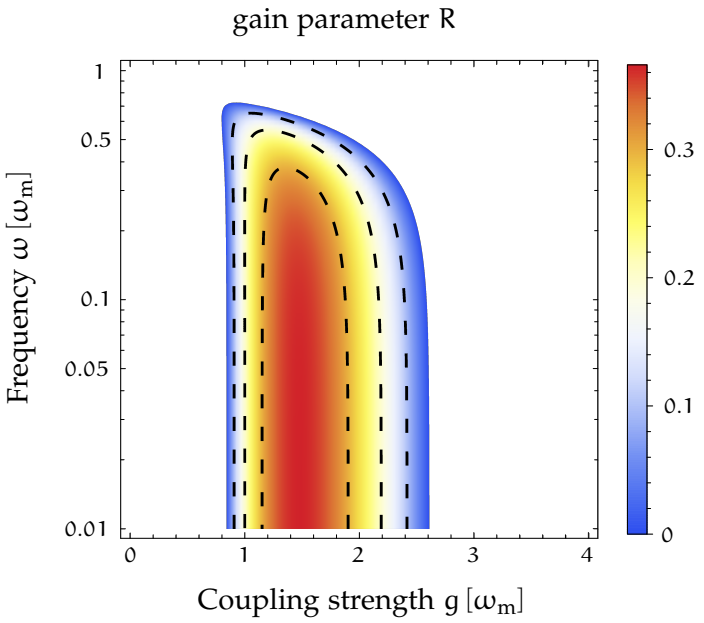

Figure 4.8: Linear-logarithmic plot of the gain parameter defined in Equation (4.73), plotted against the coupling strength g and frequency ω for the remaining parameters as in Table 4.2. We find a gain over the SQL for $g \approx 0.9 - 2.6\,\omega_m$ in almost the entire frequency range below the resonance. For our goal of $g = \omega_m$, we find a performance gain over the SQL of $\approx 20\%$. The maximal performance gain is 40% at $g \approx 1.5\omega_m$.

in Equation (2.128) must be much larger than the thermal noise. In the low-frequency limit ($\kappa_{om} \gg \omega$), this can be expressed in terms of the quantum cooperativity. It is the ratio of the mechanical oscillator's classical cooperativity and thermal occupation. It is given as

$$C_q = \frac{C_{cl}}{\bar{n}_{th}} = \frac{\Gamma_{om}}{\gamma_m}\frac{\hbar\,\omega_m}{k_B T} = \frac{4g^2\hbar}{\kappa_{om} k_B T}\,Q_m \gg 1. \tag{4.74}$$

Modern silicon-nitride membranes have exceeded quality factors of $Q_m = 10^8$ [84], thus the OMS would be quantum back-action limited for a temperature $T = 4K$, a temperature achievable with cryogenics. For higher temperatures, the quality factor must be increased to elevate the back-action effects over the thermal noise floor, and similarly, lower temperatures allow for a lower quality factor. In order to account for this and compare all OMS of frequency ω_m, once they can resolve the quantum back-action, we normalize our force noise by the quality factor Q_m.

The achievable sensitivities for the parameters in Table 4.2 are shown in Figure 4.9. In the low-frequency regime, the configuration NMO $\mapsto$ OMS shows a reduction of 20% below the SQL and almost comparable results to the integrated setup. No sub-SQL sensitivity can be achieved for the other system order OMS $\mapsto$ NMO. This is not surprising, as we saw in Section 4.3.3, that this configuration suffers additional penalties from losses. Instead of matching the parameters (4.38)–(4.40), the limiting factor for noise reduction in a realistic case

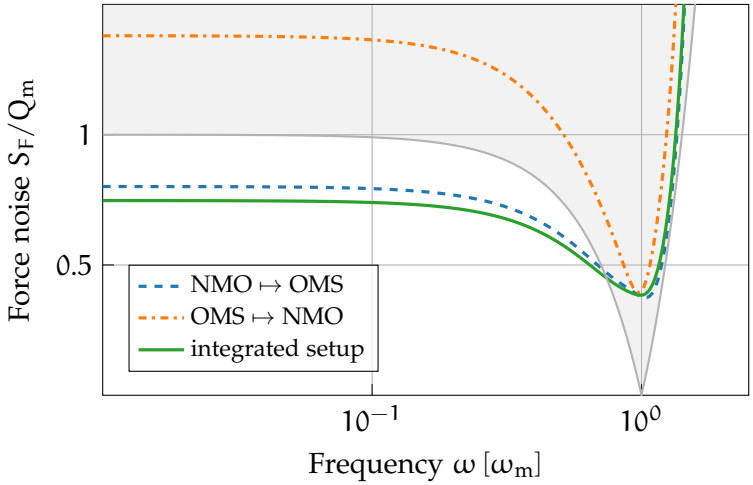

Figure 4.9: Force noise normalised to Q_m for the parameters given by Table 4.2 and temperature $T = 4$ K. For low frequencies, sub-SQL performance is possible for the integrated setup (solid green) and the case NMO ↦ OMS (dashed blue). No sub-SQL levels are possible for the case OMS ↦ NMO (dash-dotted orange). The shaded area shows levels above the SQL.

will be losses. Additionally, as losses will never be entirely avoidable, choosing the right system ordering, NMO ↦ OMS, is of utmost importance.

4.5 CONCLUSION AND OUTLOOK

In this chapter, we discussed a cascaded version of the all-optical coherent quantum noise cancellation setup proposed by Tsang and Caves [120, 141]. Instead of introducing the anti-noise path directly into the optomechanical cavity, we considered an all-optical effective negative-mass oscillator as a standalone system and removed the back-action noise of the positive mass oscillator by coupling both systems coherently via a strong drive field. Under the conditions (4.38)–(4.40), we then rediscovered the perfect cancellation of back-action noise. Afterward, we discussed deviations from the ideal conditions, including losses and the influence of the system order. We saw that for mismatched measurement strengths, $G_{om} \neq G_a$, by choosing the cavity linewidth and coupling strength in a specific way, CQNC can be recovered in the high- or low-frequency regime, or even at a specific frequency $\omega_* \neq \omega_m$. The system order will also affect the noise cancellation performance for losses and a relative mismatch of beamsplitter and down-conversion coupling. Finally, we discussed the performance of our setup for a set of realistic parameters. We showed that a quantum noise reduction of 20% below the SQL is possible for the order NMO ↦ OMS in the low-frequency regime.

To improve upon the performance laid out in the case study, the obvious solution is to reduce noise and the ancilla cavity linewidth κ_a, or if possible, increase the coupling rate g. Apart from these "trivial" suggestions, one idea discussed in the group is introducing a second laser beam to the OMS. This beam

is detuned far from the resonance frequency and is used as a cooling beam, whereas the other beam measures the mechanical oscillator on resonance. In this, the probe's quantum cooperativity (4.74) will remain constant. Therefore we could decrease the temperature of the mechanical oscillator and increase its linewidth γ_m to match the ancilla cavity linewidth κ_a closer. We assume the combination of these effects will benefit the CQNC performance, but further research is needed in this regard.

In the field of cascaded quantum systems, many interesting configurations can be discussed. For example, Karg et al. [67, 68] showed the cascade of an OMS and a spin-ensemble in a looped topology. Interesting effects can be observed by reentering the first system under a time delay or imposed phase shift. Preliminary calculations for a looped setup with our optical NMO showed no apparent benefit for the CQNC performance. However, closer inspection of different topologies, such as loops or parallel configurations, as discussed by Zeuthen et al. [147] could be an interesting idea for future projects.

Recently, colleagues in our group [64] showed that a detuned single-mode squeezer would generate frequency-dependent squeezing. Another interesting topic would be to compare the performance of such a detuned single-mode squeezer to our suggested NMO, which is, in a sense, a detuned two-mode squeezer. Of course, the detuned single-mode squeezer will never cancel quantum back-action noise for all frequencies as the NMO. Nevertheless, it would be interesting to see the possible performance levels and frequency range of a detuned single-mode squeezer in our cascaded setting.

5 CONCLUSION

This thesis aimed to illuminate two aspects of quantum parameter estimation in optomechanical systems. The concept of conditioning, or filtering, on the level of measured data; and decreasing measurement back-action noise employing back-action evading techniques, such as coherent quantum noise cancellation. For the optomechanical force sensors considered in this thesis, it was shown by Tsang et al. [123] that both these concepts are needed to estimate forces at the fundamental limit – the quantum Cramér-Rao bound.

On the side of conditioning, I discussed the different views of quantum smoothing in the literature. I started by reviewing the concept of prediction and retrodiction for continuous measurements in the quantum context. For applications in linearized optomechanics, the discussion was restricted to a suitable subclass of quantum systems; the linear Gaussian quantum systems. In this context, the governing stochastic master equations for prediction and retrodiction are reduced to the classical forward and backward Kalman filter. For quantum filtering, a fully developed theory exists [5, 9], which relies on the quantum non-demolition conditions. These conditions are not fulfilled for quantum retrodiction. Subsequently, quantum smoothing in a purely quantum scenario can yield non-physical results. I illustrated this by applying quantum smoothing to an optomechanical setup using Kalman and Wiener filters. For retrodiction, the estimates of these filters on the states' variance differed. While the differences would disappear in the case of a hybrid classical-quantum parameter estimation, these results are connected to weak-value estimates, which are not always well-defined. Additionally, as seen in the discussed example, the smoothed "state" constructed by this method is not physical, as it violates Heisenberg's uncertainty principle.

In my opinion, a general theory of quantum smoothing is needed that can encompass the different current views on quantum smoothing. Once such a theory is found, one could derive the conditions that allow for the use of classical smoothing as a limit. A good starting point seems to be the theory of quantum smoothing proposed by the group around Wiseman [45, 79, 21]. Their smoothing theory is purely quantum and produces a proper smoothed density operator. In this framework, Laverick et al. [81, 78] produced quantum extensions of the classical Mayne-Fraser-Potter and Rauch-Tung-Striebel smoothers for linear Gaussian quantum case. Another approach is taken by Tsang [119]; he tries to unify the various concepts of quantum smoothing in the context of generalized expectation values. Quantum mechanics can be seen as a generalized probability theory; thus, building a theory of quantum smoothing on this level is a reasonable approach. When applying smoothing to quantum systems, each scenario should be considered very carefully, and it should be determined if the QND conditions are also fulfilled in case of retrodiction. Also, the Kalman filters

are obtained by the restriction of the stochastic master equation to the case of linear Gaussian quantum systems. In my opinion, this gives them validity on a more fundamental level.

Regarding quantum back-action evasion, I considered a cascaded scheme for coherent quantum noise cancellation in optomechanical force sensors. I analyzed its noise reduction performance with regard to many of its parameters and conducted a case study for an experimental realization. This cascaded setup consists of an all-optical effective negative-mass oscillator, as proposed by Tsang and Caves [120], connected to an optomechanical force sensor by a laser field. The analysis showed that compared to the integrated setup [120, 141], this cascaded scheme can give more experimental freedom while giving similar noise reduction performance. In addition, I showed that in a realistic setting, where noise will play a role, a preferable order of the subsystems exists. "Pre-squeezing" the light by putting the negative-mass oscillator in front of the optomechanical sensor should always be chosen. The outlined formulation is based on linear quantum networks [25, 98], which is an excellent tool for modeling cascaded systems. It can readily be extended to more subsystems, more inputs and generally many other possible negative-mass oscillators.

A

APPENDIX

A.1 STOCHASTIC INTEGRALS

In this section, we want to give some context to the mentioned stochastic integrals in the main text. This is not a detailed instruction on how to solve these types of integrals but a clarification of their definition. For a simpler introduction, let us consider a one-dimensional stochastic system. The solution to the Langevin equation (2.9) is then reduced to

$$x_t = x_{t_0} + \int_{t_0}^{t} f(x_\tau, \tau)d\tau + \int_{t_0}^{t} g(x_\tau, \tau)dW_s(\tau), \tag{A.1}$$

with f and g functions instead of matrices A and E. The first integral is just the "standard" integral known from calculus – the Riemann integral. The second integral is with respect to the white noise process $W_s(\tau)$, which is nowhere differentiable. Therefore, this *stochastic integral* needs special treatment. To solve these, Itô [56] defined a new type of integral – the Itô stochastic integral[1]. Let us consider only the stochastic integral

$$\int_{t_0}^{T} g(x_\tau, \tau)dW_s(\tau). \tag{A.2}$$

For the definition of this integral on the time interval $[t_0, T]$, we define a sequence partitions $\Delta_n = \{\tau_j : j = 0, ..., n\}$ of this interval in n time steps with

$$t_0 = \tau_0 < \tau_1 < ... < \tau_{n-1} < \tau_n = T. \tag{A.3}$$

The norm (also called mesh) of a partition is given by the length of the longest sub-interval [49], i.e.,

$$\|\Delta_n\| = \max\left\{|\tau_j - \tau_{j-1}| : j = 1, ..., n\right\}. \tag{A.4}$$

We restrict ourselves to partitions Δ_n such that

$$\lim_{n\to\infty} \|\Delta_n\| = 0, \tag{A.5}$$

which means that as we increase the number of time steps, we arrive at the finest partition. With this, the Itô integral is defined as

$$\int_{t_0}^{T} g(x_\tau, \tau)dW_s(\tau) := \lim_{n\to\infty} \sum_{j=1}^{n} g(x_{\tau_{j-1}}, \tau_{j-1})\left(W_{\tau_j} - W_{\tau_{j-1}}\right). \tag{A.6}$$

1 We note, there exists another stochastic integral, called the Stratonovich stochastic integral [113]

Thus, the function is evaluated at the lower bound of each sub-interval in this form of integral. This evaluation at the lower bounds can be seen as the stochastic integral moving forward in time, hence the *forward* Itô integral. The corresponding *backward* Itô integral is then defined similarly, but the function is evaluated at the upper bound of the sub-interval. It reads

$$\int_{t_0}^{T} g(x_\tau, \tau) dW_s(\tau) := \lim_{n\to\infty} \sum_{j=1}^{n} g(x_{\tau_j}, \tau_j) \left(W_{\tau_j} - W_{\tau_{j-1}}\right). \tag{A.7}$$

A.2 HOMODYNE DETECTION

Homodyne detection is a phase-sensitive detection scheme from which information about an arbitrary quadrature of the measured field can be obtained. As all the schemes considered in this thesis used homodyne detection exclusively, we recall its principle. Note that we will only discuss balanced homodyne detection. More details can be found in most textbooks about quantum optics [143, 3].

To better understand the concept of homodyne detection, let us first describe how a light field is measured. This is usually done by a photodetector in which the incoming light field is converted into a current. Consider an input light signal $\hat{a}(t)$, as defined in Section 2.3.1. In the photodetector, photons are converted into electrons via the photoelectric effect. These electrons generate a current if a voltage is applied. The resulting current is proportional to the average photon number, i.e., $I(t) \propto \langle \hat{a}^\dagger(t)\hat{a}(t)\rangle$. Expanding the creation operator in the mean field and small fluctuations $\hat{a} = \alpha + \delta\hat{a}$ like in Section 2.3.2, the current is found as

$$\begin{aligned} I(t) &\propto \langle \hat{a}^\dagger(t)\hat{a}(t)\rangle && \text{(A.8)}\\ &\approx \alpha^2 + \alpha\langle \delta\hat{a}^\dagger(t) + \delta\hat{a}(t)\rangle && \text{(A.9)}\\ &= \alpha^2 + \alpha\sqrt{2}\langle \hat{x}(t)\rangle, && \text{(A.10)} \end{aligned}$$

where the amplitude quadrature was introduced as defined in Equation 2.82. We see in this method called *direct detection*, on gains only information about the amplitude.

The homodyne detection scheme adds a local oscillator field $\hat{a}_{LO}$, which is then combined with the signal $\hat{a}_{sig}$ on a 50:50 beam-splitter. The output fields of the 50:50 beam-splitter ports are a balanced combination of the inputs and can be written as

$$\hat{a}_\pm(t) = \frac{\hat{a}_{sig}(t) \pm \hat{a}_{LO}(t)}{\sqrt{2}}. \tag{A.11}$$

Each of these outputs is then measured by a photodetector as in the direct measurement. We decompose the signal field as above $\hat{a}_{sig} = \alpha_{sig} + \delta\hat{a}_{sig}$ in its mean and fluctuations. Additionally, the local oscillator is assumed to be a

coherent classical field with a mean $\langle \hat{a}_{LO}(t) \rangle = |\alpha_{LO}| e^{-i\theta_{LO}}$ such that $|\alpha_{LO}| \gg \alpha_{sig}$. Thus, one finds the currents of each output as

$$I_{\pm}(t) \approx \frac{|\alpha_{LO}|^2}{2} \pm \frac{|\alpha_{LO}|}{\sqrt{2}} \langle \hat{x}_{sig}^{\theta_{LO}}(t) \rangle, \tag{A.12}$$

where the introduced quadrature operator

$$\hat{x}_{sig}^{\theta}(t) = \frac{\hat{a}(t) e^{-i\theta} + \hat{a}^{\dagger}(t) e^{i\theta}}{\sqrt{2}}, \tag{A.13}$$

is the generalized quadrature operator such that $\hat{x}_{sig}^{0} = \hat{x}$ and $\hat{x}_{sig}^{\pi/2} = \hat{p}$.

For balanced homodyne detection, these two currents will be subtracted, and the resulting measured current is

$$I_{hom}(t) = I_{+}(t) - I_{-}(t) = \sqrt{2} |\alpha_{LO}| \langle \hat{x}_{sig}^{\theta_{LO}}(t) \rangle. \tag{A.14}$$

Thus, by this scheme, one can measure an arbitrary quadrature by changing the phase of the local oscillator θ_{LO}.

In practice, this measurement will not be perfect, be it through optical losses of the signal or the general efficiency of the photodetector. For our purposes, these effects can be regarded in the same way, as a loss of signal before reaching the homodyne detector. The way we model these losses is by a fictitious beam-splitter. Unlike the beam-splitter in the balanced homodyne scheme, this will overlay the signal with a vacuum field with a transmission $\sqrt{\eta}$ corresponding to the efficiency of our detection. The path orthogonal to the signal will be traced-out or lost to the vacuum with a transmission $\sqrt{1-\eta}$. The output of the signal after this beam-splitter is thus

$$\hat{a}_{out} = \sqrt{\eta} \hat{a}_{sig} + \sqrt{1-\eta} \hat{a}_{vac}. \tag{A.15}$$

Combing all of this, we arrive at an inefficient homodyne measurement with the homodyne current

$$I_{hom}(t) = |\alpha_{LO}| \sqrt{\eta} \langle \hat{x}_{sig}^{\theta_{LO}}(t) \rangle. \tag{A.16}$$

A schematic of this is depicted in Figure A.1.

A.3 DETAILS ON THE QUANTUM WIENER FILTER

In this chapter, we provide details on the validity of the causal Wiener filter in the quantum context and some calculations omitted in Chapter 3.

A.3.1 *Admissibility of the Wiener Filter*

In this section, we want to explain why the Wiener filter can be applied in the quantum context. This motivation was already given in the Appendix of [93], but we give a more in-depth version of this argument for completeness. The

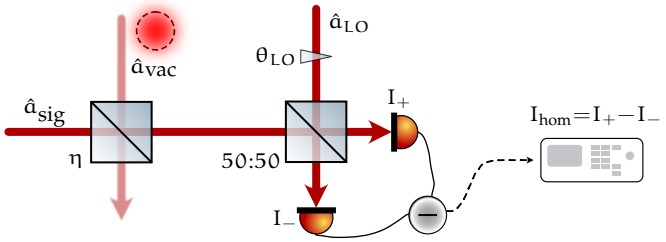

Figure A.1: Simplistic depiction of an inefficient homodyne detector. The signal field $\hat{a}_{sig}$ is overlaid with a vacuum field $\hat{a}_{vac}$ on an imbalanced beam-splitter with transmission $\sqrt{\eta}$. The lossy signal is combined with a local oscillator $\hat{a}_{LO}$ on a 50:50 beam-splitter for homodyne detection. Homodyne current I_{hom} is given by the difference I_+ and I_-. The measured quadrature can be chosen by changing the phase of the local oscillator θ_{LO}.

usual way to describe continuous measurements [60] is as a limit of projective measurements. Assume we started a measurement at a time $t_0 = T < 0$ and finished the measurement at time $t = 0$. We consider the measurement operator $\hat{y}$ pre-whitened by the Wiener filter for simplicity. Thus we describe the measurement as a projective measurement at discrete times $\hat{y}(t)$, where $\delta t = t_{i+1} - t_i = T/N$, with T the length of the measurement time, divided into N sub-intervals and the limit $N \to \infty$ is taken. Between each projective measurement, there is a free evolution given by a unitary operator

$$\hat{U} = e^{-\frac{i}{\hbar}\hat{H}\delta t}. \tag{A.17}$$

Thus given a vector of measurement data $\mathbf{y} = \{y_i\}$ one can write the conditional state[2] at time $t = 0$ as

$$\hat{\rho}_c(0) = \hat{P}_{\mathbf{y}}\hat{\rho}_{in}\hat{P}_{\mathbf{y}}^{\dagger}. \tag{A.18}$$

The projection operators on the measurement record are given by

$$\hat{P}_{\mathbf{y}} = \hat{P}(\hat{y} - y_N)\hat{U}\hat{P}(\hat{y} - y_{N-1})\hat{U}...\hat{U}\hat{P}(\hat{y} - y_i)\hat{U}...\hat{U}\hat{P}(\hat{y} - y_1)\hat{U}, \tag{A.19}$$

where each of the measurements is a "sharp" measurement in the sense that

$$\hat{P}(\hat{y} - y_i) = \delta(\hat{y} - y_i) = \int_{-\infty}^{\infty} dy\,\delta(y - y_i)|y\rangle\langle y|. \tag{A.20}$$

In the Heisenberg picture, and because the measurement operator $\hat{y}$ fulfills the QND condition (3.60a), this can be written as a product of dirac distributions [69]:

$$\hat{P}_y = \prod_{T<t<0} \delta(\hat{y}(t) - y(t)). \tag{A.21}$$

2 This state is unnormalized.

Letting $T \to \infty$ and making the discretization of the measurement record arbitrarily small $N \to \infty$, this functional delta distribution can be written as a path integral, i.e.,

$$\hat{P}_y = \prod_{-\infty<t<0} \delta(\hat{y}(t) - y(t)) \xrightarrow{N\to\infty} \int \mathcal{D}[\xi] \exp\left(i \int_{-\infty}^{0} dt\, \xi(t)[\hat{y}(t) - y(t)] \right). \tag{A.22}$$

Here, ξ is a dummy variable in the parameter space, and $\mathcal{D}[\xi]$ denotes the path integral in this parameter space. Essentially, the whole measurement record is collapsed into the projection operator onto the "path" the recorded data took.

Now, consider the characteristic function χ as in Equation (3.28b) of the conditional state after the measurement. It is given

$$\chi_{\hat{\rho}_c}(\boldsymbol{\alpha}) = \operatorname{tr}\left(\hat{P}_y \hat{\rho} \hat{P}_y \hat{D}_{\boldsymbol{\alpha}}\right) \tag{A.23}$$

$$= \operatorname{tr}\left(\hat{P}_y \hat{\rho} \hat{P}_y \exp\left(i \sum_i \alpha_i \hat{x}_i(0) \right) \right). \tag{A.24}$$

Using the other condition (3.60b) of the QND conditions (3.60), the path integral and displacement operators can be combined as

$$\chi_{\hat{\rho}_c}(\boldsymbol{\alpha}) = \operatorname{tr}\left(\hat{P}_y \hat{\rho} \hat{P}_y \exp\left(i \sum_i \alpha_i \hat{x}_i(0) \right) \right) \tag{A.25}$$

$$= \operatorname{tr}\left(\hat{\rho} \hat{P}_y \exp\left(i \sum_i \alpha_i \hat{x}_i(0) \right) \right) \tag{A.26}$$

$$= \int \mathcal{D}[\xi] \operatorname{tr}\left(\hat{\rho} \exp\left(i \sum_i \alpha_i \hat{x}_i(0) + i \int_{-\infty}^{0} d\tau\, \xi(\tau)[\hat{y}(\tau) - y(\tau)] \right) \right). \tag{A.27}$$

Because the state $\hat{\rho}$ is a Gaussian state and $\hat{x}$ is linear with zero mean $\langle \hat{x} \rangle = \operatorname{tr}(\hat{\rho}\hat{x}) = 0$, we can use that for this case $\operatorname{tr}(\hat{\rho} e^{i\hat{x}}) = e^{\langle \hat{x}^2 \rangle / 2}$. Thus, the characteristic function becomes

$$\chi_{\hat{\rho}_c}(\boldsymbol{\alpha}) = \int \mathcal{D}[\xi] \exp\left(- \left\langle \left[\sum_i \alpha_i \hat{x}_i(0) + \int_{-\infty}^{0} d\tau\, \xi(\tau) \hat{y}(\tau) \right]^2 \right\rangle / 2 \right) \tag{A.28}$$

$$\times \exp\left(-i \int_{-\infty}^{0} d\tau \xi(\tau) y(\tau) \right). \tag{A.29}$$

Now, use Equations (3.61) and (3.62),

$$\hat{x}_i(0) = \hat{R}_i(0) + \int_{-\infty}^{0} d\tau \overrightarrow{K}_i(-\tau) \hat{y}(\tau), \tag{A.30}$$

$$\langle \hat{R}_i(0) \hat{y}(\tau) \rangle = 0 \quad \forall\, \tau < 0, \tag{A.31}$$

then

$$\left\langle \left[\sum_i \alpha_i \hat{x}_i(0) + \int_{-\infty}^{0} d\tau\, \xi(\tau)\hat{y}(\tau) \right]^2 \right\rangle = \sum_{ij} \alpha_i \alpha_j \langle \hat{R}_i\, \hat{R}_j \rangle + \int_{-\infty}^{0}\int_{-\infty}^{0} d\tau d\tau' \xi'(\tau)\xi'(\tau')\langle \hat{y}(\tau)\, \hat{y}(\tau')\rangle. \tag{A.32}$$

The new variables ξ' are shifted by the factor

$$\xi'(\tau) = \xi(\tau) + \sum_i \alpha_i \overrightarrow{K}(-\tau). \tag{A.33}$$

Using these as the new integration variables, the characteristic function is given as [93]

$$\chi_{\hat{\rho}_c}(\boldsymbol{\alpha}) \approx \exp\left(-\frac{1}{2} \sum_{ij} \alpha_i \alpha_j \langle \hat{R}_i\, \hat{R}_j \rangle \right) \exp\left(i \int_{-\infty}^{0} d\tau \sum_i \alpha_i \overrightarrow{K}(-\tau) y(\tau) \right), \tag{A.34}$$

which under the definitions 3.32, one can calculate

$$-i\frac{\partial}{\partial \alpha_i} \chi_{\hat{\rho}_c}(\boldsymbol{\alpha})\Big|_{\boldsymbol{\alpha}=0} = \langle \hat{x}_i(0) \rangle^c, \tag{A.35}$$

$$-\frac{\partial^2}{\partial \alpha_i \partial \alpha_j} \chi_{\hat{\rho}}(\boldsymbol{\alpha})\Big|_{\boldsymbol{\alpha}=0} = V_{\hat{x}_i \hat{x}_j} + \langle \hat{x}_i \rangle^c \langle \hat{x}_j \rangle^c, \tag{A.36}$$

which by means of Equation (A.34) shows that Equations 3.68 and (3.69) as shown in [93]. We want to emphasize that this proof relied on the QND conditions (3.60), which are not generally fulfilled for retrodiction.

A.3.2 *Details on the Wiener Filter Results*

In this section, we give details on the Wiener filter results given in Chapter 3. We start with the steady-state spectral densities for the optomechanical system described in Section 3.3.1. In the bad cavity limit, we find

$$S_{xx} = |\chi_m|^2 \left(2\Gamma + \gamma_m(2\bar{n} + 1)\right), \tag{A.37a}$$

$$S_{yy} = \frac{1}{2} + 4\Gamma\eta S_{xx}, \tag{A.37b}$$

$$S_{xy} = 2\sqrt{\Gamma\eta} S_{xx}, \tag{A.37c}$$

$$S_{pp} = \frac{\omega^2}{\omega_m^2} S_{xx}, \tag{A.37d}$$

$$S_{py} = \frac{i\omega}{\omega_m} S_{xy}, \tag{A.37e}$$

$$S_{xp} = -\frac{i\omega}{\omega_m} S_{xx}. \tag{A.37f}$$

We first need to decompose the spectral density S_{yy} to derive the Wiener filters. We note that the poles of S_{yy} are determined by the mechanical susceptibility χ_m. The poles are found to be

$$P_{1,2} = \frac{1}{2}\left(\pm\sqrt{4\omega_m^2 - \gamma_m^2} - i\gamma_m\right), \tag{A.38}$$

$$P_{3,4} = \frac{1}{2}\left(\pm\sqrt{4\omega_m^2 - \gamma_m^2} + i\gamma_m\right), \tag{A.39}$$

$$\tag{A.40}$$

where $P_{1,2}$ lie in the LHP and $P_{3,4}$ in the UHP. Due to symmetry, we can also note that one may write $P_2 = -P_1^*$, $P_3 = P_1^*$ and $P_4 = -P_1$. For the zeros, we find the numerator as

$$\begin{aligned}\text{Numerator}(S_{yy}) = \omega^4 + \omega^2(\gamma_m^2 - 2\omega_m^2) \\ + 8\omega_m^2\gamma_m^2\eta C_{cl}(2C_{cl} + 2\bar{n} + 1) + \omega_m^4.\end{aligned} \tag{A.41}$$

The numerator has the form $\omega^4 + A\omega^2 + B^2$, which has zeros of the form $\pm\sqrt{\frac{A+B}{2}} \pm i\sqrt{\frac{B-A}{2}}$. Now, it is useful to define the effective frequency ω_{eff} and effective linewidth γ_{eff} as

$$\omega_{eff} = \left(8\eta\gamma_m^2(2C_{cl} + 2\bar{n} + 1)\omega_m^2 + \omega_m^4\right)^{\frac{1}{4}} \tag{A.42}$$

$$\gamma_{eff} = \sqrt{\gamma_m^2 + 2\omega_{eff}^2 - 2\omega_m^2}, \tag{A.43}$$

because then we find the zeros analogous to the poles as

$$Z_{1,2} = \frac{1}{2}\left(\pm\sqrt{4\omega_{eff}^2 - \gamma_{eff}^2} - i\gamma_{eff}\right), \tag{A.44}$$

$$Z_{3,4} = \frac{1}{2}\left(\pm\sqrt{4\omega_{eff}^2 - \gamma_{eff}^2} + i\gamma_{eff}\right). \tag{A.45}$$

$$\tag{A.46}$$

From this, we define the effective susceptibility $\chi_{eff} = \frac{1}{\omega_{eff}^2 - \omega^2 - i\gamma_{eff}\omega}$. The spectral density is then decomposed as

$$S_{yy} = \frac{1}{2}\frac{|\chi_m|^2}{|\chi_{eff}|^2} = \frac{1}{\sqrt{2}}\left(\frac{\chi_m}{\chi_{eff}}\right)\frac{1}{\sqrt{2}}\left(\frac{\chi_m^*}{\chi_{eff}^*}\right) = s_y^+ s_y^-. \tag{A.47}$$

For the causal part of S_{xy}/s^- we find

$$\left[\frac{S_{xy}}{s^-}\right]_+ = \sum_{i=1}^{2}\frac{\text{Res}[\frac{S_{xy}}{s^-}, P_i]}{\omega - P_i}. \tag{A.48}$$

Thus, the position Wiener filter is

$$\overrightarrow{K}_x(\omega) = \frac{1}{s_y^+(\omega)}\left[\frac{S_{xy}(\omega)}{s^-(\omega)}\right]_+ \tag{A.49}$$

$$= \frac{1}{\sqrt{2}}\frac{(\omega-P_1)(\omega-P_1)}{(\omega-Z_1)(\omega-Z_1)}\frac{\mathrm{Res}_1(\omega-P_2)+\mathrm{Res}_2(\omega-P_1)}{(\omega-P_1)(\omega-P_2)} \tag{A.50}$$

$$= \frac{1}{\sqrt{2}}\frac{\mathrm{Res}_1(\omega-P_2)+\mathrm{Res}_2(\omega-P_1)}{(\omega-Z_1)(\omega-Z_2)} \tag{A.51}$$

$$= \frac{1}{\sqrt{2}}\frac{\mathrm{Res}_1(\omega+P_1^*)-\mathrm{Res}_1^*(\omega-P_1)}{(\omega-Z_1)(\omega-Z_2)} \tag{A.52}$$

$$= \frac{2(i\,\mathrm{Im}(\mathrm{Res}_1\,\omega)+\mathrm{Re}(\mathrm{Res}_1\,P_1^*))}{\sqrt{2}(\omega-Z_1)(\omega-Z_2)}. \tag{A.53}$$

From here, we find,

$$\overrightarrow{K}_x(\omega) = \alpha(1-i\omega\beta)\chi_{\mathrm{eff}}(\omega), \tag{A.54}$$

with

$$\alpha = 4\gamma_m\sqrt{\gamma_m C_{cl}\eta}(2C_{cl}+2\bar{n}+1)\frac{\omega_m^2}{\omega_m^2+\omega_{\mathrm{eff}}^2}, \tag{A.55}$$

$$\beta = \frac{\gamma_m+\gamma_{\mathrm{eff}}}{\omega_{\mathrm{eff}}^2-\omega_m^2+\gamma_m^2+\gamma_{\mathrm{eff}}\gamma_m}. \tag{A.56}$$

For the variance, we need to derive the integral

$$V_{xx} = \int_{-\infty}^{\infty}\frac{d\omega}{2\pi}S_{xx}(\omega) - \left[\frac{S_{xy}(\omega)}{s_y^-(\omega)}\right]_+\left[\frac{S_{xy}(\omega)}{s_y^-(\omega)}\right]_+^*. \tag{A.57}$$

This is most efficiently done by treating $\omega \to z$ as a complex variable and then performing a contour integral on a half-circle in the LHP or UHP. From the residue theorem, it follows that the contour integral around a closed loop with poles inside is given by the sum over the residues inside the loop $\times 2\pi i$[3]. For the situation considered, we have the quantities above $\to 0$ for $|z| \to \infty$. Thus, the integral along the half circle vanishes due to Jordan's lemma. Therefore, the integral along the real axis can be calculated from the residues of the singularities in the chosen half-plane. First, we calculate the unconditional variance:

$$\int_{-\infty}^{\infty}\frac{d\omega}{2\pi}S_{xx}(\omega) = 2\pi i\frac{1}{2\pi}\sum_{P\in\mathrm{UHP}}\mathrm{Res}[S_{xx}(\omega),P] \tag{A.58}$$

$$= \frac{2\Gamma+\gamma_m(2\bar{n}+1)}{2\gamma_m} = C_{cl}+\bar{n}+\frac{1}{2}. \tag{A.59}$$

Now, for the estimation part, we find that

$$\left|\left[\frac{S_{xy}(\omega)}{s_y^-(\omega)}\right]_+\right|^2 = \frac{\alpha^2(1+\beta^2\omega^2)}{2(\omega-P_1)(\omega-P_2)(\omega-P_3)(\omega-P_4)}, \tag{A.60}$$

3 i for a half-circle in the upper half-plane, -i for a half-circle in the lower half-plane.

and by the residue theorem, we find the integral

$$\int_{-\infty}^{\infty} \frac{d\omega}{2\pi} \left| \left[\frac{S_{xy}(\omega)}{s_y^-(\omega)} \right]_+ \right|^2 = \frac{\alpha^2(1+\beta^2\omega_m^2)}{4\gamma_m\omega_m^2}. \tag{A.61}$$

From these expressions, we can derive the conditional position variance

$$V_{xx} = C_{cl} + \bar{n} + \frac{1}{2} - \frac{\alpha^2(1+\beta^2\omega_m^2)}{4\gamma_m\omega_m^2} \tag{A.62}$$

$$= \frac{-\gamma_m + \sqrt{\gamma_m^2 + 2\omega_m\left(-\omega_m + \sqrt{8C_{cl}(2C_{cl}+2\bar{n}+1)\gamma_m^2\eta + \omega_m^2}\right)}}{8C_{cl}\eta\gamma_m}. \tag{A.63}$$

The calculations for the momentum filter, momentum variance and covariance are completely analogous by noting that $\hat{p} = i\omega\hat{x}/\omega_m$.

We perform the inverse Fourier transform to arrive at the Wiener filter in the time domain. We write

$$\overrightarrow{K}(t) = \int d\omega\, \overrightarrow{K}(\omega) e^{-i\omega t} = \int d\omega\, \alpha(1 - i\omega\beta)\chi_{eff}(\omega) e^{-i\omega t} \tag{A.64}$$

$$\begin{aligned} &= \Theta(t)\alpha e^{-\frac{\gamma_{eff}}{2}t}\left(\beta\cos\left(\frac{1}{2}\sqrt{4\omega_{eff}^2 - \gamma_{eff}^2}\,t\right)\right. \\ &\left. + \frac{2-\beta\gamma_{eff}}{\sqrt{4\omega_{eff}^2 - \gamma_{eff}^2}}\sin\left(\frac{1}{2}\sqrt{4\omega_{eff}^2 - \gamma_{eff}^2}\,t\right)\right) \end{aligned} \tag{A.65}$$

$$\approx \alpha\beta e^{-\frac{\gamma_{eff}}{2}t}\cos\left(\frac{1}{2}\sqrt{4\omega_{eff}^2 - \gamma_{eff}^2}\,t\right)\Theta(t), \tag{A.66}$$

as the sin term will go to zero for the large frequency limit. Performing this limit for the constants will lead to Equation (3.93). The calculations for the momentum filter and the retrodiction filter are analogous.

Regarding the variance of the relative distance, we first derive the relative estimate for the position

$$V_{\Delta x\Delta x} = \langle (\langle\hat{x}(\omega)\rangle^c - \langle\hat{x}(\omega)\rangle^r)(\langle\hat{x}(\omega)\rangle^c - \langle\hat{x}(\omega)\rangle^r)\rangle \tag{A.67}$$

$$= \langle (\overrightarrow{K}(\omega)\hat{y}(\omega) - \overleftarrow{K}(\omega)\hat{y}(\omega))(\overrightarrow{K}(\omega)\hat{y}(\omega) - \overleftarrow{K}(\omega)\hat{y}(\omega))\rangle \tag{A.68}$$

$$= \int_{-\infty}^{\infty} \frac{d\omega}{2\pi} S_{yy}(\omega)\left(|\overrightarrow{K}(\omega)|^2 + |\overleftarrow{K}(\omega)|^2 - 2\overleftarrow{K}(\omega)^2\right) \tag{A.69}$$

$$= \int_{-\infty}^{\infty} \frac{d\omega}{2\pi} 2 * \left| \left[\frac{S_{xy}(\omega)}{s_y^-(\omega)} \right]_+ \right|^2 - 2 * \int_{-\infty}^{\infty} \frac{d\omega}{2\pi} S_{yy}\overleftarrow{K}(\omega)^2 \tag{A.70}$$

$$= 2 * \frac{\alpha^2(1+\beta^2\omega_m^2)}{4\gamma_m\omega_m^2} - 2 * \int_{-\infty}^{\infty} \frac{d\omega}{2\pi} S_{yy}\overleftarrow{K}(\omega)^2. \tag{A.71}$$

No compact expression is found for the second integrand. It is, in principle, a simple but very tedious calculation. We wrote a script in *Mathematica* that calculates the pole integral using the residue theorem. The result of our calculation

by hand and of the script was compared with the result of Meng et al. [86, 88], yielding the same result:

$$V_{\Delta x \Delta x} = \frac{\alpha^2 \beta^2}{\gamma_m + \gamma_{eff}} \left(1 + \frac{2\gamma_m \gamma_{eff}}{\omega_m^2 + \omega_{eff}^2} \right). \tag{A.72}$$

The other variances of the relative quadratures are calculated in the same manner, giving the results as in Equations (3.126).

A.4 ORDER INDEPENDENCE IN IMPERFECT CQNC

In this section, we will provide proof why the system order in Section 4.3 can be ignored in the lossless cases ($\kappa_{bath} = 0$ and $\eta = 1$) with matched beam-splitter g_{BS} and down-conversion coupling g_{DC}. We start from the Equation (4.21) for the output quadratures of the cascaded system,

$$\hat{\mathbf{x}}'_{out,2} = T_2^{loss} \begin{pmatrix} T_1^{loss} & 0 & 0 \\ 0 & \mathbb{1}_{4\times4} & 0 \\ 0 & 0 & \mathbb{1}_{2\times2} \end{pmatrix} \begin{pmatrix} \hat{\mathbf{x}}_{in} \\ \hat{\mathbf{x}}_{bath,1} \\ \hat{\mathbf{x}}_{vac,1} \\ \hat{\mathbf{x}}_{bath,2} \\ \hat{\mathbf{x}}_{vac,2} \end{pmatrix} \tag{A.73}$$

$$= T_{total} \hat{\mathbf{x}}_{in,total}. \tag{A.74}$$

Without losses, the output matrix T_{total} is reduced to

$$T_{total} = T_2 \begin{pmatrix} T_1 & 0 \\ 0 & \mathbb{1} \end{pmatrix} \tag{A.75}$$

$$= \left(P_{in}^i P_{in}^j \,|\, P_{in}^i P_{bath}^j \,|\, P_{bath}^i \right), \tag{A.76}$$

where $i, j = \{NMO, OMS\}$ stand for the respective subsystems. Depending on the system order chosen, we find the output quadratures as

$$\begin{pmatrix} \hat{x}_{out} \\ \hat{p}_{out} \end{pmatrix} = P_{in}^{OMS} P_{in}^{NMO} \begin{pmatrix} \hat{x}_{in} \\ \hat{p}_{in} \end{pmatrix} + P_{in}^{OMS} P_{bath}^{NMO} \begin{pmatrix} \hat{x}_a \\ \hat{p}_a \end{pmatrix} + P_{bath}^{OMS} \begin{pmatrix} 0 \\ F \end{pmatrix}, \tag{A.77}$$

or

$$\begin{pmatrix} \hat{x}_{out} \\ \hat{p}_{out} \end{pmatrix} = P_{in}^{NMO} P_{in}^{OMS} \begin{pmatrix} \hat{x}_{in} \\ \hat{p}_{in} \end{pmatrix} + P_{in}^{NMO} P_{bath}^{OMS} \begin{pmatrix} 0 \\ F \end{pmatrix} + P_{bath}^{NMO} \begin{pmatrix} \hat{x}_a \\ \hat{p}_a \end{pmatrix}. \tag{A.78}$$

The calculated spectral densities will be independent of the system order, if

$$P_{in}^{NMO} P_{in}^{OMS} S_{in} (P_{in}^{NMO} P_{in}^{OMS})^\dagger = P_{in}^{OMS} P_{in}^{NMO} S_{in} (P_{in}^{OMS} P_{in}^{NMO})^\dagger \tag{A.79a}$$

$$P_{in}^{NMO} P_{bath}^{NMO} S_F (P_{in}^{NMO} P_{bath}^{OMS})^\dagger = P_{bath}^{OMS} S_F P_{bath}^{OMS\,\dagger} \tag{A.79b}$$

$$P_{in}^{OMS} P_{bath}^{NMO} S_a (P_{in}^{OMS} P_{bath}^{NMO})^\dagger = P_{bath}^{NMO} S_a P_{bath}^{NMO\,\dagger}, \tag{A.79c}$$

with S_{in}, S_F and S_a input spectral densities of the input field, the force and the ancilla cavity.

We will now calculate the P-matrices of each subsystem for this lossless case without detuning ($\Delta_{om} = \Delta_c = 0$). For the OMS, we find the drift and input matrices

$$\begin{aligned} M_{OMS} &= \begin{pmatrix} -\kappa_{om}/2 & 0 & 0 & 0 \\ 0 & -\kappa_{om}/2 & -g & 0 \\ 0 & 0 & 0 & \omega_m \\ -g & 0 & -\omega_m & -\gamma_m \end{pmatrix}, \\ K^{in}_{OMS} &= \begin{pmatrix} \sqrt{\kappa_{om}} & 0 \\ 0 & \sqrt{\kappa_{om}} \\ 0 & 0 \\ 0 & 0 \end{pmatrix}, \; K^{bath}_{OMS} = \begin{pmatrix} 0 & 0 \\ 0 & 0 \\ 0 & 0 \\ 0 & \sqrt{\gamma_m} \end{pmatrix}. \end{aligned} \tag{A.80}$$

We then find the input P-matrix

$$P^{OMS}_{in} = (K^{in\,\top}_{OMS}(i\omega\mathbb{1} - M_{OMS})^{-1}K^{in}_{OMS} - \mathbb{1} \tag{A.81}$$

$$= \begin{pmatrix} \frac{\kappa_{om}/2 - i\omega}{\kappa_{om}/2 + i\omega} & 0 \\ -g^2\kappa_{om}\chi^2_{om}\chi_m & \frac{\kappa_{om}/2 - i\omega}{\kappa_{om}/2 + i\omega} \end{pmatrix} \tag{A.82}$$

$$= \begin{pmatrix} e^{i\phi} & 0 \\ -g^2_{om}\chi_m & e^{i\phi} \end{pmatrix}. \tag{A.83}$$

For brevity, we introduced a complex coupling strength $g^2_{om} = g^2\kappa_{om}\chi^2_{om}$, such that $|g_{om}|^2 = G_{om}$. The bath P-matrix is found as

$$P^{OMS}_{bath} = (K^{in\,\top}_{OMS}(i\omega\mathbb{1} - M_{OMS})^{-1}K^{bath}_{OMS} \tag{A.84}$$

$$= \begin{pmatrix} 0 & 0 \\ 0 & g\sqrt{\gamma_m}\sqrt{\kappa_{om}}\chi_{om}\chi_m \end{pmatrix} \tag{A.85}$$

$$= \begin{pmatrix} 0 & 0 \\ 0 & g_{om}\sqrt{\gamma_m}\chi_m \end{pmatrix}. \tag{A.86}$$

For the NMO, in addition to no losses and no detuning, we also consider that beam-splitter and down-conversion coupling are matched, i.e., $g_{BS} = g_{DC} = g_a/2$. Thus, the corresponding drift and input matrices are

$$\begin{aligned} M_{NMO} &= \begin{pmatrix} -\kappa_c/2 & 0 & 0 & 0 \\ 0 & -\kappa_a/2 & -g_a & 0 \\ 0 & 0 & -\kappa_a/2 & \Delta_a \\ -g_a & 0 & -\Delta_a & -\kappa_a/2 \end{pmatrix}, \\ K_{NMO}^{in} &= \begin{pmatrix} \sqrt{\kappa_c} & 0 \\ 0 & \sqrt{\kappa_c} \\ 0 & 0 \\ 0 & 0 \end{pmatrix}, \; K_{NMO}^{bath} = \begin{pmatrix} 0 & 0 \\ 0 & 0 \\ \sqrt{\kappa_a} & 0 \\ 0 & \sqrt{\kappa_a} \end{pmatrix}. \end{aligned} \tag{A.87}$$

The P-matrices are derived similarly to the OMS. We find the input P-matrix

$$P_{in}^{NMO} = \begin{pmatrix} \frac{\kappa_c/2-i\omega}{\kappa_c/2+i\omega} & 0 \\ -g_a^2\kappa_c\chi_c^2\chi_a & \frac{\kappa_c/2-i\omega}{\kappa_c/2+i\omega} \end{pmatrix} \tag{A.88}$$

$$= \begin{pmatrix} e^{i\phi} & 0 \\ -g_a^2\kappa_c\chi_c^2\chi_a & e^{i\phi} \end{pmatrix} \tag{A.89}$$

$$= \begin{pmatrix} e^{i\phi} & 0 \\ -g_{anc}^2\chi_a & e^{i\phi} \end{pmatrix}, \tag{A.90}$$

where we introduced another complex coupling strength $g_{anc} = g_a^2\kappa_c\chi_c^2$ such that $|g_{anc}|^2 = G_a$. The corresponding bath P-matrix is

$$P_{bath}^{NMO} = \begin{pmatrix} 0 & 0 \\ \frac{g_a\sqrt{\kappa_a}\sqrt{\kappa_c}\chi_c\chi_a}{\chi_{anc}\Delta_a} & g_a\sqrt{\kappa_a}\sqrt{\kappa_c}\chi_c\chi_a \end{pmatrix} \tag{A.91}$$

$$= \begin{pmatrix} 0 & 0 \\ \frac{g_{anc}\sqrt{\kappa_a}\chi_a}{\chi_{anc}\Delta_a} & g_{anc}\sqrt{\kappa_a}\chi_a \end{pmatrix}, \tag{A.92}$$

with $\chi_{anc} = \frac{1}{i\omega+\kappa_a/2}$.

We can now calculate the needed matrix products in Equation (A.79). We find

$$P_{in}^{OMS} \cdot P_{in}^{NMO} = \begin{pmatrix} e^{i(\phi+\theta)} & 0 \\ g_{anc}^2\,\chi_a\,e^{i\theta} + g_{om}^2\,\chi_m\,e^{i\phi} & e^{i(\phi+\theta)} \end{pmatrix} \tag{A.93}$$

$$= P_{in}^{NMO} \cdot P_{in}^{OMS}, \tag{A.94}$$

and

$$P_{in}^{OMS} \cdot P_{bath}^{NMO} = e^{i\theta}\,P_{bath}^{NMO}, \tag{A.95}$$

$$P_{in}^{NMO} \cdot P_{bath}^{OMS} = e^{i\phi}\,P_{bath}^{OMS}. \tag{A.96}$$

Thus, the input matrix product is commutative, and the other product differs by a complex phase. For the calculation of the output spectra, this phase will vanish. As a result, the output spectrum for the lossless case with matched beam-splitter and down-conversion coupling $g_{BS} = g_{DC} = \frac{1}{2}g_a$ is the same for both system orders.

LIST OF FIGURES

LIST OF TABLES

ACRONYMS

LHP lower-half complex plane

UHP upper-half complex plane

SQL standard quantum limit

CQNC coherent quantum-noise cancellation

QND quantum non-demolition

QMFS quantum mechanics-free subspace

POVM positive operator-valued measure

NMO negative-mass oscillator

OMS optomechanical sensor

SME stochastic master equation

RWA rotating wave approximation

BIBLIOGRAPHY

[1] Y. Aharonov, D. Z. Albert, and L. Vaidman. How the result of a measurement of a component of the spin of a spin-1/2 particle can turn out to be 100. *Physical Review Letters*, 60(14):1351–1354, Apr. 1988. doi:10.1103/physrevlett.60.1351.

[2] W. Arveson. *Noncommutative Dynamics and E-Semigroups*. Springer, New York, 2003. doi:10.1007/978-0-387-21524-2.

[3] H.-A. Bachor and T. C. Ralph. *A Guide to Experiments in Quantum Optics*. Wiley, July 2019. doi:10.1002/9783527695805.

[4] F. Bariani, H. Seok, S. Singh, M. Vengalattore, and P. Meystre. Atom-based coherent quantum-noise cancellation in optomechanics. *Physical Review A - Atomic, Molecular, and Optical Physics*, 92:043817, 10 2015. doi:10.1103/physreva.92.043817.

[5] V. P. Belavkin. Quantum stochastic calculus and quantum nonlinear filtering. *Journal of Multivariate Analysis*, 42(2):171–201, Aug. 1992. doi:10.1016/0047-259x(92)90042-e.

[6] V. P. Belavkin. Nondemolition principle of quantum measurement theory. *Foundations of Physics*, 24(5):685–714, May 1994. doi:10.1007/bf02054669.

[7] D. W. Berry, M. J. W. Hall, and H. M. Wiseman. Stochastic heisenberg limit: Optimal estimation of a fluctuating phase. *Physical Review Letters*, 111(11), Sept. 2013. doi:10.1103/physrevlett.111.113601.

[8] R. S. Bondurant and J. H. Shapiro. Squeezed states in phase-sensing interferometers. *Phys. Rev. D*, 30:2548–2556, Dec 1984. doi:10.1103/PhysRevD.30.2548.

[9] L. Bouten, R. V. Handel, and M. R. James. An introduction to quantum filtering. *SIAM Journal on Control and Optimization*, 46(6):2199–2241, Jan. 2007. doi:10.1137/060651239.

[10] W. P. Bowen and G. J. Milburn. *Quantum Optomechanics*. CRC Press, jun 2020. ISBN 9780367575199.

[11] V. Braginsky and F. Khalili. Gravitational wave antenna with QND speed meter. *Physics Letters A*, 147(5-6):251–256, July 1990. doi:10.1016/0375-9601(90)90442-q.

[12] V. B. Braginsky, Y. I. Vorontsov, and K. S. Thorne. Quantum nondemolition measurements. *Science*, 209(4456):547–557, 1980. doi:10.1126/science.209.4456.547.

[13] V. B. Braginsky, M. L. Gorodetsky, F. Y. Khalili, and K. S. Thorne. Energetic quantum limit in large-scale interferometers. *AIP Conference Proceedings*, 523:180, 2 2001. doi:10.1063/1.1291855.

[14] O. Bratteli and D. W. Robinson. *Operator Algebras and Quantum Statistical Mechanics 2*. Springer Berlin Heidelberg, 1981. doi:10.1007/978-3-662-09089-3.

[15] O. Bratteli and D. W. Robinson. *Operator Algebras and Quantum Statistical Mechanics 1*. Springer Berlin Heidelberg, 1987. doi:10.1007/978-3-662-02520-8.

[16] H.-P. Breuer and F. Petruccione. *The Theory of Open Quantum Systems*. Oxford University PressOxford, Jan. 2007. doi:10.1093/acprof:oso/9780199213900.001.0001.

[17] M. Brunelli, D. Malz, A. Schliesser, and A. Nunnenkamp. Stroboscopic quantum optomechanics. *Physical Review Research*, 2(2), May 2020. doi:10.1103/physrevresearch.2.023241.

[18] A. Buonanno and Y. Chen. Quantum noise in second generation, signal-recycled laser interferometric gravitational-wave detectors. *Physical Review D*, 64:042006, 7 2001. doi:10.1103/PhysRevD.64.042006.

[19] H. J. Carmichael. Quantum trajectory theory for cascaded open systems. *Physical Review Letters*, 70:2273, 4 1993. doi:10.1103/PhysRevLett.70.2273.

[20] C. M. Caves, K. S. Thorne, R. W. P. Drever, V. D. Sandberg, and M. Zimmermann. On the measurement of a weak classical force coupled to a quantum-mechanical oscillator. i. issues of principle. *Reviews of Modern Physics*, 52(2):341–392, Apr. 1980. doi:10.1103/revmodphys.52.341.

[21] A. Chantasri, I. Guevara, K. T. Laverick, and H. M. Wiseman. Unifying theory of quantum state estimation using past and future information. *Physics Reports*, 930:1–40, Oct. 2021. doi:10.1016/j.physrep.2021.07.003.

[22] S. Chapman. On the brownian displacements and thermal diffusion of grains suspended in a non-uniform fluid. *Proceedings of the Royal Society of London. Series A, Containing Papers of a Mathematical and Physical Character*, 119(781):34–54, May 1928. doi:10.1098/rspa.1928.0082.

[23] Y. Chen. Macroscopic quantum mechanics: theory and experimental concepts of optomechanics. *Journal of Physics B: Atomic, Molecular and Optical Physics*, 46:104001, 5 2013. doi:10.1088/0953-4075/46/10/104001.

[24] A. A. Clerk, M. H. Devoret, S. M. Girvin, F. Marquardt, and R. J. Schoelkopf. Introduction to quantum noise, measurement, and amplification. *Reviews of Modern Physics*, 82:1155–1208, 4 2010. doi:10.1103/RevModPhys.82.1155.

[25] J. Combes, J. Kerckhoff, and M. Sarovar. The SLH framework for modeling quantum input-output networks. *Advances in Physics: X*, 2(3):784–888, May 2017. doi:10.1080/23746149.2017.1343097.

[26] J. B. Conway. *A Course in Functional Analysis*. Springer New York, 2007. doi:10.1007/978-1-4757-4383-8.

[27] S. L. Danilishin. Quantum speed meter in laser gravitational antennas. *Optics and Spectroscopy*, 96(5):727–733, Sept. 2004. doi:10.1134/1.1753638.

[28] S. L. Danilishin, E. Knyazev, N. V. Voronchev, F. Y. Khalili, C. Gräf, S. Steinlechner, J.-S. Hennig, and S. Hild. A new quantum speed-meter interferometer: measuring speed to search for intermediate mass black holes. *Light: Science and Applications*, 7(1), May 2018. doi:10.1038/s41377-018-0004-2.

[29] S. L. Danilishin, F. Y. Khalili, and H. Miao. Advanced quantum techniques for future gravitational-wave detectors. *Living Reviews in Relativity 2019 22:1*, 22:1–89, 4 2019. doi:10.1007/s41114-019-0018-y.

[30] L. Diósi. Continuous quantum measurement and itô formalism. *Physics Letters A*, 129(8-9):419–423, June 1988. doi:10.1016/0375-9601(88)90309-x.

[31] A. C. Doherty, A. Szorkovszky, G. I. Harris, and W. P. Bowen. The quantum trajectory approach to quantum feedback control of an oscillator revisited. *Philosophical Transactions of the Royal Society A: Mathematical, Physical and Engineering Sciences*, 370(1979):5338–5353, Nov. 2012. doi:10.1098/rsta.2011.0531.

[32] G. A. Einicke. *Smoothing, Filtering and Prediction - Estimating The Past, Present and Future*. InTech, 2 2012. doi:10.5772/2706.

[33] I. Florescu. *Probability and stochastic processes*. Wiley-Blackwell, 2014. ISBN 978-0-470-62455-5. URL `https://www.wiley.com/en-us/Probability+and+Stochastic+Processes-p-9780470624555`.

[34] D. Fraser and J. Potter. The optimum linear smoother as a combination of two optimum linear filters. *IEEE Transactions on Automatic Control*, 14 (4):387–390, 1969. doi:10.1109/TAC.1969.1099196.

[35] D. C. Fraser. *A new technique for the optimal smoothing of data*. PhD thesis, Massachusetts Institute of Technology, 1967. URL `https://dspace.mit.edu/handle/1721.1/13543`.

[36] S. Gammelmark, B. Julsgaard, and K. Mølmer. Past quantum states of a monitored system. *Phys. Rev. Lett.*, 111:160401, Oct 2013. doi:10.1103/PhysRevLett.111.160401.

[37] C. W. Gardiner. Driving a quantum system with the output field from another driven quantum system. *Physical Review Letters*, 70:2269, 4 1993. doi:10.1103/PhysRevLett.70.2269.

[38] C. W. Gardiner and P. Zoller. *Quantum Noise: A Handbook of Markovian and Non-Markovian Quantum Stochastic Methods with Applications to Quantum Optics*. Springer, 2004. ISBN 9783540223016. URL https://link.springer.com/book/9783540223016.

[39] T. Gebremariam, Y. X. Zeng, M. Mazaheri, and C. Li. Enhancing optomechanical force sensing via precooling and quantum noise cancellation. *Science China Physics, Mechanics and Astronomy 2019 63:1*, 63:1–11, 6 2019. doi:10.1007/s11433-019-9424-y.

[40] C. Gerry and P. Knight. *Introductory Quantum Optics*. Cambridge University Press, 2004. doi:10.1017/CBO9780511791239.

[41] V. Gorini, A. Kossakowski, and E. C. G. Sudarshan. Completely positive dynamical semigroups of n-level systems. *Journal of Mathematical Physics*, 17(5):821–825, 1976. doi:10.1063/1.522979.

[42] J. Gough. How to estimate past quantum measurement interventions after continuous monitoring. *Russian Journal of Mathematical Physics*, 27 (2):218–227, Apr. 2020. doi:10.1134/s1061920820020089.

[43] C. Gräf, B. W. Barr, A. S. Bell, F. Campbell, A. V. Cumming, S. L. Danilishin, N. A. Gordon, G. D. Hammond, J. Hennig, E. A. Houston, S. H. Huttner, R. A. Jones, S. S. Leavey, H. Lück, J. Macarthur, M. Marwick, S. Rigby, R. Schilling, B. Sorazu, A. Spencer, S. Steinlechner, K. A. Strain, and S. Hild. Design of a speed meter interferometer proof-of-principle experiment. *Classical and Quantum Gravity*, 31(21):215009, Oct. 2014. doi:10.1088/0264-9381/31/21/215009.

[44] A. Grossmann. Parity operator and quantization of δ-functions. *Communications in Mathematical Physics*, 48(3):191–194, Oct. 1976. doi:10.1007/bf01617867.

[45] I. Guevara and H. Wiseman. Quantum state smoothing. *Physical Review Letters*, 115(18), Oct. 2015. doi:10.1103/physrevlett.115.180407.

[46] I. A. Guevara Prieto. *Quantum State Smoothing*. PhD thesis, Griffith University, 2016. URL https://research-repository.griffith.edu.au/handle/10072/367795.

[47] K. Hammerer, M. Aspelmeyer, E. S. Polzik, and P. Zoller. Establishing Einstein-Poldosky-Rosen channels between nanomechanics and atomic ensembles. *Physical Review Letters*, 102:020501, 1 2009. doi:10.1103/physrevlett.102.020501.

[48] T. Heinosaari and M. Ziman. *The Mathematical Language of Quantum Theory: From Uncertainty to Entanglement*. Cambridge University Press, 2011. doi:10.1017/CBO9781139031103.

[49] O. Hijab. *Introduction to Calculus and Classical Analysis*. Springer International Publishing, 2016. doi:10.1007/978-3-319-28400-2.

[50] S. Hofer. *Quantum Control of Optomechanical Systems*. PhD thesis, Universität Wien, 2015. URL https://utheses.univie.ac.at/detail/34525.

[51] S. G. Hofer and K. Hammerer. Entanglement-enhanced time-continuous quantum control in optomechanics. *Physical Review A*, 91(3), Mar. 2015. doi:10.1103/physreva.91.033822.

[52] A. Holevo. *Probabilistic and Statistical Aspects of Quantum Theory*. Edizioni della Normale, 2011. doi:10.1007/978-88-7642-378-9.

[53] A. S. Holevo. On singular perturbations of quantum dynamical semigroups. *Mathematical Notes*, 103:133–144, 3 2018. doi:10.1134/S0001434618010157.

[54] Z. Huang and M. Sarovar. Smoothing of gaussian quantum dynamics for force detection. *Phys. Rev. A*, 97:042106, Apr 2018. doi:10.1103/PhysRevA.97.042106.

[55] R. L. Hudson and K. R. Parthasarathy. Quantum Ito's formula and stochastic evolutions. *Communications in Mathematical Physics*, 93(3):301–323, Sept. 1984. doi:10.1007/bf01258530.

[56] K. Itô. Stochastic integral. *Proceedings of the Imperial Academy*, 20(8):519 – 524, 1944. doi:10.3792/pia/1195572786.

[57] K. Itô. On stochastic differential equations. *Memoirs of the American Mathematical Society*, 0:0–0, 1951. doi:10.1090/memo/0004.

[58] K. Jacobs. *Stochastic Processes for Physicists: Understanding Noisy Systems*. Cambridge University Press, 2010. doi:10.1017/CBO9780511815980.

[59] K. Jacobs. *Quantum measurement theory and its applications*. Cambridge University Press, 1 2014. doi:10.1017/cbo9781139179027.

[60] K. Jacobs and D. A. Steck. A straightforward introduction to continuous quantum measurement. *Contemporary Physics*, 47(5):279–303, Sept. 2006. doi:10.1080/00107510601101934.

[61] M. T. Jaekel and S. Reynaud. Quantum limits in interferometric measurements. *Europhys. Lett.*, 13(4):301–306, oct 1990. doi:10.1209/0295-5075/13/4/003.

[62] P. Janotta and H. Hinrichsen. Generalized probability theories: what determines the structure of quantum theory? *Journal of Physics A: Mathematical and Theoretical*, 47:323001, 8 2014. doi:10.1088/1751-8113/47/32/323001.

[63] B. Julsgaard, A. Kozhekin, and E. S. Polzik. Experimental long-lived entanglement of two macroscopic objects. *Nature 2001 413:6854*, 413:400–403, 9 2001. doi:10.1038/35096524.

[64] J. Junker, D. Wilken, N. Johny, D. Steinmeyer, and M. Heurs. Frequency-dependent squeezing from a detuned squeezer. *Physical Review Letters*, 129(3), July 2022. doi:10.1103/physrevlett.129.033602.

[65] T. Kailath, A. H. Sayed, and B. Hassibi. *Linear Estimation*. Prentice Hall information and system sciences series. Pearson, Upper Saddle River, NJ, Mar. 2000.

[66] R. E. Kalman and R. S. Bucy. New results in linear filtering and prediction theory. *Journal of Basic Engineering*, 83:95–108, 3 1961. doi:10.1115/1.3658902.

[67] T. M. Karg, B. Gouraud, C. T. Ngai, G.-L. Schmid, K. Hammerer, and P. Treutlein. Light-mediated strong coupling between a mechanical oscillator and atomic spins 1 meter apart. *Science*, 369(6500):174–179, July 2020. doi:10.1126/science.abb0328.

[68] Karg, Thomas Michael. *Strong light-mediated coupling between a membrane oscillator and an atomic spin ensemble*. PhD thesis, University of Basel, 2020. URL `https://edoc.unibas.ch/78413/`.

[69] F. Khalili, S. Danilishin, H. Miao, H. Müller-Ebhardt, H. Yang, and Y. Chen. Preparing a mechanical oscillator in non-gaussian quantum states. *Physical Review Letters*, 105(7), Aug. 2010. doi:10.1103/physrevlett.105.070403.

[70] F. Y. Khalili. Optimal configurations of filter cavity in future gravitational-wave detectors. *Physical Review D - Particles, Fields, Gravitation and Cosmology*, 81:122002, 6 2010. doi:10.1103/physrevd.81.122002.

[71] F. Y. Khalili and Y. Levin. Speed meter as a quantum nondemolition measuring device for force. *Physical Review D*, 54(8):4735–4737, Oct. 1996. doi:10.1103/physrevd.54.4735.

[72] F. Y. Khalili and E. Zeuthen. Quantum limits for stationary force sensing. *Physical Review A*, 103:043721, 4 2021. doi:10.1103/physreva.103.043721.

[73] A. S. Kholevo. There exists a non-standard dynamical semigroup on. *Russian Mathematical Surveys*, 51(6):1206, 12 1996. doi:10.1070/RM1996v051n06ABEH003009.

[74] H. J. Kimble, Y. Levin, A. B. Matsko, K. S. Thorne, and S. P. Vyatchanin. Conversion of conventional gravitational-wave interferometers into quantum nondemolition interferometers by modifying their input and/or output optics. *Physical Review D*, 65:022002, 12 2001. doi:10.1103/PhysRevD.65.022002.

[75] A. Kolmogoroff. Über die analytischen methoden in der wahrscheinlichkeitsrechnung. *Mathematische Annalen*, 104(1):415–458, Dec. 1931. doi:10.1007/bf01457949.

[76] J. Lammers. *State preparation and verification in continuously measured quantum systems*. PhD thesis, Leibniz Universität Hannover, 2018. URL https://www.repo.uni-hannover.de/handle/123456789/3888.

[77] K. Landsman. *Foundations of Quantum Theory: From Classical Concepts to Operator Algebras (Fundamental Theories of Physics)*. Springer, 2017. doi:10.1007/978-3-319-51777-3.

[78] K. T. Laverick. Quantum Rauch-Tung-Striebel smoothed state. *Phys. Rev. Research*, 3:033196, Aug 2021. doi:10.1103/PhysRevResearch.3.033196.

[79] K. T. Laverick, A. Chantasri, and H. M. Wiseman. Quantum state smoothing for linear gaussian systems. *Physical Review Letters*, 122(19), May 2019. doi:10.1103/physrevlett.122.190402.

[80] K. T. Laverick, A. Chantasri, and H. M. Wiseman. General criteria for quantum state smoothing with necessary and sufficient criteria for linear gaussian quantum systems. *Quantum Studies: Mathematics and Foundations*, 8(1):37–50, Apr. 2020. doi:10.1007/s40509-020-00225-7.

[81] K. T. Laverick, A. Chantasri, and H. M. Wiseman. Linear gaussian quantum state smoothing: Understanding the optimal unravelings for alice to estimate bob's state. *Phys. Rev. A*, 103:012213, Jan 2021. doi:10.1103/PhysRevA.103.012213.

[82] C. K. Law. Interaction between a moving mirror and radiation pressure: A hamiltonian formulation. *Physical Review A*, 51(3):2537–2541, Mar. 1995. doi:10.1103/physreva.51.2537.

[83] G. Lindblad. On the generators of quantum dynamical semigroups. *Communications in Mathematical Physics*, 48(2):119 – 130, 1976. doi:cmp/1103899849.

[84] D. Mason, J. Chen, M. Rossi, Y. Tsaturyan, and A. Schliesser. Continuous force and displacement measurement below the standard quantum limit. *Nature Physics 2019 15:8*, 15:745–749, 5 2019. doi:10.1038/s41567-019-0533-5.

[85] D. Q. Mayne. A solution of the smoothing problem for linear dynamic systems. *Automatica*, 4:73–92, 12 1966. doi:10.1016/0005-1098(66)90019-7.

[86] C. Meng. *Optomechanical state preparation via strong measurement*. PhD thesis, The University of Queensland, 2022. URL https://espace.library.uq.edu.au/view/UQ:eda377c.

[87] C. Meng, G. A. Brawley, J. S. Bennett, M. R. Vanner, and W. P. Bowen. Mechanical squeezing via fast continuous measurement. *Physical Review Letters*, 125(4), July 2020. doi:10.1103/physrevlett.125.043604.

[88] C. Meng, G. A. Brawley, S. Khademi, E. M. Bridge, J. S. Bennett, and W. P. Bowen. Measurement-based preparation of multimode mechanical states. *Science Advances*, 8(21), May 2022. doi:10.1126/sciadv.abm7585.

[89] H. Miao, S. Danilishin, H. Müller-Ebhardt, H. Rehbein, K. Somiya, and Y. Chen. Probing macroscopic quantum states with a sub-heisenberg accuracy. *Physical Review A*, 81(1), Jan. 2010. doi:10.1103/physreva.81.012114.

[90] H. Miao, R. X. Adhikari, Y. Ma, B. Pang, and Y. Chen. Towards the fundamental quantum limit of linear measurements of classical signals. *Physical Review Letters*, 119:050801, 8 2017. doi:10.1103/physrevlett.119.050801.

[91] A. Motazedifard, F. Bemani, M. H. Naderi, R. Roknizadeh, and D. Vitali. Force sensing based on coherent quantum noise cancellation in a hybrid optomechanical cavity with squeezed-vacuum injection. *New Journal of Physics*, 18:073040, 7 2016. doi:10.1088/1367-2630/18/7/073040.

[92] H. Müller-Ebhardt. *On quantum effects in the dynamics of macroscopic test masses*. PhD thesis, Leibniz Universität Hannover, 2009. URL `https://www.repo.uni-hannover.de/handle/123456789/7316`.

[93] H. Müller-Ebhardt, H. Rehbein, C. Li, Y. Mino, K. Somiya, R. Schnabel, K. Danzmann, and Y. Chen. Quantum-state preparation and macroscopic entanglement in gravitational-wave detectors. *Physical Review A*, 80(4), Oct. 2009. doi:10.1103/physreva.80.043802.

[94] C. B. Møller, R. A. Thomas, G. Vasilakis, E. Zeuthen, Y. Tsaturyan, M. Balabas, K. Jensen, A. Schliesser, K. Hammerer, and E. S. Polzik. Quantum back-action-evading measurement of motion in a negative mass reference frame. *Nature*, 547:191–195, 7 2017. doi:10.1038/nature22980.

[95] M. A. Nielsen and I. L. Chuang. *Quantum Computation and Quantum Information: 10th Anniversary Edition*. Cambridge University Press, 12 2010. doi:10.1017/cbo9780511976667.

[96] B. Noble. *Methods based on the Wiener-Hopf technique for the solution of partial differential equations*. AMS Chelsea Publishing. American Mathematical Society, 2 edition, Jan. 1988. ISBN 9780828403320.

[97] R. A. Norte, J. P. Moura, and S. Gröblacher. Mechanical resonators for quantum optomechanics experiments at room temperature. *Physical Review Letters*, 116:147202, 4 2016. doi:10.1103/physrevlett.116.147202.

[98] H. I. Nurdin, M. R. James, and A. C. Doherty. Network synthesis of linear dynamical quantum stochastic systems. *SIAM Journal on Control and Optimization*, 48(4):2686–2718, 2009. doi:10.1137/080728652.

[99] S. Olivares. Quantum optics in the phase space. *The European Physical Journal Special Topics*, 203(1):3–24, Apr. 2012. doi:10.1140/epjst/e2012-01532-4.

[100] E. S. Polzik and K. Hammerer. Trajectories without quantum uncertainties. *Annalen der Physik*, 527:A15–a20, 1 2015. doi:10.1002/andp.201400099.

[101] H. Rehbein. *On the enhancement of future gravitational wave laser interferometers and the prospects of probing macroscopic quantum mechanics*. PhD thesis, Leibniz Universität Hannover, 2009. URL https://www.repo.uni-hannover.de/handle/123456789/7335.

[102] M. Rossi. *Quantum Measurement and Control of a Mechanical Resonator*. PhD thesis, University of Copehagen, 2020. URL https://nbi.ku.dk/english/theses/phd-theses/massimiliano-rossi.

[103] M. Rossi, D. Mason, J. Chen, Y. Tsaturyan, and A. Schliesser. Measurement-based quantum control of mechanical motion. *Nature*, 563 (7729):53–58, Oct. 2018. doi:10.1038/s41586-018-0643-8.

[104] M. Rossi, D. Mason, J. Chen, and A. Schliesser. Observing and verifying the quantum trajectory of a mechanical resonator. *Physical Review Letters*, 123(16), Oct. 2019. doi:10.1103/physrevlett.123.163601.

[105] J. Schweer. Non-standard dynamical semigroups on the CAR algebra. Master's thesis, Leibniz Universität Hannover, 2018.

[106] J. Schweer, D. Steinmeyer, K. Hammerer, and M. Heurs. All-optical coherent quantum-noise cancellation in cascaded optomechanical systems. *Physical Review A*, 106(3), Sept. 2022. doi:10.1103/physreva.106.033520.

[107] A. Serafini. *Quantum Continuous Variables*. CRC Press, 2017. doi:10.1201/9781315118727.

[108] I. Siemon, A. S. Holevo, and R. F. Werner. Unbounded generators of dynamical semigroups. *Open Systems & Information Dynamics*, 24(04): 1740015, 2017. doi:10.1142/S1230161217400157.

[109] S. K. Singh, M. Mazaheri, J.-X. Peng, and M. Asjad. Enhanced weak force sensing through atom-based coherent noise cancellation in a hybrid cavity optomechanical system, 2022. URL https://arxiv.org/abs/2201.10805.

[110] A. Sinha. *Linear systems : optimal and robust control*. CRC Press, 2007. ISBN 9780849392177. URL https://www.routledge.com/Linear-Systems-Optimal-and-Robust-Control/Sinha/p/book/9780849392177.

[111] D. Steinmeyer. *Subsystems for all-optical coherent quantum-noise cancellation*. PhD thesis, Leibniz Universität Hannover, 2019. URL https://www.repo.uni-hannover.de/handle/123456789/9232.

[112] W. F. Stinespring. Positive functions on C*-algebras. *Proceedings of the American Mathematical Society*, 6(2):211–216, 1955. doi:10.1090/s0002-9939-1955-0069403-4.

[113] R. L. Stratonovich. A new representation for stochastic integrals and equations. *SIAM Journal on Control*, 4(2):362–371, May 1966. doi:10.1137/0304028.

[114] S. Särkkä. *Bayesian Filtering and Smoothing*. Institute of Mathematical Statistics Textbooks. Cambridge University Press, 2013. doi:10.1017/CBO9781139344203.

[115] D. Tan, S. Weber, I. Siddiqi, K. Mølmer, and K. Murch. Prediction and retrodiction for a continuously monitored superconducting qubit. *Physical Review Letters*, 114(9), Mar. 2015. doi:10.1103/physrevlett.114.090403.

[116] H. L. V. Trees. *Detection, Estimation, and Modulation Theory, Part I*. Wiley & Sons, 9 2001. doi:10.1002/0471221082.

[117] M. Tsang. Time-symmetric quantum theory of smoothing. *Physical Review Letters*, 102:250403, 6 2009. doi:10.1103/PhysRevLett.102.250403.

[118] M. Tsang. Optimal waveform estimation for classical and quantum systems via time-symmetric smoothing. *Physical Review A - Atomic, Molecular, and Optical Physics*, 80:033840, 9 2009. doi:10.1103/PhysRevA.80.033840.

[119] M. Tsang. Generalized conditional expectations for quantum retrodiction and smoothing. *Physical Review A*, 105(4), Apr. 2022. doi:10.1103/physreva.105.042213.

[120] M. Tsang and C. M. Caves. Coherent quantum-noise cancellation for optomechanical sensors. *Physical Review Letters*, 105:123601, 9 2010. doi:10.1103/physrevlett.105.123601.

[121] M. Tsang and C. M. Caves. Evading quantum mechanics: Engineering a classical subsystem within a quantum environment. *Physical Review X*, 2: 031016, 9 2012. doi:10.1103/physrevx.2.031016.

[122] M. Tsang, J. H. Shapiro, and S. Lloyd. Quantum theory of optical temporal phase and instantaneous frequency. II. continuous-time limit and state-variable approach to phase-locked loop design. *Physical Review A*, 79(5), May 2009. doi:10.1103/physreva.79.053843.

[123] M. Tsang, H. M. Wiseman, and C. M. Caves. Fundamental quantum limit to waveform estimation. *Physical Review Letters*, 106:090401, 3 2011. doi:10.1103/physrevlett.106.090401.

[124] W. G. Unruh. Quantum noise in the interferometer detector. In P. Meystre and M. O. Scully, editors, *Quantum Optics, Experimental Gravity, and Measurement Theory*, pages 647–660. Springer US, 1983. ISBN 978-1-4613-3712-6. URL https://doi.org/10.1007/978-1-4613-3712-6_28.

[125] H. Vahlbruch, M. Mehmet, K. Danzmann, and R. Schnabel. Detection of 15 db squeezed states of light and their application for the absolute calibration of photoelectric quantum efficiency. *Physical Review Letters*, 117:110801, 9 2016. doi:10.1103/physrevlett.117.110801.

[126] G. Vasilakis, V. Shah, and M. V. Romalis. Stroboscopic backaction evasion in a dense alkali-metal vapor. *Physical Review Letters*, 106(14), Apr. 2011. doi:10.1103/physrevlett.106.143601.

[127] J. von Neumann. *Mathematische Grundlagen der Quantenmechanik*. Springer Berlin Heidelberg, 1996. doi:10.1007/978-3-642-61409-5.

[128] S. Vyatchanin and E. Zubova. Quantum variation measurement of a force. *Physics Letters A*, 201(4):269–274, 1995. doi:https://doi.org/10.1016/0375-9601(95)00280-G.

[129] S. P. Vyatchanin and A. B. Matsko. Quantum speed meter based on dissipative coupling. *Physical Review A*, 93(6), June 2016. doi:10.1103/physreva.93.063817.

[130] J. E. Wall. *Control and estimation for large-scale systems having spatial symmetry*. PhD thesis, Massachusetts Institute of Technology, 1978. URL `https://willsky.lids.mit.edu/ssg/ssg_theses/ssg_theses_1974_1999/Wall_PhD_78.pdf`.

[131] J. E. Wall, A. S. Willsky, and N. R. Sandell. On the fixed-interval smoothing problem. *Stochastics*, 5:1–41, 2011. doi:10.1080/17442508108833172.

[132] D. F. Walls and G. J. Milburn. *Quantum optics*. Springer, 2008. doi:10.1007/978-3-540-28574-8.

[133] W. Wasilewski, K. Jensen, H. Krauter, J. J. Renema, M. V. Balabas, and E. S. Polzik. Quantum noise limited and entanglement-assisted magnetometry. *Physical Review Letters*, 104:133601, 3 2010. doi:10.1103/physrevlett.104.133601.

[134] C. Weedbrook, S. Pirandola, R. García-Patrón, N. J. Cerf, T. C. Ralph, J. H. Shapiro, and S. Lloyd. Gaussian quantum information. *Reviews of Modern Physics*, 84(2):621–669, May 2012. doi:10.1103/revmodphys.84.621.

[135] H. L. Weinert. *Fixed Interval Smoothing for State Space Models*. Springer US, 2001. doi:10.1007/978-1-4615-1691-0.

[136] R. Werner. Quantum harmonic analysis on phase space. *Journal of Mathematical Physics*, 25(5):1404–1411, May 1984. doi:10.1063/1.526310.

[137] T. A. Wheatley, D. W. Berry, H. Yonezawa, D. Nakane, H. Arao, D. T. Pope, T. C. Ralph, H. M. Wiseman, A. Furusawa, and E. H. Huntington. Adaptive optical phase estimation using time-symmetric quantum smoothing. *Physical Review Letters*, 104(9), Mar. 2010. doi:10.1103/physrevlett.104.093601.

[138] N. Wiener. *Extrapolation, Interpolation, and Smoothing of Stationary Time Series: With Engineering Applications*. The MIT Press, 8 1949. doi:10.7551/mitpress/2946.001.0001.

[139] E. Wigner. On the quantum correction for thermodynamic equilibrium. *Physical Review*, 40(5):749–759, June 1932. doi:10.1103/physrev.40.749.

[140] M. Wimmer. *Coupled nonclassical systems for coherent backaction noise cancellation*. PhD thesis, Leibniz Universität Hannover, 2016. URL `https://www.repo.uni-hannover.de/handle/123456789/8957`.

[141] M. H. Wimmer, D. Steinmeyer, K. Hammerer, and M. Heurs. Coherent cancellation of backaction noise in optomechanical force measurements. *Physical Review A - Atomic, Molecular, and Optical Physics*, 89:053836, 5 2014. doi:10.1103/physreva.89.053836.

[142] H. M. Wiseman. Weak values, quantum trajectories, and the cavity-QED experiment on wave-particle correlation. *Physical Review A*, 65(3), Feb. 2002. doi:10.1103/physreva.65.032111.

[143] H. M. Wiseman and G. J. Milburn. *Quantum Measurement and Control*. Cambridge University Press, 2009. doi:10.1017/CBO9780511813948.

[144] M. Wolf. Quantum channels and operations - guided tour, 2012. URL: `https://www-m5.ma.tum.de/foswiki/pub/M5/Allgemeines/MichaelWolf/QChannelLecture.pdf`.

[145] J. Yan and J. Jing. Backaction-noise suppression and system stabilization in double-mode optomechanical systems. *Annalen der Physik*, 533:2100119, 7 2021. doi:10.1002/andp.202100119.

[146] H. Yonezawa, D. Nakane, T. A. Wheatley, K. Iwasawa, S. Takeda, H. Arao, K. Ohki, K. Tsumura, D. W. Berry, T. C. Ralph, H. M. Wiseman, E. H. Huntington, and A. Furusawa. Quantum-enhanced optical-phase tracking. *Science*, 337(6101):1514–1517, Sept. 2012. doi:10.1126/science.1225258.

[147] E. Zeuthen, E. S. Polzik, and F. Y. Khalili. Trajectories without quantum uncertainties in composite systems with disparate energy spectra. *PRX Quantum*, 3:020362, 6 2022. doi:10.1103/PRXQuantum.3.020362.

[148] J. Zhang and K. Mølmer. Prediction and retrodiction with continuously monitored gaussian states. *Phys. Rev. A*, 96:062131, Dec 2017. doi:10.1103/PhysRevA.96.062131.

[149] K. Zhang, P. Meystre, and W. Zhang. Back-action-free quantum optomechanics with negative-mass bose-einstein condensates. *Physical Review A - Atomic, Molecular, and Optical Physics*, 88:043632, 10 2013. doi:10.1103/physreva.88.043632.

LIST OF PUBLICATIONS

PEER-REVIEWED JOURNAL ARTICLES

- J. Schweer, D. Steinmeyer, K. Hammerer, and M. Heurs "All-optical coherent quantum-noise cancellation in cascaded optomechanical systems", *Physical Review A*, **106**(3), 033520 (2022).

Curriculum Vitæ

Jakob Schweer

E-Mail: jakob.schweer@aei.mpg.de

Education

2018 – 2023	**PhD Physics**, Leibniz University Hanover PhD student within the Institute for Gravitational Physics Group of Quantum Control Thesis: "Quantum Back-Action Evasion and Filtering in Optomechanical Systems"
2013 – 20018	**M. Sc.** in Physics, Leibniz University Hanover Supervisor: Prof. Reinhard Werner Institute of Theoretical Physics Group of Quantum Information Thesis: "Non-standard Dynamical Semigroups on the CAR Algebra"
2009 – 2014	**B. Sc.** in Physics, Leibniz University Hanover Supervisor: Prof. Domenico Giulini Institute of Theoretical Physics Group of String Theory, Gravitation and particle physics Thesis: "Mathematische Aspekte der Geschwindigkeitsaddition in der speziellen Relativitätstheorie"
2006 – 2009	**Abitur**, Fachgymnasium Wirtschaft Wunstorf